BOSTON UNIVERSITY

COLLEGE OF ENGINEERING

Dissertation

NOVEL COMPUTATIONAL AND INSTRUMENTATION METHODOLOGIES

FOR BIOLOGICAL FOURIER-TRANSFORM ION CYCLOTRON RESONANCE

MASS SPECTROMETRIC (FT-ICR MS) IMAGING

by

KONSTANTIN AIZIKOV

B.A., Brandeis University 1997
M.S., Boston University 2002
M.S., Boston University 2009

Submitted in partial fulfillment of the

requirements for the degree of

Doctor of Philosophy

2010

Approved by

First Reader

_____
Peter B. O'Connor, Ph. D.
Professor
Department of Chemistry
Warwick University, Coventry, UK

Second Reader

_____
Lev B. Levitin, Ph. D.
Professor
Department of Electrical and Computer Engineering
Boston University, Boston

Third Reader

_____
Ron Knepper, Ph. D.
Professor
Department of Electrical and Computer Engineering
Boston University, Boston

Fourth Reader

_____
Alexander Sergienko, Ph. D.
Professor
Department of Electrical and Computer Engineering
Boston University, Boston

Fifth Reader

_____
Ron M.A. Heeren, Ph. D.
Professor
FOM Institute and
Department of Chemistry
Utrecht University, Utrecht NL

NOVEL COMPUTATIONAL AND INSTRUMENTATION METHODOLOGIES FOR BIOLOGICAL FOURIER-TRANSFORM ION CYCLOTRON RESONANCE MASS SPECTROMETRIC (FT-ICR MS) IMAGING

(Order No.   )

KONSTANTIN AIZIKOV

Boston University, College of Engineering, 2010

Major Professor: Peter B. O'Connor, Ph.D., Professor of Chemistry, Warwick University, Coventry, UK.

ABSTRACT

Mass spectrometry imaging (MSI) is an emerging experimental methodology whose primary objective is the investigation of spatial variation of molecular composition within and across selected biological tissues to enable biomarker discovery, molecular diagnosis, and studies of drug metabolism, among other applications. The two major challenges, therefore, are the unambiguous identification and precise localization of biologically relevant compounds. These challenges can be recast as a problem of improving the accuracy and resolution of mass analyzers as well as the accuracy of the sample positioning robotics.

The first part of this work reports on the progress and outlines the strategies of application of a recently developed high resolution spectral analysis technique, called the Filter Diagonalization Method (FDM), for the investigation of space-charge related phenomena inside the detection cell of a Fourier Transform Ion Cyclotron Resonance Mass Spectrometer (FT-ICR MS), understanding of which lies at the heart of the quest for further improvements in mass accuracy and resolution.

The FDM spectrographic analysis revealed previously unobserved rapid isotope-beat space-charge induced ICR frequency modulations, shown to reach up to +/- 400 ppm even on high quality spectra. The application of this methodology to the investigation of a frequently observed but previously unexplained phenomenon in FT-ICR MS, the Spontaneous Loss of Coherence Catastrophe, conclusively demonstrated that it is tied directly to the space charge effect and magnetron expansion.

The second part of this work reports on the development of the ionization source and vacuum compatible high precision sample positioning robotics for biological MSI applications, purpose built for FT-ICR MS. The complete design and implementation is reported herein, along with the demonstration of its performance and biological application.

The XY-positioning stage capable of operating under 10^{-8} mbar vacuum with submicron positioning accuracy along the entire ranges of motion of 100x100 mm was designed, built, and installed into the ionization sources of three MALDI FT-ICR MS instruments. Two dimensional chemo-spatial maps of rat brain tissue selections were constructed with 150 micron spatial resolution, identifying multiple ionic species with their distinct and discreet spatial localizations. These demonstrated performance characteristics greatly surpass current state-of-the-art robotics available for MALDI MSI and shift the effort of further improvements in spatial resolution to the ionization methodologies, and other ion source design issues, such as laser optics.

Contents:

List of Tables:

List of Figures:

Chapter 1

Background

1.1 Introduction to Mass spectrometry

Mass Spectrometry (MS) is an analytical technique for determining the elemental composition of molecules. It traces its roots to the discovery of beams of positively charged ions by Eugen Goldstein in 1886, which, at the time of his discovery, he called "Kanalstrahlen" or canal rays (anode rays in more modern terms). The consequent work on "rays of positive electricity" led Sir Joseph John Thomson to the discovery of isotopes.(Thomson 1913)(The first prototype of a modern mass spectrometer, called a positive ray spectrograph (figure 1.1.a), was designed in 1917 by Arthur Jeffry Dempster,(Dempster 1918) shortly followed by the first reported mass spectrum (figure 1.1.b) by Francis William Aston in 1918.(Aston 1919)
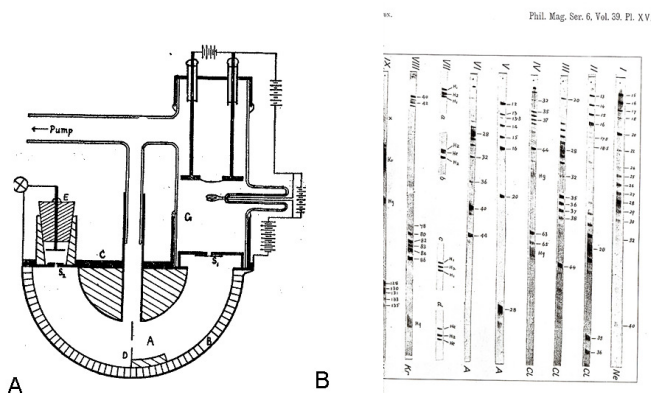
Figure 1.1 a) a schematics of the positive ray spectrograph reported by A.J. Demtster in 1917; (Dempster 1918) b) the first mass spectrum reported by F.W Aston in 1918.(Aston 1919)

Rapid progress in subsequent decades has contributed significantly to the development of the MS technique, through advances in instrumentation, applications, and methods development, making it today one of the most ubiquitous analytical methodologies. It is used in multitudes of diverse applications: from airport security to archeology, from space exploration to bio-medicine. The reason for its widespread adoption is the unmatched sensitivity and accuracy of the technique, for example, an analyte at a concentration of one part per billion can be detected and distinguished within a chemically complex mixture,(Moyer, Budnik et al. 2003) while mass differences as little as that between a proton and an antiproton can be quantified by carefully conducted mass spectrometric studies.(Brown, Gabrielse et al. 1997)

Mass spectrometers provide researchers with information on the mass to charge ratio m/z (where m is a molecular weight in Daltons (Da), and z is a number of elementary charges; 1 Da ~ 1.6×10^{-17} Kg , 1 unit charge ~ 1.6×10^{-19} Coulombs) of analytes. From the precise mass of analytes or from the mass of their fragments, exact chemical composition can be determined. This mass information is obtained from the observed behavior of gaseous charged analyte particles in electric or combination electric and magnetic fields. Therefore, every mass spectrometer must contain at least three conceptually distinct components: a means to ionize the analyte into the gas phase (an ion source), a means to separate the ions by their m/z (a mass analyzer), and a means to detect the ions (a detector).

1.2 Ionization

The majority of functional elements within living organisms consist of macromolecules and their non-covalent complexes in the solid, liquid, or liquid crystalline state. For that reason it is imperative that ionization methods employed in biological mass spectrometry be efficient yet gentle enough for biopolymers and biologically relevant complexes to survive the vaporization and ionization events intact. Although, there is a wide variety of ionization techniques in the field, by far the most commonly used methods are electrospray ionization (ESI) (Fenn, Mann et al. 1989) and matrix-assisted laser desorption/ionization (MALDI),(Karas, Bachmann et al. 1987) the enventions of which garnered the 2002 Nobel Prize in Chemistry.
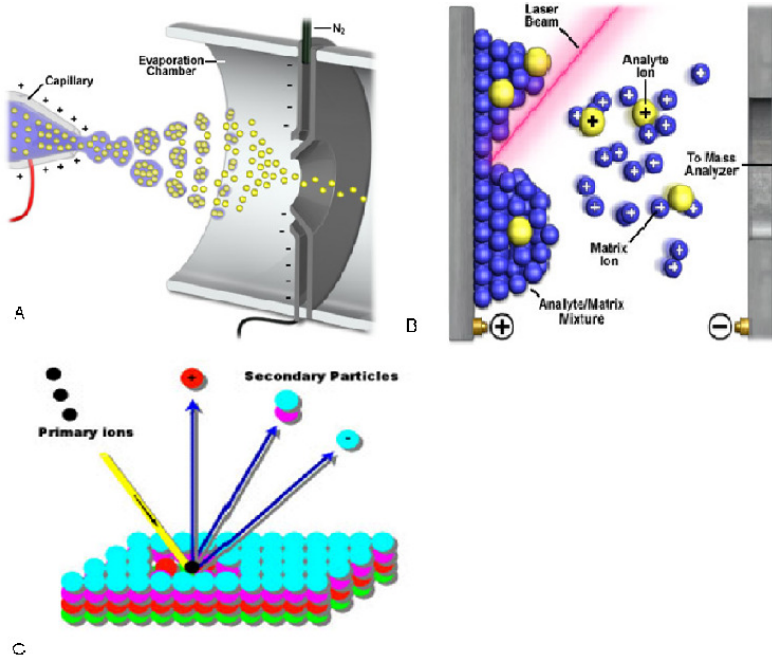
Figure 1.2 Schematics of (a) ESI, (b) MALDI, and (c) secondary ionization techniques.

In the contemporary application of the ESI technique (figure 1.2.a), analytes may be dissolved in a slightly acidic solution (to promote protonation), loaded into glass capillaries, and exposed to a steep potential drop (1-2 kV). This electric field facilitates droplet formation at the surface of the spray tip and draws these charged droplets towards the inlet of a mass spectrometer. The evaporating droplet goes through a series of decompositions, called Coulombic explosions, when repulsive Coulombic forces outweigh the surface tension at the Rayleigh limit, ultimately resulting in ions desorbing from the droplet altogether. At this point gas-phase ions are transported into the mass analyzer by means of the strong potential gradient.

The MALDI method (figure 1.2.b) was introduced by Franz Hillenkamp and Michael Karas in 1987,(Karas, Bachmann et al. 1987) who demonstrated the ability to ionize intact proteins of up to 67 KDa with this technique.(Karas and Hillenkamp 1988) In MALDI, analytes typically are co-crystallized with a matrix compound, a small aromatic organic acid, the structure of which is optimized to absorb energy at the wavelength of the laser and transfer it to the analyte. The crystalline mixture is desorbed by a laser pulse, and excitation of the matrix vaporizes both the matrix and the sample with concomitant ionization. The exact ionization mechanism is not known as of yet, and is the source of the ongoing debate whether the charge transfer taking place during the desorption event is the result of photo-ionization reaction at or right after the laser pulse, or results from evaporation (similar to ESI) of charged matrix-analyte clusters. The particular attributes of MALDI, its high sensitivity, tolerance to contaminants, and the ability for *in situ* ionization within biological tissues, make MALDI the ideal ionization

methodology for biological mass spectrometry imaging (MSI).(Caldwell and Caprioli 2005; McDonnell and Heeren 2007)

Another technique commonly employed in the context of biological MSI is secondary ionization mass spectrometry (SIMS). In the SIMS approach (figure 1.3.c) the sample in the solid state is bombarded with a focused primary ion beam, which results in ejection of secondary ions off its surface. This phenomenon was first observed by Sir Joseph John Thomson in 1910.(Thomson 1910) and the first prototype ion source was reported in 1949 by Herzog and Viehböck.(Herzog and Viehböck 1949) Even though it is one of the oldest ionization techniques in MS, SIMS has found new utility in biological MSI, as it has been demonstrated to be a powerful tool for monitoring small metabolites and pharmaceuticals in tissue samples with minimal sample preparation and superb spatial resolution of 100 nm and less.

1.3 Fourier Transform Ion Cyclotron Resonance Mass Spectrometer

1.3.1 Introduction

Once the sample is ionized, it is subjected to mass analysis. Although there are a wide variety of mass analyzers available, one in particular, the Fourier transform ion cyclotron resonance mass spectrometer (FT-ICR MS), is the undisputed leaders in terms of mass accuracy and resolution. Research, that led Alan G. Marshall and Melvin B. Comisarow to the discovery of FT-ICR MS(Comisarow and Marshall 1974; Comisarow 1985; Amster 1996; Marshall, Hendrickson et al. 1998) in the late 1960's built upon the discoveries of the cyclotron by Ernest O. Lawrence in 1920's(Lawrence and Livingston

1932) and the Penning trap (Gabrielse and Mackintosh 1984; Guan and Marshall 1995) by Hans G. Dehmelt (who named his invention after the Dutch physicist Franc M. Penning), for which both groups were awarded Nobel Prizes in Physics in 1939 and 1989, respectively.

Briefly, in FT-ICR MS charges are trapped radially in a homogeneous axial magnetic field, while they are trapped axially in a quadrupole electric field. Through the application of an RF sweep to two radially opposite plates the ions are coherently excited to their respective cyclotron orbits, where the orbiting ion clouds induce alternating image charge in the detection plates. This image charge is converted to current, amplified, sampled, and recorded, creating a so-called transient signal. The transient signal may than be Fourier transformed into a frequency domain spectrum, calibrated, and converted into a mass spectrum (figure 1.3). The non destructive nature of FT-ICR charge detection allows the ions to travel hundreds of meters or even kilometers in the course of an experiment. This long duration of observation translates into ultrahigh resolving power, generally reaching $\sim 10^6$, and mass accuracy routinely in the low to sub ppm ranges.
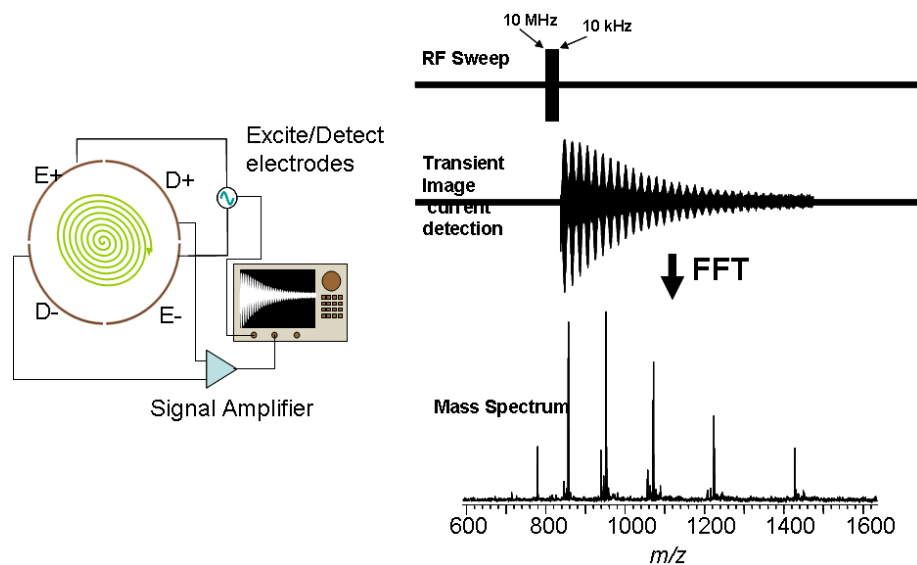
Figure 1.3 Workflow of a typical FT-ICR MS experiment

1.3.2 Charged Particle in the Magnetic Field

The fundamental principle underlying the Ion Cyclotron Resonance (ICR) phenomenon lies in the interaction between an electric charge q and a magnetic field $\mathbf{B}$. Once in the magnetic field, charged particles orbit in the plane perpendicular to the magnetic field due to the centripetal Lorentz force $\mathbf{F}$ given by

$$\mathbf{F}=q(\mathbf{v}\times\mathbf{B}) \tag{1.1}$$

where q is the charge of the particle, $\mathbf{v}$ its velocity, and $\mathbf{B}$ is the magnetic field. Rewriting the Lorentz force equation for the plane (xy) perpendicular to the magnetic field (z) results in the following equation:

$$F=qB_z v_{xy} \tag{1.2}$$

Since the general equation for a centripetal force in an *xy*-plane is

$$F = ma = m\frac{v_{xy}^2}{r} \qquad (1.3)$$

1.2 and 1.3 may be combined, taking into account that *v/r* can be substituted by angular frequency ω:

$$\omega_c = \frac{qB}{m} \qquad (1.4)$$

where ω_c is the fundamental cyclotron frequency of a particle with the charge *q* and mass *m* in the magnetic field *B*. One important observation is that the cyclotron frequency is independent of the radius of the ion's orbit, hence also independent of its velocity and the kinetic energy. I most other types of mass spectrometers (with the exception of the orbitrap (Makarov 2000; Scigelova and Makarov 2006; Makarov and Denisov 2009)) the kinetic energy spread defines ultimate mass resolution. The fact that the ICR frequency is independent from ionic kinetic energy is key to the superb resolving power of FT-ICR MS.

1.3.3 Charged Particle in the Penning Trap

In the Penning trap, while the Lorentz force prevents ions from escaping radially, they are confined axially by the electric field. The potential of this electric field ideally varies quadratically with axial position *z*, causing a harmonic oscillation of the ions in this direction with frequency ω_z(Brown and Gabrielse 1986)

$$\omega_z = \sqrt{\frac{2qV_T\alpha}{ma^2}} \tag{1.5}$$

where, V_T is the trapping potential, α is the trap geometry coefficient, and a is the distance between the trapping plates of the cell.

The addition of the potential in the z direction introduces an additional term in equation 1.1 resulting in

$$\mathbf{F}=q(\mathbf{v}\times\mathbf{B})+q\mathbf{E} \tag{1.6}$$

where $\mathbf{E}$ is the electric field. Similarly to equation 1.3, the force in the plane perpendicular to the magnetic field can be reduced to

$$F = ma = m\omega^2 r = qB\omega r - \frac{qV_T\alpha}{a^2}r \tag{1.7}$$

where r is the radial distance to the z axis. Rewriting 1.7 results in the quadratic equation

$$\omega^2 - \frac{qB\omega}{m} + \frac{qV_T\alpha}{ma^2} = 0 \tag{1.8}$$

The solution for 1.8 combined with equations 1.4 and 1.5 produces two rotational frequencies in the plane perpendicular to the magnetic field:

$$\omega_+ = \frac{\omega_c}{2} + \sqrt{\left(\frac{\omega_c}{2}\right)^2 - \frac{\omega_z^2}{2}} \tag{1.9}$$

$$\omega_- = \frac{\omega_c}{2} - \sqrt{\left(\frac{\omega_c}{2}\right)^2 - \frac{\omega_z^2}{2}} \tag{1.10}$$

These resulting frequencies, ω_+ and ω_-, are the reduced cyclotron and magnetron frequencies (figure 1.4). The reduced cyclotron frequency is very close in value to the fundamental cyclotron frequency ω_c, whereas the magnetron frequncy ω_- is closely related to the potential energy.(Brown and Gabrielse 1986) Moreover, taking into account the fact that $\omega_+ \approx \omega_c$, it follows from 1.9, 1.10, and 1.5 that

$$\omega_- = \frac{\omega_z^2}{2\omega_+} \approx \frac{\omega_z^2}{2\omega_c} = \frac{V\alpha}{a^2 B} \qquad (1.11)$$

Which clearly indicates that ion's magnetron motion is independent of m/z and, given the hyperbolic shape of the trapping potential, is always expanding.
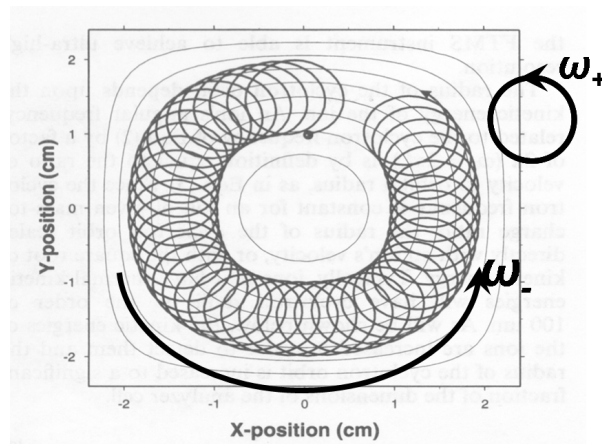
Figure 1.4 Trajectories of ions in an ICR cell in the plane perpendicular to the magnetic field, where ω_+ and ω_-, are the reduced cyclotron and magnetron frequencies.(Adapted from Amster 1996)

1.4 Mass Spectrum

As discussed previously, the image charge induced on the detection plates by the orbiting ions is converted into the alternating electrical current, amplified, digitized, and recorded. The stored transient signal is then Fourier transformed into a frequency domain spectrum. Although a number of techniques are available for conversion of the frequency spectrum into a mass spectrum,(Ledford, Rempel et al. 1984; Wang and Marshall 1988; Easterling, Mize et al. 1999; Bruce, Anderson et al. 2000; Masselon, Tolmachev et al. 2002) a graph of ion intensity as a function of m/z, they all rely on the fact that m/z value is inversely proportional to the ICR frequency.

1.4.1 Ion Intensities

As in any other spectrum, one of the most important informational components of a mass spectrum is the intensity of its peaks. Typically either the area under the peak or its height is used as a measure of it intensity. The intensities of peaks are directly related to the number of charges registered by a detector for a given m/z, however, this itself is a function of multiple parameters. First of all, the ionization efficiency ranges greatly from compound to compound. More over, ion suppression(King, Bonfiglio et al. 2000; Knochenmuss, Stortelder et al. 2000) causes ionization to vary even further, depending on the composition and complexity of the sample. Additionally, since most of the experiments are conducted with external ionization sources, nonlinearity of transmission efficiency across ion optics causes further distortion to the quantitative composition of the sample. Lastly, the detection efficiency is also known to be nonlinear across a wide enough m/z range. Therefore, it is important to note that MS peak abundances are

generally a poor measure of the relative concentrations of different analytes in the sample. Nevertheless, they are extremely useful for comparing between chemically identical analytes, such as those that differ by stable isotope composition, as is the case in isotope labeling experiments(Ong and Mann 2006) or in hydrogen-deuterium exchange studies.(Engen, Smithgall et al. 1999)

1.4.2 Mass Accuracy

The most important piece of information in a mass spectrum is the *m/z* values of the ions determined by the position of their peaks. The measure of the precision provided by an instrument is called mass accuracy and is defined in ppm's as

$$Mass\,Accuracy = \frac{(M_{Exo} - M_{Th}) \times 10^6}{M_{Th}} \qquad (1.12)$$

where, M_{Exp} and M_{Th} are the experimentally observed and the theoretical mass values respectively. Mass accuracy fundamentally depends on the type of mass analyzer, the calibration approaches, and the experimental conditions.

Currently FT-ICR MS provide by far the most accurate mass measurements of all available mass analyzers. It is impossible to overemphasize the importance of high mass accuracy in the assignment of unambiguous chemical composition. Both for small molecules,(Marshall, Hendrickson et al. 1998; Marshall 2000) or a large biopolymers,(Spengler 2004; Zubarev and Mann 2007) mass accuracy plays a vital role in compound identification. Theoretical calculations demonstrate the relationship between the mass accuracy of a protein's mass spectrum and the ability to uniquely

identify amino acid the composition of that protein,(Shen, Tolic et al. 2001) a relationship

that varies with the size of a protein and the proteome of the host organism. For instance,

1 ppm mass accuracy is sufficient for a unique identification of a 4 kDa yeast protein,

while 0.1 ppm will result in less than 40% probability of success for a match to a 1.5 kDa

C. elegans protein.

1.4.3 Resolution and Resolving power

Resolution and resolving power are also critical concepts that define the quality of

a mass spectrum. Resolution is a measure of the ability to distinguish two adjacent

peaks; it is measured in m/z and represents the spacing between two adjacent peaks.

Resolving power, on the other hand, is a unitless value defined as

$$R_p = \frac{m/z}{\Delta(m/z)_{FWHM}} \tag{1.13}$$

Note, that in FT-ICR MS, $(m/z)/\Delta(m/z) = \omega_c/\Delta\omega_c = v/\Delta v$, where v is the cyclotron

frequency in Hz. Moreover, taking into account the fact that, under the assumption of a

non-decaying transient,(Comisarow and Marshall 1976; Marshall 1979; Marshall and

Hendrickson 2001) Δv_{FWHM}, is given as

$$\Delta v = 1.2066/T \tag{1.14}$$

where T is the duration of the recorded FT-ICR signal, and that the equation 1.4 can be

rewritten in more conventional units as

$$\nu = 1.53561184 \times 10^7 \times \frac{zB}{m} \tag{1.15}$$

the resolving power can be expressed as

$$m/\Delta m = \nu/\Delta\nu = .08288\nu \times T = 1.2727 \times 10^7 \times \frac{zBT}{m} \tag{1.16}$$

This indicates that the resolving power depends on the instrumentation, namely, higher

magnetic fields result in better resolving power. And it shows that experimental

conditions that accommodate longer acquisition times and higher charge states are also

more advantageous. Finally, it is also evident from equation 1.16 that resolving power is

not uniform across the *m/z* range, being inversely proportional to *m/z* value. Since the

resolving power is closely related to mass accuracy, higher *m/z* species, therefore, result

in higher mass error rates.

1.4.4 Deleterious Effects

It is apparent from the previous discussion, that the stability of the ICR

frequencies and long acquisition times are imperative for high resolution and accurate

mass measurements. The two factors, causing the most deleterious effects on these, are

space charge and magnetron expansion.

The space charge effect is the result of coulombic interactions between and within

ion clouds in an ICR cell. Primarily, it affects the instantaneous trapping field (the third

term in equation 1.8) experienced by the ions. To account for it, equations 1.9 and 1.10

can be augmented(Jeffries, Barlow et al. 1983) to

$$\omega_{\pm} = \frac{\omega_c}{2}\left(1 \pm \sqrt{1 - 4\left(\frac{qV_TG_T}{ma^2} + \frac{q^2\rho G_i}{\varepsilon_0 m}\right)/\omega_c^2}\right) \qquad (1.17)$$

where G_T is the geometry factor of a specific ICR cell, G_i is the geometry factor of an ion

cloud, ε_0 permittivity of a vacuum, and, ρ, is the ion density. Coulombic repulsion within

ion packets cause cloud de-phasing reducing the charge density ρ. This affects both the

duration of the observable signal and the stability of the resonant frequency, causing

frequency "drift".(Bruce, Anderson et al. 1993; Guan, Wahl et al. 1993; Nikolaev,

Miluchihin et al. 1995) Furthermore, there is an interaction between the ion packet and

its image charge(Gorshkov, Marshall et al. 1993; Xiang, Grosshans et al. 1993) that is

also ρ dependant and results in an observable resonant frequency change, expressed as

$$\Delta\omega = \frac{\rho}{4\pi^2\varepsilon_0 B(r_{trap}^2 - r_{ion}^2)} \qquad (1.18)$$

where r_{trap} and r_{ion} are cylindrical cell and cyclotron motion radii, respectively. The

instabilities introduced by those phenomena increase both the peak width and the

uncertainty in peak position, hence reducing the resolving power together with mass

accuracy.

Unlike cyclotron motion, magnetron motion is associated with potential

energy(Brown and Gabrielse 1986) (the trapping potential landscape is shown in figure

1.5) and, therefore, its radius expands over time. The temporal evolution of magnetron

motion results in ion packet's exposure to increasing inhomogeneities in the trapping

field. It also creates variations in instantaneous trapping voltage experienced by the ion

packets, but unlike space charge, magnetron motion induced fluctuations are not due to varying charge density ρ, but are caused by the geometry of the trapping potentials. Additionally, the image charge induced frequency modulations will also be nonlinear because of the time variation in ion distance to the radial ICR cell walls.
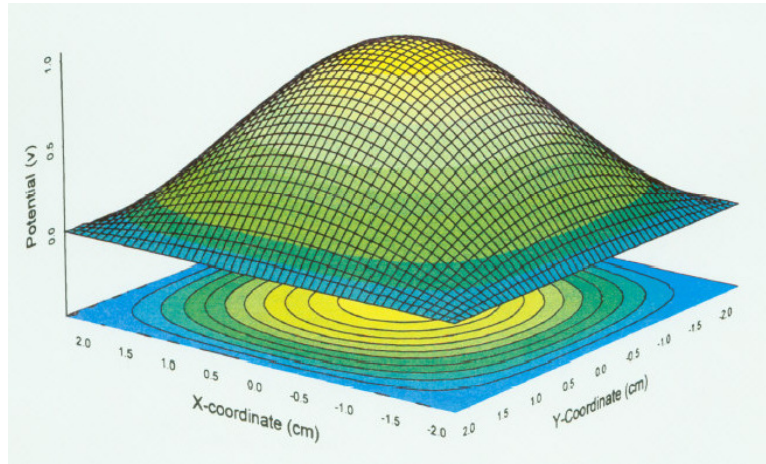
Figure 1.5 Landscape of the trapping potential in the Penning trap.(Amster 1996)

Both space charge and magnetron expansion are the main factors limiting mass accuracy and resolution; they have been identified as the main causes of the most undesirable effects in FT-ICR MS. For example, space charge is known to cause frequency drifts and peak coalescence.(Amster 1996; Marshall, Hendrickson et al. 1998) Here in this work, other deleterious effects of space charge and magnetron motion will be explored, including the hitherto unobserved isotope-beat space-charge induced frequency modulations and the phenomenon of the sudden catastrophic loss of transient signal, known as the spontaneous loss of coherence catastrophe, which has not been explained up till now. A detailed understanding of these space charge and magnetron motion-

related phenomena, such as that presented in subsequent chapters of this work, is critical

for the understanding of how these deleterious effects can be avoided or accounted for, in

order that FT-ICR mass spectra of the highest possible mass accuracy and resolution can

be obtained.

1.5 Mass Spectrometry Imaging

As mentioned previously, mass spectrometry imaging (MSI) is the technique for

identifying biologically relevant molecules simultaneous to their localization in tissues.

Recent advances in instrumentation, ionization techniques, sample preparation, and

computational methodologies have enabled mass spectrometers to be used for biological

imaging purposes.

Since the spatial distribution of biological molecules is inseparably linked to their

function, accurate chemo-spatial characterization of relevant molecules within a tissue

can provide vital biological information, information that is obscured if the architecture

of the tissue is destroyed during sample preparation. This technology has provided

indispensible insights into, for example, the biophysics(Kleinfeld, Kampf et al. 2004) of

the fatty acid transport into adipocytes, abnormalities of which are leading causes of a

variety of diseases (*e.g.* obesity, diabetes, and hypertension, among others). MSI is

becoming more commonplace in histological diagnostics and currently is extensively

used in the field of molecular pathology, investigating the molecular basis of numerous

diseases including Parkinson's,(Pierson, Norris et al. 2004) Alzheimer's,(Puglielli, Tanzi

et al. 2003; Cutler, Kelly et al. 2004; Rohner, Staab et al. 2005) muscular

dystrophy,(Touboul, Piednoel et al. 2004) obesity, and cancer.(Chaurand, Schwartz et al. 2004; Chaurand, Schwartz et al. 2004) Therefore, the applications of MSI are immense.

1.5.1 Types of Mass Spectrometry Imaging

MSI techniques may be differentiated fundamentally by the types of ionization they employ. Currently, since the most commonly used methods are MALDI and secondary ionization, this discussion will focus mostly on these imaging methodologies.
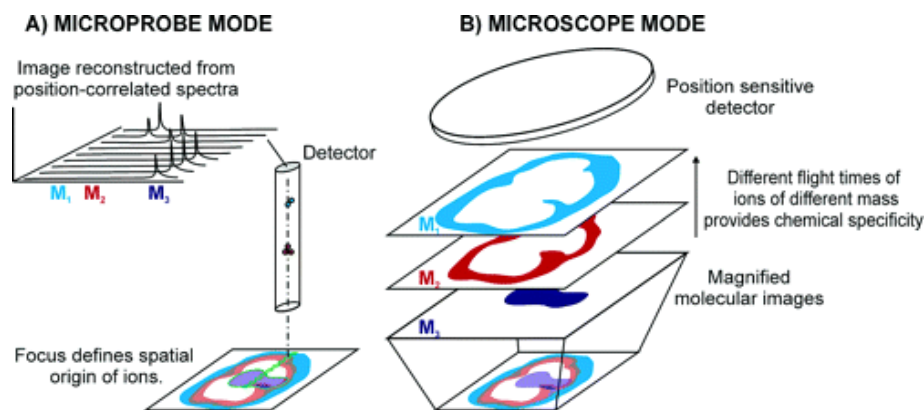
Figure 1.6 Schematics of a typical MSI experiment in either (a) microprobe, or (b) microscope modes.(McDonnell and Heeren 2007)

1.5.1.1 SIMS MSI

Secondary ionization MSI experiments, due to the nature of the ionization process employed, are exclusively conducted in the microprobe mode (figure 1.6.a), the method that consists of rastering the surface under investigation into a grid of pixels. SIMS analysis is thus conducted independently on each pixel, and the mass spectrum is stored along with its spatial information. This is repeated until all the pixels are analyzed.

Raster size in SIMS is determined by the diameter of the primary ion beam. Depending on the primary ions used, it might vary, but the typical range is 100-200nm. Smaller sizes have also been reported,(Chabala, Soni et al. 1995) but the use of these sources have results so far only in production of atomic ions, rendering them of limited use for biological MSI.

The chemical resolution, or the range of ionic species available for detection, can be varied with primary ion beam intensity. For instance, low intensity beams (10^{13} primary ion impacts per cm^2) can produce intact up to molecular ions 1 kDa. This is referred to as static SIMS, since this type of ionization causes very little damage to the surface of the tissue under investigation, or, in other words, the experiment is conducted on the *static* tissue. In contrast to static, dynamic SIMS imaging uses very high intensity beams, causing substantial molecular fragmentation, and, therefore, focuses on the analysis of smaller metabolites or their fragments.

1.5.1.2 MALDI MSI

MALDI, being a more gentle ionization method than SIMS, is typically preferred in the investigations of larger biopolymers, *i.e.* peptides, lipids, and proteins. Similar to SIMS imaging, this technique can be used in either microprobe or microscope modes (figure 1.6).

MALDI imaging in microprobe mode is conceptually the same as in SIMS except that the vaporization and ionization is achieved via a laser and matrix as opposed to an ion beam. Microscope mode (figure 1.6), in contrast, consists of ionizing the sample over

a wide area at once and preserving the spatial distribution of the ions within the ionized area until the image of these ions is read out by the detector. It requires ion-optics capable of preserving spatial distribution of ions and a detector that is position sensitive. Since FT-ICR MS is not a position sensitive detection technique, further discussion will be focused solely on microprobe MSI.

The level of raster granularity or spatial resolution is limited by the physics of MALDI. The most important factors determining spatial resolution are the diameter and the energy of the laser beam. Importantly, they are tightly interconnected variables that must be balanced between each other. The smaller the laser spot diameter, the higher the energy that is required to achieve similar levels of ionization due to higher levels of heat dissipation in tissue. On the other hand, higher laser energies lead to higher levels of undesired ion fragmentation. The compromise between the laser beam width and its intensity is typically reached at the ranges of 100-300 microns.

The spatial resolution MALDI MSI can be further improved to reach a pixel size below the width of the laser by the use of the "oversampling" technique.(Jurchen, Rubakhin et al. 2005) A typical oversampling MS imaging experiment consists of complete sample ablation at the initial position, followed by moving the sample by a fraction of the laser spot size and collecting spectra (until sample exhaustion as well), hence acquiring sub-laser-spot-size information. The trade off of this technique, however, is a reduction in the signal to noise ratio (SNR), since the amount of analyte drops proportionally to the decrease in surface area. So that a second significant tradeoff

in MSI is that the spatial resolution available is limited by the sensitivity required which often directly relates to the ion statistical abundance and accuracy needed.

The chemical resolution of MALDI MSI may be manipulated by the choice of laser and matrix used.(Zenobi and Knochenmuss 1998; Reyzer, Hsieh et al. 2003; Schwartz, Reyzer et al. 2003; Rohner, Staab et al. 2005) For example, when paired with a typical nitrogen laser (at 337nm), α-cyano-4-hydroxycinnamic acid (CHCA) provides the best ionization efficiency for smaller molecular weights. 2,5-dihydroxybenzoic acid (DHB) may be best suited for medium sizes, while sinapinic acid(SA) is more efficient for macromolecular species.

1.5.2 Challenges

1.5.2.1 On-Tissue Ionization

A number of factors make ionization *in situ* much more difficult than ionization of purified chemical species. Most importantly, the intermolecular interactions within biological tissues may be much stronger than those of homogeneous purified compounds in typical MS experiments. Additionally, only a small fraction of molecules at the very surface of the tissue are exposed to the matrix in MALDI MSI. These factors together substantially decrease amount of gaseous analyte ions liberated by the desorption event, which reduces sensitivity.

Intrinsic chemical complexity of biological tissues inevitably leads to ion suppression. This phenomenon manifests in a preferential increase in ionization

efficiency of one compound at the expense of another. Ion suppression severely distorts relative abundances of ionic species, which may lead to ambiguities in chemo-spatial images.

Another confounding factor of *in situ* MALDI analysis is analyte migration during MALDI sample preparation, which is responsible for spatial distortions in the resulting signal. Analytes on the surface of the tissue may diffuse when exposed to matrix solutions during matrix deposition. A number of methodologies may be employed to minimize this effect, a good example of which is electrospray deposition.(Kruse and Sweedler 2003)

Additionally, varying ion populations inside a mass spectrometer in the course of a MSI experiment lead to inconsistent space-charge conditions. This leads to degradation in raster-to-raster reproducibility as well as loss in spectra quality, in terms of mass accuracy and resolution. Hence, all aspects of a chemo-spatial map are adversely affected by the immense heterogeneity and complexity of biological tissues.

1.5.2.1 Instrumentation and Spatial Resolution

Aside from the physics of ionization, fundamental properties of biological tissues, and challenges in sample preparation, instrumentation is of vital importance to the ability to spatially discriminate chemical signals in tissue samples. For example, non-uniform energy distribution across an ionizing beam limits how finely a sample can be rasterized, an effect, which is especially pronounced in "oversampling" MALDI MSI experiments. Since a typically MALDI laser has a cross section with a Gaussian energy distribution

complete sample exhaustion within a given raster cannot be guaranteed without infringing on the adjacent raster. This, in turn, results in decreased image "sharpness".

Finally, an indisputably critical aspect in obtaining high quality MSI results is the ability to move and position the tissue under investigation with sufficient precision to provide the desired spatial resolution. This manifests itself in two challenges, therefore, that need to be addressed: the precision of the positioning devices and their range of motion. Unfortunately, the current state-of-the-art commercial robotics available for this purpose are subject to a general trade-off between positioning accuracy and range of motion, *i.e.* devices that excel in positioning accuracy suffer from limited range of motion and *vice versa*. For example, usually, ultra fine positioning of <50 nm is achieved by in-source vacuum-compatible stages equipped with piezoelectric motors, so called "inchworms". They operate under horizontal load with typical ranges of motion of up to 1.0 cm. This setup is most common for SIMS imaging. Contrastingly, the robotics for longer ranges, 100 mm and more, usually consist of externally mounted stepper motors transmitting the motion to the sample plate *via* vacuum feedthroughs, and can operate under either horizontal or vertical loads. The achievable positional accuracy on commercially available such devices can reach ~10 microns. Typically, these devices are installed on MALDI MS and MSI instruments

While the need for high positioning accuracy is obvious because it dictates the rasterizing ability of a given MSI technique, the requirements for the long ranges of motion for ideal sample positioning robotics come in part from the necessity to image

large tissue selections and even whole organisms.(Khatib-Shahidi, Andersson et al. 2006) Another need for robotics with large ranges of motion, which relates to the previous discussion on mass accuracy, is to introduce internal calibrants,(Mize and Amster 2000; O'Connor and Costello 2000) ionic species of known *m/z*, into the mass spectrometer in order to recalibrate mass spectra to compensate for raster-to-raster variations in spectra caused by changing space-charge conditions during MSI experiments. Identical experimental conditions experienced by the calibrant and analyte ions allow for substantial decrease in mass error through internal recalibration. Since the calibrants may be deposited in a separate location from the interrogated tissue material, the positioning device must fulfill the requirement that it sustain repeated prolonged travels without loss of positioning accuracy.

.

1.6 Summary and Statements of purpose

Mass spectrometry imaging is an exciting emerging MS methodology to characterize spatial variation of chemical signals across samples such as selected biological tissues, with great promise to facilitate biomarker discovery and molecular diagnosis, among numerous other applications. Unfortunately, obtaining high quality mass spectra in FT-ICR MSI that have the highest achievable mass accuracy and resolution is potentially confounded by space charge and magnetron motion phenomena. Furthermore, currently available sample positioning robotics technology limits the positional accuracy and range of motion of acquisition, which imposes limits on the size

and spatial resolution of the MS images that are possible with this technology. This work addresses both of these challenges by developing computational and instrumentation methodologies to achieve higher mass and spatial resolution in FT-ICR MS imaging experiments.

The first part of this work develops strategies of application of the Filter Diagonalization Method (FDM), a recently developed technique for high resolution spectral analysis to investigate of space-charge related phenomena inside the detection cell of a FT-ICR MS, in order that these phenomena be better understood and accounted for in mass spectra. The specific focus is given to:

1. **Use of the Filter Diagonalization Method in the Study of Space Charge Related Frequency Modulation in FT-ICR MS**: The Filter Diagonalization Method (FDM) is a recently developed computational technique capable of extracting resonance frequencies and amplitudes from very short transient signals. Although it requires stable resonance frequencies and is slower than the Fast Fourier Transform (FFT), FDM has a resolution and accuracy that is unmatched by the FFT or any other comparable techniques. This unique feature of FDM makes it an ideal tool for tracing space charge induced frequency modulations in Fourier Transform Ion Cyclotron Resonance (FT-ICR) cells, which are shown to reach +/-400 ppm even for such simple spectra as substance P.(Aizikov and O'Connor 2006)

2. **The Spontaneous Loss of Coherence Catastrophe in FT-ICR MS**:

The Spontaneous Loss of Coherence Catastrophe (SLCC) is a

frequently observed, yet poorly understood, space-charge related effect

in Fourier Transform Ion Cyclotron Resonance Mass Spectrometry.

The temporal frequency behavior reproduced by frequency shift

analysis using the FDM shows the complex nature of the SLCC, which

can be explained by a combination of factors occurring concurrently,

governed by electrostatics and ion packet trajectories inside the Penning

Trap.(Aizikov, Mathur et al. 2009)

The second part of this work describes the design, construction, and application of

the an ionization source and vacuum compatible high precision sample positioning

robotics for biological MSI applications, purpose built for FT-ICR MS, which has

positional accuracy and range of motion performance characteristics that far exceed

current commercially available units, thereby enabling FT-ICR MSI with more detail

than previously possible. The specific focus is given to:

1. **Vacuum Compatible Sample Positioning Device for MALDI FT-ICR**

MSI: This work discusses a two-dimensional positioning stage designed

to address these issues. The stage is capable of operating in ~1e-8 mbar

vacuum. The range of motion is set to 100x100 mm to accommodate

large samples, while the positioning accuracy is demonstrated to be less

than 0.4 micron under vertical load over the entire range. This device was integrated into three different MALDI FT-ICR instruments and showed no detectable RF noise. The "oversampling" MALDI-MSI experiments, under which the sample is completely ablated at each position, followed by the target movement of the distance smaller then the laser beam, conducted on the custom-built 7T FT-ICR MS demonstrate the stability and positional accuracy of the stage robotics which delivers high spatial resolution mass spectral images at a fraction of the laser spot diameter.

2. **MALDI FT-FT ICR Imaging: Instrumentation and Methods:** This work describes the construction and application of a new MALDI source for FT-ICR mass spectrometry imaging as a result of a collaborative effort with prof. Ron M.A. Heeren of AMOLF (Amsterdam, NL). The source includes a translational X-Y positioning stage with a $10\,cm^2$ range of motion for analysis of large sample areas, a quadrupole for mass selection and an external octopole ion trap with electrodes for the application of an axial potential gradient for ion ejection. A LC MALDI MS/MS run demonstrates the utility of the new source for data- and position-dependent experiments. A FT-ICR MS imaging experiment of a coronal rat brain section yields ~**200** unique peaks from m/z 400-1200 with corresponding mass-selected images images.

Chapter 2

Use of Filter Diagonalization Method in the Study of Space Charge Related Frequency modulations in Fourier Transform Ion Cyclotron Resonance Mass Spectrometry

2.1 Introduction

With the increasing number of completed and nearly completed genomes, research interest is shifting to proteomics,(Hoog and Mann 2004) which is the study of the structure and function of the translated proteins. Due to its high sensitivity, accuracy, and reproducibility, mass spectrometry is one of the primary technologies used in this field. One of the most important factors in identifying and sequencing proteins as well as identifying and localizing posttranslational modifications in proteins is the accuracy of the experimentally determined masses.(Clauser, Baker et al. 1999) Fourier transform mass spectrometry (FTMS)(Marshall 2000) produces the best mass accuracy and resolving power currently available.

Current FTMS instruments are capable of routinely producing measurements with ~1 ppm accuracy internally calibrated(Lorenz, Maziarz et al. 1999; O'Connor and Costello 2000; Flora, Hannis et al. 2001) and ~5 ppm externally calibrated.(Easterling, Mize et al. 1997; Hannis and Muddiman 2000) Recent studies in proteomics show that determination of amino acid composition of tryptic peptides requires at least 0.1 ppm mass accuracy.(Spengler 2004)'(Norbeck, Monroe et al. 2005) One of the major

fundamental factors determining FTMS mass accuracy limits is the "space-charge"

effect, which arises from columbic interactions among ions within the FT-ICR cell,

causing frequency shifts in time with periodicities equal to the beat frequencies of

different ion packets (note, Wineland and Dehmelt(Wineland and Dehmelt 1975)

demonstrated that ions of the same m/z do not experience the same space charge induced

frequency modulations that are observed between ions of different m/z). Due to the very

fast nature of the "space-charge" phenomena, techniques for its analysis must operate on

short transient signals. The Fast Fourier Transform (FFT),(Press, Flannery et al. 1986)

however, is limited to a resolution of $\Delta \omega = 2\pi / N\tau$, where N is the number of data

points and τ is the sampling time, and cannot generally provide detailed information on

frequency shifts within a transient.

Other FT based signal processing methods such as wavelet and chirplet(Mann and

Haykin 1992) transforms as well as the shifted-basis technique(Savitski, Ivonin et al.

2004), although having lower uncertainty, suffer from the same shortcoming of the

resolving power being directly proportional to the length of the transient. On the other

hand high-resolution techniques such as linear prediction(Loo, Krahling et al. 1990; Guan

and Marshall 1997) or Prony method based techniques(Marple 1987; Roy, Sumpter et al.

1991) are very computationally expensive.

The Filter Diagonalization Method (FDM)(Wall and Neuhauser 1995; Wall and

Neuhauser 1995; Mandelshtam and Taylor 1997; Hu, Van et al. 1998; Mandelshtam and

Taylor 1998; Hu, De Angelis et al. 2000; Mandelshtam 2001; Mandelshtam 2003) is a

recently developed signal-processing algorithm based on a linear algebra mathematical

formalism, which finds the exact solution of the harmonic inversion problem(Mandelshtam and Taylor 1998) and, theoretically, can achieve infinite resolution if the resonant frequencies are stable. FDM has been shown to provide superb accuracy on short transient signals, and, compared to other high-resolution computational techniques, is very quick (e.g. FDM's time complexity scales quasi linearly with the number of data points, which puts it in the same order as the FFT). These two factors make it an ideal tool for frequency shift chasing experiments as shown here. These results could be used for reference deconvolution(Bruce, Anderson et al. 1993; Guan, Wahl et al. 1993) to improve mass accuracy.

2.2 Theory

Although detailed description is available in the literature,(Wall and Neuhauser 1995; Wall and Neuhauser 1995; Mandelshtam and Taylor 1997; Hu, Van et al. 1998; Mandelshtam and Taylor 1998; Mandelshtam 2001; Mandelshtam 2003) a brief description of FDM's main features, structure, and functionality compiled from the above references is provided since it is new in the field of FTMS. The main objective of FDM is to interpolate complex amplitudes d_k's and complex frequencies ω_k's from a time signal $C(t_n)$

$$C(t_n) = c_n \equiv \sum_{k=1}^{K} d_k e^{-in\tau\omega_k}, \tag{1}$$

which is defined on an equidistant time grid $t_n = n\tau$, n=0,1,…,N-1 with complex

frequencies $\omega_k = 2\pi f_k - i\gamma_k$ (including damping γ_k), where N is the number of data

points, τ is the time step, and f_k is the frequency in Hz. Even though the fitting problem

of Eq. (1) is highly nonlinear, the solution can be obtained by pure linear algebra if one

assumes Lorentzian line shape and uniform sampling rate.

The unique feature of FDM is the association of C_n with a time correlation

function of a hypothetical quantum system described by a complex symmetric

Hamiltonian operator $\hat{\Omega}$ with complex eigenvalues ω_k and the initial state Φ_0

$$c_n = (\Phi_0 \,|\, e^{-in\tau\hat{\Omega}}\Phi_0),\tag{2}$$

which redefines the problem of fitting the observed time signal C_n to Eq. (1) as one of

diagonalizing $\hat{\Omega}$ or, equivalently, its evolution operator $\hat{U}$ over a single step, where

$\hat{U} = e^{-i\tau\hat{\Omega}}$. Furthermore if Y_k is a set of orthonormal eigenvectors which

diagonalizes $\hat{U}$, then

$$\hat{U} = e^{-i\tau\hat{\Omega}} = \sum_k e^{-i\tau\omega_k} |Y_k)(Y_k|\tag{3}$$

and from Eq. (1), (2) and (3) corresponding abundance values, d_k, can be calculated as

$$d_k = (\Phi_0 \,|\, Y_k)(Y_k \,|\, \Phi_0) = (Y_k \,|\, \Phi_0)^2\tag{4}$$

Although neither $\hat{\Omega}$ nor $\hat{U}$ are explicitly available, their matrix elements in an appropriately chosen basis can be reconstructed from the observed time signal. For instance, $\hat{U}$ can be reconstructed using Krylov type finite-time Fourier (Mandelshtam and Taylor 1997) basis described by

$$\Psi_j = \Psi(z_j) = \sum_{n=0}^{M} (\hat{U}/z_j)^n \Phi_0, \qquad (5)$$

where $z_j = e^{-i\varphi_j}, \varphi_j = \omega_j \tau, \varphi_{min}/\tau < \omega_k < \varphi_{max}/\tau, j = 1,2,...,K_{win}$, and the matrix elements (note, the basis is not orthonormal) can be obtained from

$$U^{(p)}(\varphi_j, \varphi_{j'}) = U^{(p)}[j, j'] = (\Psi_j | \hat{U}^p \Psi_{j'}) = \sum_{n=0}^{M} \sum_{n'=0}^{M} (z_{j'}/z_j)^n c_{n+n'+p} z_{j'}^{-(n+n')}, \qquad (6)$$

where $p = 0,1,2\ldots$, and M is the one half of the transient length. Now, the fitting problem of Eq. (1) is recast into generalized eigenvalue problem

$$U^{(1)} B_k = u_k U^{(0)} B_k, \qquad (7)$$

where $u_k = e^{-i\tau\omega_k}$ are eigenvalues and B_k are eigenvectors of the system, note that B_k are normalized with respect to $U^{(0)}$, and the intensities d_k can be recovered(Mandelshtam and Taylor 1997; Hu, Van et al. 1998) as

$$\sqrt{d_k} = \sum_{j=1}^{K_{win}} B_{jk} \sum_{n=0}^{M} c_n e^{in\varphi_j} \qquad (8)$$

By using a rectangular window Fourier basis Eq. (6), and moving into the frequency domain where interaction between adjacent points is small and the matrices are diagonally dominant with the richest informational content along the main diagonal(Hu,

Van et al. 1998) the computational effort for solving the generalized eigenvalue problem

Eq. (7) becomes much smaller. More importantly, the size of the matrices, $K_{win,}$ can be

relatively small, in practice ranging from 3 to 100.(Hu, Van et al. 1998) These two

factors let us achieve quasi-linear computational complexity, which is comparable to that

of FFT. However, construction of the $\hat{U}$ matrices imposes a large constant prefactor so

that while FDM scales well, it is slower than the FFT.

One of the major advantages of FDM over FFT is its resolution. The Fast Fourier

Transform is limited in peak width to $\Delta\omega = 2\pi / N\tau$. In theory FDM can have infinite

resolution. In practice, infinite resolution is achievable only if the local average density

of peaks $\rho(\omega)$ satisfies

$$\rho(\omega) \equiv 2\pi / \delta\omega \leq N\tau / 2, \tag{9}$$

where $\delta\omega$ is the spacing between the adjacent peaks.(Mandelshtam 2001)

While FDM has a resolution advantage which is reported in this manuscript, it

also has some disadvantages compared to FFT. Specifically, the local nature of the basis

can generate spurious values or "false" solutions to Eq. (7). These spurious values, while

annoying, can be purged. There are a number of ways to get rid of them(Wall and

Neuhauser 1995; Wall and Neuhauser 1995) but the most simple and efficient one is

solving Eq. (7) for overlapping K_{win}'s and dropping out those solutions which appear

only once.(Wall and Neuhauser 1995; Wall and Neuhauser 1995) Furthermore, due to

the fact that it is not an approximation technique and solves Eq. (1) exactly, FDM

experiences substantial difficulties in cases when the frequencies are not stable, for example under "space-charge" conditions.

2.3 Methods

In this study an in-house C++ implementation of the FFT square window FDM was used, which is integrated into the Boston University Data Analysis (BUDA) system(O'Connor P 2002) and is available as open source software. The constructions of the matrices described by Eq. (11) and (12) were implemented following the method described by Hu et al.(Hu, Van et al. 1998) To make the calculations faster, the FFTW implementation of the FFT(Matteo Frigo and Johnson 2005) was used in place of the discrete FT as described in the above reference. Use of the FFT limited the granularity of the $\Delta\omega$, or to be more precise the spacing between adjacent frequencies φ_j in Eq. (6), to $2\pi/N\tau$ and consequently increased the minimal length of the transient signals necessary to provide the same accuracy (for the spectra used, the transient length of 1 millisecond or 1K data points generally satisfied the criteria for selected peaks). Modified CLAPAC code(Anderson, Bai et al. 1999) was used for solving the generalized eigenvalue problem.

For testing the FDM implementation, theoretical spectra were generated in-house with 1 mega-point lengths and 1 MHz sampling rate based on isotopic abundances calculated using IsoPro 3.0.(Senko; Yergey 1983) The conversion from m/z to frequency domain was done according to the calibration equation $f = \frac{z}{m}A - B$, where $A = $ 107079830.92 and $B = $ -0.69 which differ slightly from the values used in the calibration

of the experimental spectra, this caused a slight difference in frequency domain between the two. Real spectra of Substance P were acquired on a homebuilt ESI FTMS instrument(Pittman, Thomson et al. 2004) (1 mega-point length with 1 MHz acquisition rate). Frequency chasing experiments were performed on transient domains ranging from 1000 to 20000 data points starting with the 0 offset and shifting depending on the experiment from 1 to 200 data points into transient. K_{win} ranged from 4-11 points.
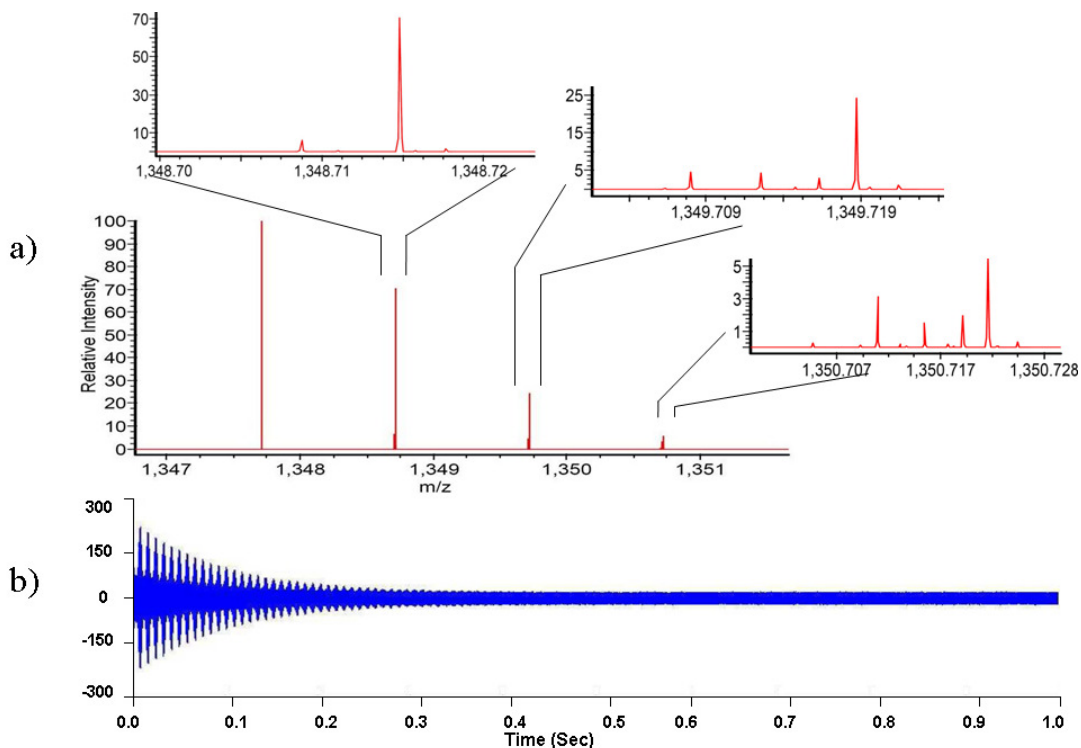
Figure 2.1 a) Theoretical Mass spectrum of Substance P using isotopic abundances calculated by IsoPro 3.0 (*m/z* vs. Relative Intensity) and b) the corresponding transient signal of 1 second (1M data points) duration sampled at 1MHz rate with the damping constant of 10. The signal was generated using stable frequencies.

2.4 Results and Discussion

In order to test the fundamental capabilities of FDM, theoretical spectra were generated

where the exact signal composition was defined *a priori* with an absence of frequency

shift modulation. A theoretical transient signal (Figure 2.1) of length 1 second (1 M data

points) with sampling rate of 1 MHz and damping of 10 s^{-1} was generated using

frequencies and abundances from Supplementary Table, calculated from the known

elemental composition of substance P using IsoPro 3.0.(Senko; Yergey 1983) In

particular, the fine structures of the A+1, A+2, and A+3 isotopes were included. (The A

ion at 1347.712, being the monoisotopic peak, has no fine structure). Performance

studies of the two methods were conducted on the first 1, 0.5, 0.25, 0.1, 0.01, and 0.001

seconds of the transient (Figure 2.2). Note that while the FFT generates a spectrum and

then peak centroids must be calculated from it by non-linear least squares fitting, FDM

first generates a line list by solving Eq. (7) and (8) and Figure 2.2 (right) is generated

subsequently by applying a sum of lorentzian line shapes to the data in Table 2.1. Figure

2.2 clearly shows that the FFT fails to resolve the fine structure of the spectrum

(producing only the major peaks) even at 1M points (1.0 s.) with 80000 resolving power

(Figure 2.1a) and fails to resolve even the main isotopic peaks when the first 0.01 s

(Figure 2.2e) of the signal is used. In contrast, FDM produces all the peaks from

Supplementary Table at 0.25 s and some peak merging takes place as the signal is

shortened beyond the limit imposed by Eq. (13) for these peaks. FDM, however, still

produces a bona fide isotopic distribution with reasonably good abundance ratios even

when the transient length is only 1 ms (Table 2.1.e). This aspect of FDM algorithm could

be particularly useful for mass spectrometry of short lived radionuclides.(Stolzenberg, Audi et al. 1990)

In general the peak merging is a result of the violation of inequality Eq. (13). These merged peaks can be thought of as poorly resolved peaks.(Mandelshtam 2001) The merging is accompanied by increase in error (Table 2.1), or the difference between the peaks recovered by the overlapping K_{win}. This error serves as an uncertainty measure and has been used to filter out the spurious peaks.(Wall and Neuhauser) Note that, even with a 1 ms transient, the monoisotopic peak at 158906.79 Hz is resolved almost exactly with an error of $\sim 7*10^{-4}$ ppm. In general, as long as condition Eq. (13) holds the FDM is capable of achieving "infinite" resolution,[20] with errors only due to noise and inherent computational round off errors.
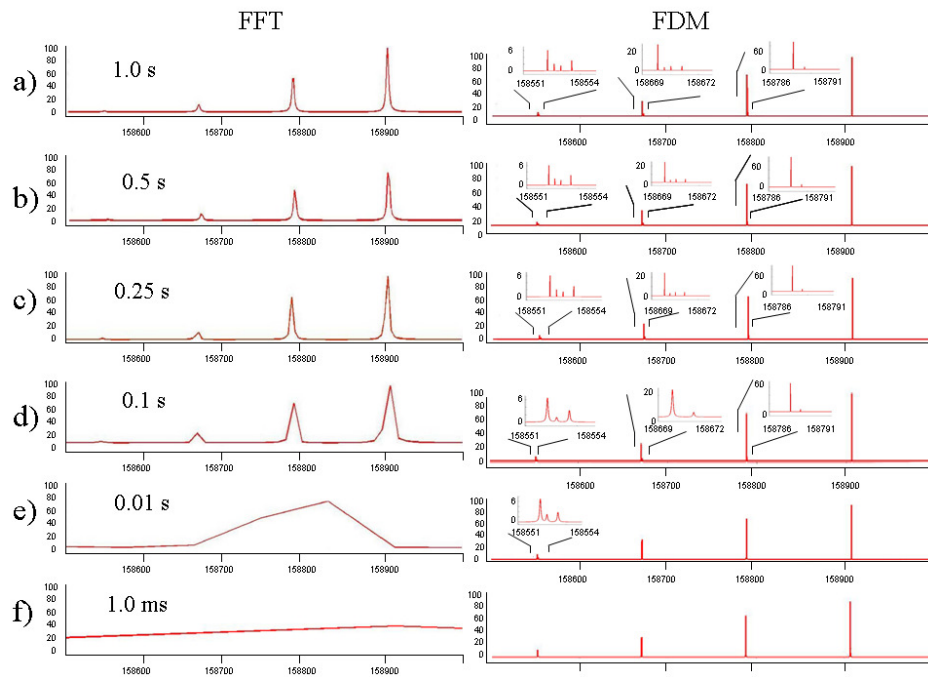
Figure 2.2 Frequency spectrum recovered from the first a) 1M, b) 0.5 M, c) 0.25M, d) 0.1M, e) 0.01M, and f) 1000 data points of the transient signal in Figure 2.1b using the

FFT (left) and using the FDM (right). The FDM "spectrum" is constructed from a Lorentzian fit to the peak list from Table 2.1.

a)

Frequency	Intensity %	Err (ppm)
158906.79730	100	0.00E+00
158789.32990	5.99999792	4.41E-07
158788.50580	69.9999968	0.00E+00
158671.80090	4.00000051	-8.82E-07
158671.21309	4.00014895	4.37E-05
158670.86039	2.99979559	5.20E-05
158670.50770	25.0000252	-1.58E-06
158553.91744	2.66580469	3.74E-04
158553.33059	1.5001432	4.37E-05
158552.97840	1.99991672	1.26E-05
158552.62630	5.99995247	6.94E-07
Standard diviation		1.10E-04

b)

Frequency	Intensity %	Err (ppm)
158906.79730	99.99999	0.00E+00
158789.32990	6.000238	1.89E-06
158788.50580	70.00086	6.31E-08
158671.80090	3.999848	-1.44E-05
158671.21294	4.005262	1.04E-03
158670.85986	2.997183	3.43E-03
158670.50769	24.99762	6.57E-05
158553.91750	3.000049	2.60E-05
158553.33052	1.500441	5.31E-04
158552.97842	1.999132	-1.54E-04
158552.62630	5.992714	-2.87E-05
Standard diviation		1.05E-03

c)

Frequency	Intensity	Err (ppm)
158906.79730	99.99997	0.00E+00
158789.32990	6.01434	4.09E-06
158788.50580	69.98557	-3.78E-07
158671.80087	4.00325	1.81E-04
158671.21081	4.04751	1.44E-02
158670.85443	2.98175	3.76E-02
158670.50759	24.97024	7.04E-04
158553.91819	2.98400	-4.37E-03
158553.33971	1.43732	-5.74E-02
158552.98745	2.05093	-5.71E-02
158552.62775	6.08859	-9.17E-03
Standard deviation		2.79E-02

d)

Frequency	Intensity	Err (ppm)
158906.79730	100.00000	0.00E+00
158789.32990	6.00000	-1.89E-07
158788.50580	70.00000	0.00E+00
158671.77770	4.48080	1.46E-01
158671.21310	N.A	0.00E+00
158670.86040	N.A	0.00E+00
158670.50952	25.47574	-1.15E-02
158553.91067	3.12141	4.31E-02
158553.17399	1.24473	9.88E-01
158552.97840	N.A	0.00E+00
158552.63673	6.50813	-6.58E-02
Standard deviation		2.99E-01

e)

Frequency	Intensity	Err (ppm)
158906.79730	100.00000	6.29E-07
158789.32990	N.A	0.00E+00
158788.53934	74.63911	-2.11E-01
158671.80090	N.A	0.00E+00
158671.21310	N.A	0.00E+00
158670.86040	N.A	0.00E+00
158670.75691	36.23842	-1.57E+00
158553.86888	3.75961	3.07E-01
158553.16842	2.87426	1.02E+00
158552.97840	N.A	0.00E+00
158552.74257	8.94472	-7.33E-01
Standard deviation		6.37E-01

f)

Frequency	Intensity	Err (ppm)
158906.79719	99.99497	7.12E-04
158789.32990	N.A	0.00E+00
158788.56981	75.14601	-4.03E-01
158671.80090	N.A	0.00E+00
158671.21310	N.A	0.00E+00
158670.86040	N.A	0.00E+00
158670.75387	36.16970	-1.55E+00
158553.91750	N.A	0.00E+00
158553.33060	N.A	0.00E+00
158552.97840	N.A	0.00E+00
158553.07004	12.50209	-2.80E+00
Standard deviation		9.14E-01

Table 2.1 Frequencies and abundances recovered by FDM from the first a) 1M, b) 0.5 M, c) 0.25M, d) 0.1M, e) 0.01M, and f) 1000 data points of the transient signal in Figure 2.1b. Errors correspond to the difference between the calculated and FDM recovered frequencies. "N.A." indicates that FDM could not resolve the frequencies within allowed error (10 ppm).

Although FDM performance in terms of accuracy on signals with no frequency modulation is by far superior to that of FFT, FDM, whose main assumption is that the resonant states are stable, does not perform that well when frequency shifts are substantial. Thus it generally fails to provide better mass accuracy when used in place of FFT on real FTMS signals. However, the ability to lock in on frequencies in extremely short transients (as seen in previous example, Figure 2.2) implies that FDM is a good tool for studying frequency shifts during FTMS experiments. To test the performance of

FDM in following shifts through a transient, a theoretical signal of 0.5 s length was generated, where 140080.1276 Hz frequency was modulated through 0.0005 Hz (3.6 ppb) with a frequency of 10 Hz (Figure 2.3), and sampled at 1 MHz with signal to noise ratio of 2 in the time domain. The frequency chasing experiment was performed with 0.5 millisecond (500 data points) transient domains stepping 200 data points into the raw data. While the signal to noise ratio of 2 in the theoretical signal, input to the FDM algorithm, clearly resulted in some noise in the output, the FDM was able to create an output signal which reproduced the frequency vs. time plot from Figure 2.3a with sub ppb accuracy. Note, that FDM also generated several spurious glitches, which were discussed above.
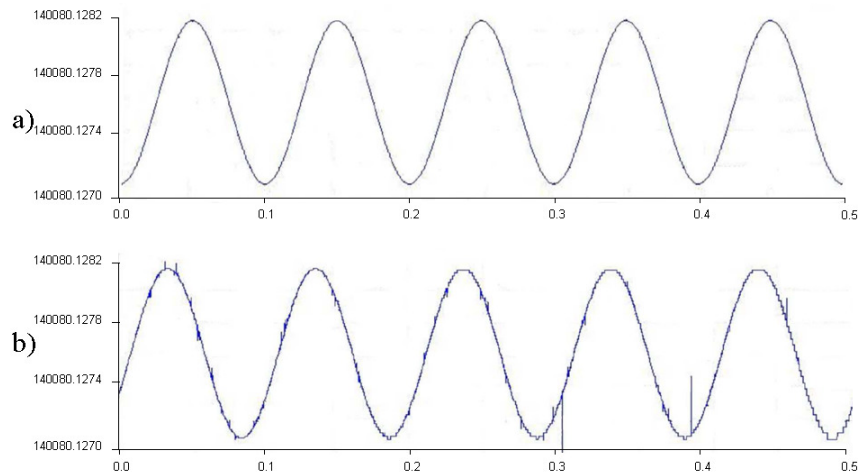
Figure 2.3 a) a theoretical signal of 140080.1276 Hz, 0.5 S long modulated over .0005 Hz with frequency 10Hz, sampled at 1 MHz. b) FDM output for the chasing experiment at signal to noise ratio of 2. The experiment was conducted on 500 data point transient domains stepping 200 data points into transient.
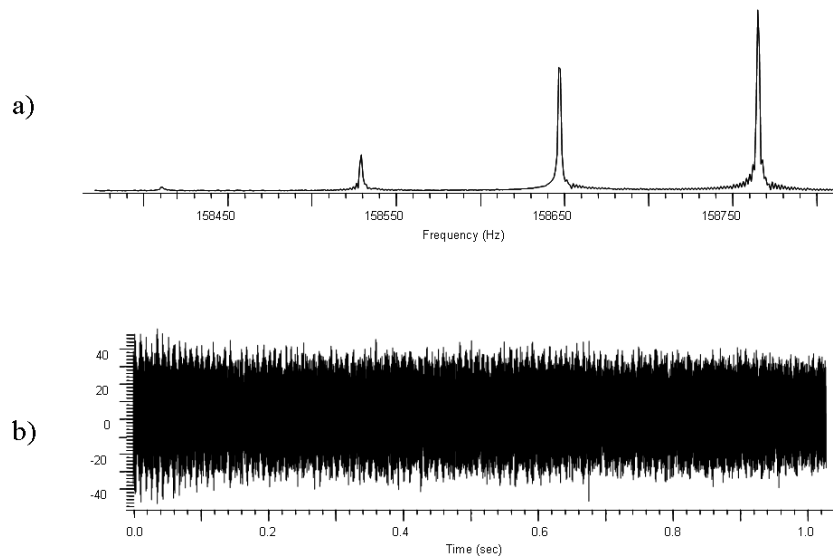
Figure 2.4 a) frequency spectrum and b) transient signal of a Substance P spectrum used for "real world" frequency chasing calculations.

The same frequency chasing experiments were conducted on a real substance P spectrum (Figure 2.4) chasing the three major isotopic peaks using 20 millisecond transient domains (20000 data points) stepping 200 data points into the transient for each FDM calculation through the first 0.5 S of the transient. This calculation produced the frequency shift plots in Figure 2.5 for the A+2, A+1, and A ion peaks of the isotopic distribution respectively. While there are some FDM spurious glitches in the frequency shift plots, the isotopic peaks are clearly modulated at several different, but superimposed, frequencies. For example, all three spectra show a negative frequency dip at ~ 0.13 s and another at ~0.28 s. Additionally, there appears to be a more rapid modulation every ~0.02 seconds. However, these frequency shift plots are rather chaotic.
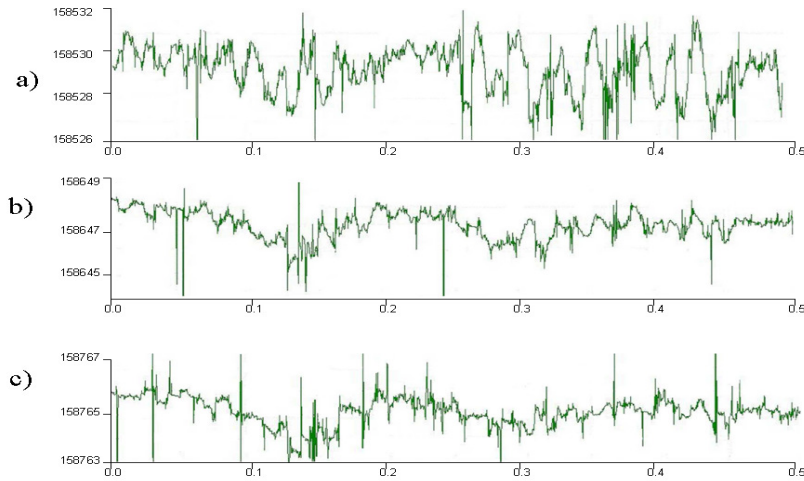
Figure 2.5 Frequency shift plots (20 ms, 0.2 μs shifts) of the first 0.5 seconds of the Substance-P spectrum (Figure 2.4) of the a) 158530 Hz, b) 158647 Hz, and c) 158765 Hz peaks
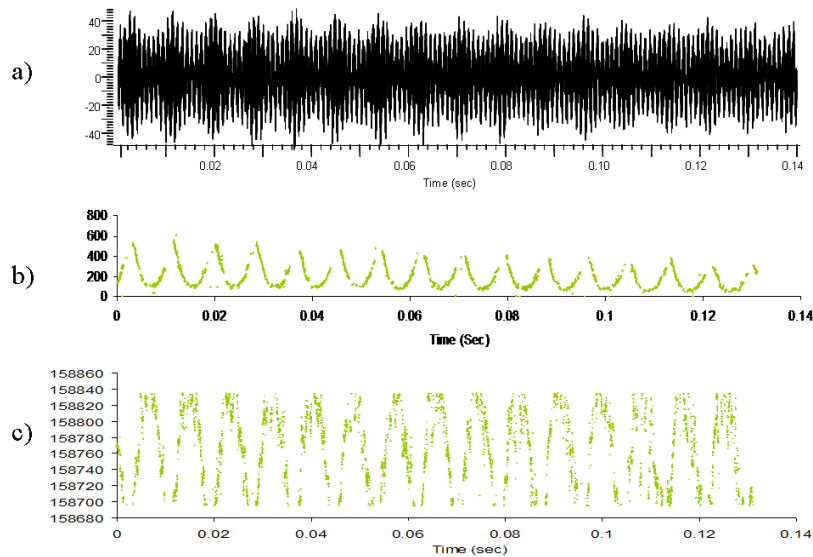
Figure 2.6 The frequency chasing experiment conducted on a) the first 0.13 seconds of the Substance-P spectrum (Figure 2.4), chasing 158647 Hz peak using a 1K data point (1 millisecond) transient domain stepping 1 data point (1 microsecond) into the transient. b) intensity vs. time plot. c) frequency shift plot.

Since the monoisotopic peak at 158760 Hz has no fine structure and satisfies the

Equation (9) on very short transients (1000 data points), a detailed frequency chasing

experiment was expected to show a simpler and cleaner structure. Thus, a frequency

chasing experiment was performed on this peak using 1 ms (1000 data points) stepping 1 μs (1 data point) into the transient for the first 0.13 s of the transient. The isotopic beat pattern is faithfully reproduced in both abundance (Figure 2.6b) and frequency shifts (Figure 2.6c). These frequency shifts occur every 0.01 s (122.07 Hz) which corresponds well with the $\Delta\omega$ between the first two isotopic peaks. Thus these frequency shifts are clearly due to the "beating" frequency of the isotopes. Interestingly, the magnitude of this frequency shift is approximately +/- 75 Hz, which corresponds to +/- 400 ppm at ~158 kHz. However, even though the ions are shifting in frequency by +/- 400 ppm during the transient, the FFT is still able to achieve 1-2 ppm mass accuracy on this spectrum. Thus, the FFT effectively averages out these cyclic frequency shifts to achieve its results.

The level of accuracy and detail produced by these frequency shift chasing experiments depends directly on the transient signal lengths. For instance the frequency chasing experiment in Figure 2.5 does not show as much modulation as Figure 2.6 in spite of being carried out on the same experimental data set, due to the averaging effect. When 20 ms, or, equivalently, 20000 data points were used, the transient signal length was extended over more than one "beat" (Figure 2.6a) causing the averaging out of the intra "beat" frequency modulations. On the other hand, by shortening of the signal in the frequency chasing experiments, depending on the choice of a peak, reliability of the results might suffer as was discussed above.

In terms of computational performance, although FDM has the same time complexity as the FFT it is much slower due to the computational cost of construction of

the U matrices. Moreover, frequency chasing experiments scale to $(NlogN)^2$ time

complexity making these studies quite expensive. On average, a typical frequency

chasing experiment, depending on the length of the transient and other parameters, takes

10 – 20 minutes on a Pentium IV 3.6 GHz system with 1 GB RAM running Windows$^{®}$

XP. However, the fact that FDM is highly parallelizable makes it easy to implement it on

parallel computer architecture, which will tremendously improve FDM's performance

and speed for frequency chasing experiments.

2.5 Conclusions

FDM is a signal processing technique, which although slower than FFT, provides

better accuracy. Computation speed and the fact that FDM requires stable resonance

states (i.e. no frequency shifts) makes it a poor choice as a direct alternative to FFT in the

analysis of FTMS data, which are dominated by space charge frequency shifts. In a

simple substance P spectrum, these frequency shifts are shown to reach 400 ppm. On the

other hand, the improved accuracy of FDM on short transients makes it an ideal tool for

frequency chasing experiments, which give a unique insight into space charge effects and

provide frequency shift functions, which potentially can be used in reference

deconvolution. Another area where high resolution on short transient signals might prove

useful is with LC-FTMS hybrid instruments which attempt to operate on sub-second

transients and with accurate mass measurements of short-lived radionuclides.

Chapter 3

The Spontaneous Loss of Coherence Catastrophe in Fourier Transform Ion Cyclotron Resonance Mass Spectrometry

3.1 Introduction

Since the introduction of the soft ionization methods(Karas, Bachmann et al. 1987; Tanaka, Waki et al. 1988; Fenn, Mann et al. 1989) mass spectrometry has been steadily gaining prominence, and is currently one of the most important experimental techniques in the biosciences. It is impossible to imagine contemporary proteomics, genomics, or glycobiology without mass spectrometric analytical methods. There is an increasing number of different types of mass spectrometers and hybrid instruments being developed and deployed every year starting from simple quadrupole(Paul 1990) instruments up to hybrid Fourier Transform Mass Spectrometers (FTMS).(Senko, Hendrickson et al. 1997; Mikhail E. Belov, Harold R. Udseth et al. 2004; Jebanathirajah, Pittman et al. 2005; O'Connor, Pittman et al. 2006)

In general, requirements for higher mass accuracy and resolving power of the contemporary mass spectrometers are becoming more and more pronounced.(Zubarev and Mann 2007) As studies have shown,(Spengler 2004; Norbeck, Monroe et al. 2005) proteomic experiments require sub-ppm mass accuracy for unique determination of peptide amino acid composition. Currently FTMS(Comisarow and Marshall 1974; Marshall 2000) instruments are established leaders in mass accuracy and resolving

power, capable of achieving ~1 ppm accuracy internally calibrated(Lorenz, Maziarz et al. 1999; O'Connor and Costello 2000; Flora, Hannis et al. 2001; Belov, Zhang et al. 2003) and ~5 ppm externally calibrated(Easterling, Mize et al. 1997; Hannis and Muddiman 2000) under normal conditions, yet routine measurements in the sub 0.1 ppm region have not yet been reported in the literature. It is a substantial challenge for instrumentation, theorists, and experimental scientists to break through this 100 ppb "barrier".

The major contributor to mass error in FTMS is space-charge – a phenomenon rising from the columbic interaction between and within ion clouds in the Ion Cyclotron Resonance (ICR) cells. Frequency shifts due to space-charge were reported to be greater than +/- 400 ppm within an isotopic beat,(Aizikov and O'Connor 2006) which affects both position and width of the peaks although these periodic shifts tend to mostly average out over a long transient. Substantial effort has been invested and there have been attempts previously made to study it *in situe*,(Guan, Wahl et al. 1993; Nikolaev, Miluchihin et al. 1995) yet the phenomenon remains poorly studied due to its rather fast nature, which requires frequency shift analysis on very short segments of transient signals. Most of the widely used signal processing techniques are not applicable to the task. For Fourier Transform (FT) based techniques such as the FFT,(Cooley and Tukey 1965) wavelet and chirplet transforms,(Mann and Haykin 1992) and the shifted basis technique(Savitski, Ivonin et al. 2004) the limiting factor is the FT uncertainty principle.(Smith 2003) For such high-resolution techniques as linear prediction(Farrar, Elling et al. 1992; Guan and Marshall 1997) and Prony method based techniques,(Marple

1987; Roy, Sumpter et al. 1991) the limiting factors are the time complexity of the calculations and poor tolerance for noise which generates false positives (hence rendering these techniques impractical for experimental data).

The Filter Diagonalization Method (FDM)(Neuhauser 1990; Neuhauser 1994; Wall and Neuhauser 1995; Mandelshtam and Taylor 1997; Hu, Van et al. 1998; Mandelshtam, Taylor et al. 1998; Chen and Mandelshtam 2000; Mandelshtam 2001; Mandelshtam 2003) is a recent addition(Aizikov and O'Connor 2006) to the repertoire of computational techniques in mass spectrometry which addresses these issues. Like the FFT, it finds a solution for the generic harmonic inversion problem(Mandelshtam and Taylor 1998; Mandelshtam, Taylor et al. 1998) (HIP) Eq. (1)

$$C(t_n) = c_n \equiv \sum_{k=1}^{K} d_k e^{-in\tau\omega_k},$$ (1)

where d_k's and ω_k's are complex amplitudes and complex frequencies respectively, and $C(t_n)$ is a time signal defined on an equidistant time grid $t_n = n\tau$, $n=0,1,\dots,N-1$, where N is the number of data points, τ is the time step, and complex frequencies $\omega_k = 2\pi f_k - i\gamma_k$ include damping γ_k.

Because FDM's resolution depends not on the length of the transient signal, but rather on the local peak density(Mandelshtam 2001) it bypasses the FT uncertainty principle(Neuhauser 1994) and is thus capable of operating on very short transients. Even 1000 data points (1 ms with a 1 MHz acquisition rate) can provide sufficient information for the FDM to produce resolution defined only by the damping constant γ_k (Eq.1) in frequency, and consequently, in mass domains,(Aizikov and O'Connor 2006) while having the similar time complexity in computation to the FFT. It is reliable under

noisy conditions,(Chen and Mandelshtam 2000) and, it reproduces complete information

about a peak, namely position, amplitude, width, decay parameter, and phase. All of

these factors make it an ideal technique for studying rapid space-charge induced

frequency modulations in FTMS.
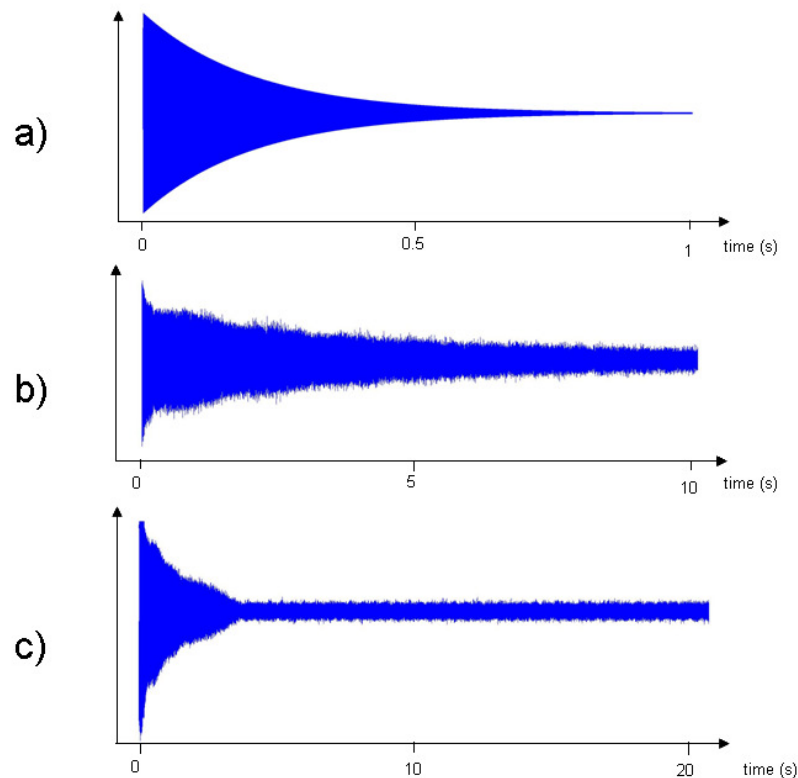
Figure 3.1 Examples of the transient signals: a) hypothetical exponentially decaying sinusoidal signal; b) transient of a high resolution substance-P spectrum; c) an example of SLCC where a period of exponential decay is followed by a rapid non-correlated decay.

This manuscript presents application of the FDM to the study of a space-charge

related frequency behavior of ion clouds in ICR called the Spontaneous Loss of

Coherence Catastrophe (SLCC), colloquially known as the "nipple effect". Unlike the

theoretical behavior of a transient signal that decays exponentially (figure 3.1a) or that

acquired under near ideal conditions (figure 3.1b), during the SLCC, a transient starts off with exponential decay, but at some point, which can be somewhat controlled by changing the number of ions in the cell, the transient collapses and dies out rather quickly (figure 3.1c) forming a nipple-like shape. This is a space-charge related phenomenon which directly depends on the number of charges in the ICR cell, an observation which was also reproduced by computer simulations.(Nikolaev, Heeren et al. 2007) When the number of charges is relatively low, the nipple effect is not observed in the experimental lifetime (figure 3.1b). On the other hand, it is easy to reproduce this particular behavior (figure 3.1c) by overloading the cell. Understanding of the ion cloud's behavior during the SLCC should give insight into its behavior under high space-charge conditions in general, which potentially can be used in modeling, deconvolution, and data reduction in FTMS, improving mass accuracy and resolution.

3.2 Methods

The experiments were conducted on custom MALDI-FTICRMS(Pittman, Thomson et al. 2004) and ESI –qQq-FTICRMS(Jebanathirajah, Pittman et al. 2005; O'Connor, Pittman et al. 2006) instruments, both based on 7 T actively shielded Cryomagnetics magnets, and equipped with capacitively coupled cylindrical cell(Beu and Laude 1992) with additional external trapping plates. All the experiments were conducted in the positive ion mode. The ions were trapped with +15V during the excite event, but the potential was lowered to +1V during detection. The MALDI instrument is equipped with 355 nm Nd:YAG laser, a novel modular data system,(Mize, Taban et al. 2004) a low noise amplifier,(Mathur, Knepper et al. 2007) and a 16 bit ADC, with ion

optics consisting of a pair of hexapoles driven by RF oscillators(O'Connor, Costello et al. 2002; Mathur and O'Connor 2006) and separated by a thin gate valve.(Pittman and O'Connor 2005) The analytes and matrices used in the experiments, substance P (MW 1347), renin substrate (MW 1759), Angiotensinogen (1-13) (MW 1645.9), Caesium Iodide, 2,5-dihydroxy benzoic acid (DHB), and sinapinic acid (SA) were purchased from Sigma Chemical Co. (St. Louis, MO).

For all the MALDI experiments DHB and SA were dissolved in methanol:acetonitrile:water (2:2:1) to make saturated solutions. For each sample, 0.5 uL of the 100 pM/mL standard aqueous solution was applied on a target on top of the matrix crystals using the dried droplet method.(Kussmann, Nordhoff et al. 1997) The acquisition rate was set at 1 MHz, and up to 4 second transients were stored.

Electrospray solutions of substance-p were prepared in 49:49:2 methanol:water:formic acid solvents and that of Cesium Iodide in 70:30 water:methanol. The isolation of the species of interest was done in Q1. The ions were axially cooled by pulsing Nitrogen gas twice (2 ms pulse, 2 mbar backing pressure, pulsing to $1.4*10^{-5}$ mbar in the cell) into the cell during a two minute cool down period after ion injection into the cell and prior to the excitation event. Substance-p 25 second transients were acquired in heterodyne mode at 10 kHz sampling rate and those of Cesium Iodide at 4 MHz (direct detection mode) using IonSpec electronics.

The ESI-FTICRMS(Jebanathirajah, Pittman et al. 2005; O'Connor, Pittman et al. 2006) used in this study is a hybrid instrument with a triple quad front end, consisting of mass resolving quadrupole, ion accumulation and collision cell linear trap, and a

transmission quadrupole coupled with a set of ion guide hexapoles via the thin gate valve.(Pittman and O'Connor 2005) The instrument is equipped with the electron gun for ECD (Zubarev, Kelleher et al. 1998; Zubarev, Kruger et al. 1999; Leymarie, Costello et al. 2003; Adamson and Hakansson 2007) experiments, which was used in all the Electron Promoted Ion Coherence (EPIC)(Kaiser and Bruce 2005; Kaiser and Bruce 2007; Kaiser, Weisbrod et al. 2008) experiments. The electron beam was turned on during the detection event only. The current on the electron gun heater was set at 1.2 A, 4.7 V , and the voltage on the reflector was set at -1.0 V to propel electrons into the cell, while kept at +7.0 V otherwise.

Data analysis was performed on the latest release of the Boston University Data Analysis (BUDA)(O'Connor P 2002) system (soon to be available online). All frequency chasing experiments were performed using an FFTW(Matteo Frigo and Johnson 2005)-based, in-house C++ implementation of the FFT square window FDM(Aizikov and O'Connor 2006) integrated into BUDA.

In order to produce the frequency behavior picture, frequency shift calculations(Aizikov and O'Connor 2006) were conducted on the acquired spectra. For the Angiotensinogen transients the monoisotopic peak at ~65 kHz was monitored. The parameters for FDM used were: K_{win} of 7, 5 milliseconds (5000 data points) of the time domain window, stepping 5 microseconds (5 data points) into the transient. For the frequency shift analysis of the Cesium Iodide (Cs_1I_2+) 272.7 kHz peak was studied, with K_{win} of 5, 0.75 milliseconds (3000 data points) of the time domain window, stepping 1 microsecond (4 data points) into the transient.
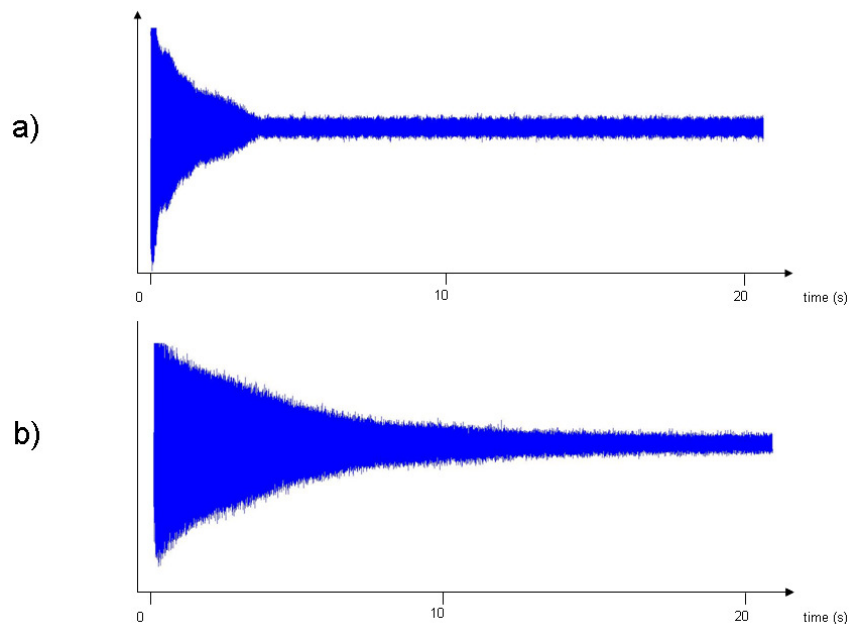
Figure 3.2 An illustration of an effect EPIC has on SLCC: a) a SLCC during substance-P signal acquisition; b) complete elimination of SLCC by applying EPIC (all other experimental parameters are kept the same).

3.3 Results

An illustration of different time domain signals is presented in figure 3.1. A transient of a hypothetical exponentially decaying harmonic signal is shown in figure 3.1a. Figure 3.1b shows that of a nearly ideally shaped experimental transient of Substance-P, and 1c is an example of the SLCC transient of Substance-P with its characteristic concave shape.

The application of EPIC can eliminate the SLCC altogether. Figure 3.2a shows the example of the nipple effect in the course of ESI-FTICRMS experiment. By turning the electron beam on during the detection, yet keeping all the other experimental

conditions the same, it was possible to achieve a nearly ideal exponentially decaying

signal (fig. 3.2b), which looks almost identical to that in figure 3.1a.
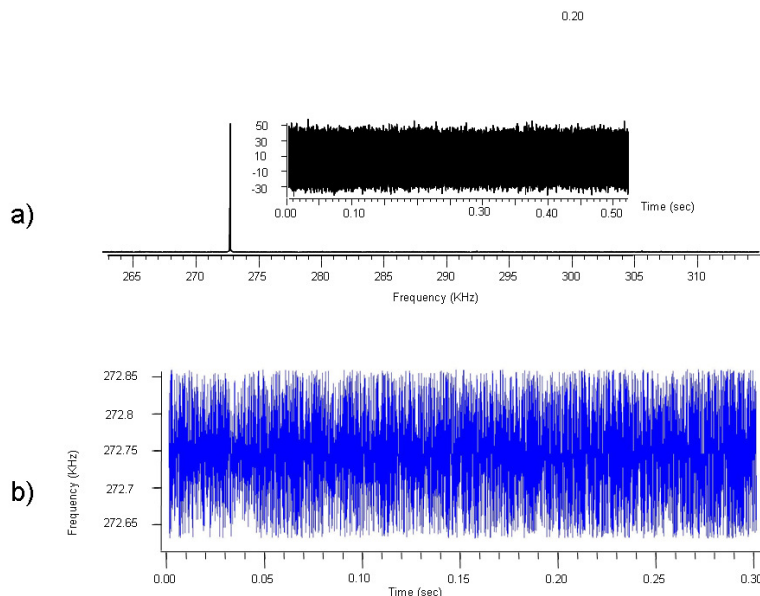
Figure 3.3 a) A frequency domain spectrum and the transient of an isolated Cesium
Iodide cluster and b) the frequency shift modulation calculations of the ICR peak at
272.75 kHz.

Figure 3.3a shows the ESI-FTICR frequency spectrum of an isolated Cs_2I_1+

cluster and its time domain signal (see the insert). An FDM frequency shift calculation is

shown in figure 3.3b. In order to detect periodic frequency modulations, the FFT was

performed on the frequency shift calculation results. Figure 3.4 presents Fourier

transforms of the frequency shift calculations conducted on the Cesium Iodide signals

without (fig. 3.4a) and with (fig. 3.4b) electron beam on. There are two general regions

in the frequency domain where modulations were stable and systematic. The major peak

is at double that of axial frequency (the factor of two is due to the cell's symmetry in Z

direction), which should be in the vicinity of 700 Hz.(Marshall, Hendrickson et al. 1998)

The minor peak is centered at the native ICR frequency in the standard Cs_2I_1+ spectrum, but is conspicuously absent in the Cs_2I_1+ EPIC signal.
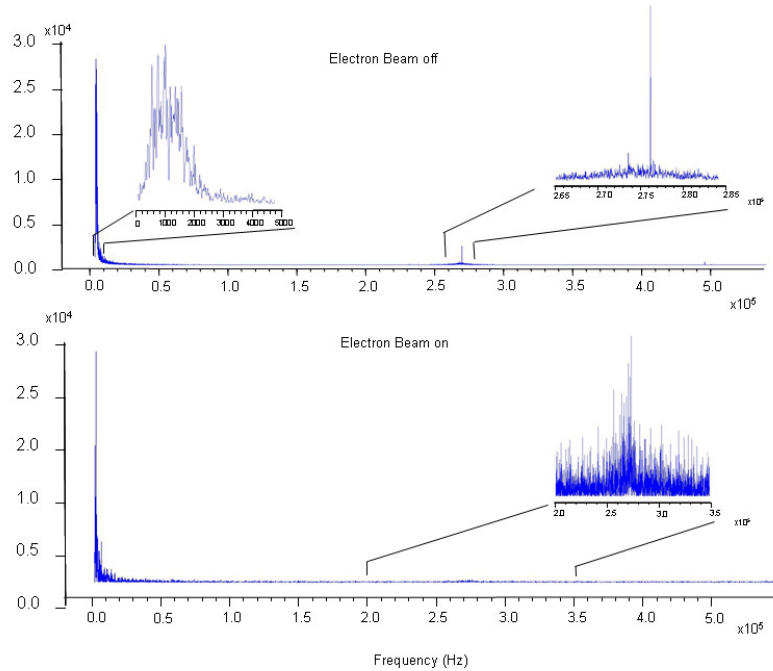
Figure 3.4 A Fourier Transform of the frequency shift calculations (see fig. 3.3b) conducted on the Cesium Iodide signals acquired without (a) and with (b) application of EPIC.

Frequency shift analysis calculations using FDM of the SLCC Angiotensinogen signals (figure 3.5a) are shown in figure 3.5 reproduce the evolution of the amplitude (I, II) and frequency (III) parameters of the induced harmonic signal (damping constant and phase are also produced by FDM but are omitted due to the clutter produced by isotopic beat pattern(Hofstadler, Bruce et al. 1994; Easterling, Amster et al. 1999) and noise). The temporal behavior of the amplitude, d_k from equation 1 follows exactly the outline of the transient signal in pre- as well as post-nipple stages).
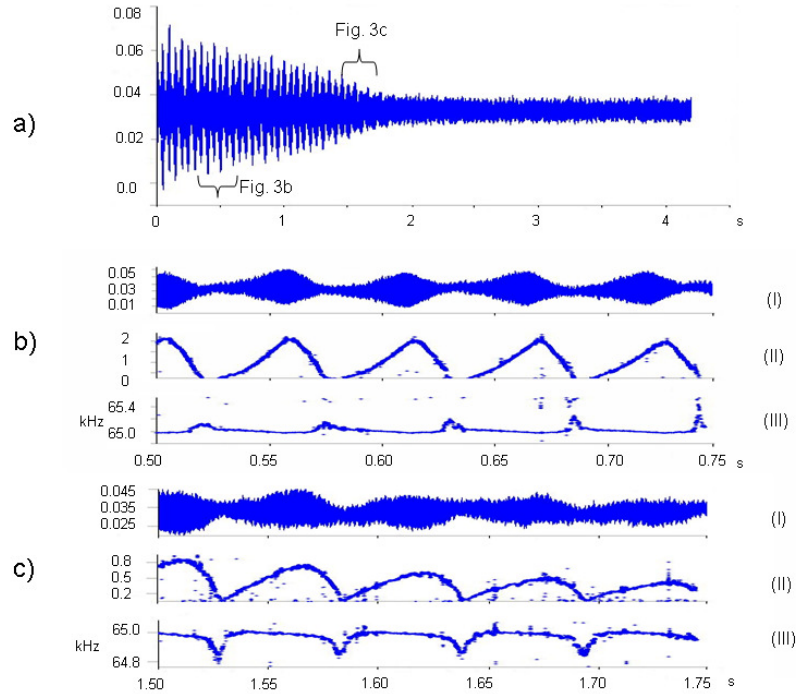
Figure 3.5 The results of the frequency shift calculations conducted on (a) the experimental SLCC of angiotensinogen. (I) is the magnification of the region of the time domain transient signal under investigation, (II) its amplitude d_k, and (III) frequency f_k temporal behaviors calculated using FDM.

The frequency behavior of the ions (Figure 3.5b, c: III) through the SLCC has several signature features. Initially, frequency spikes are observed, which correspond in time with minima in the time domain transient isotopic beat pattern. These frequency spikes increase in magnitude with time (figure 3.5b III), whereas the baseline stays relatively constant. Later, during the SLCC, these spikes "flip" becoming negative dips (figure 3.5c III). The dips also coincide with the amplitude minima. This behavior is consistent and a second set of data is available in the supplementary materials.

Figure 3.6a presents a simple plot of the inhomogeneities of the electric field inside the ICR cell experienced by a coherently excited ion cloud. As long as the

contributions of magnetron and axial motions are small (orbit I), an ion packet does not experience much deviation from the largely hyperbolic electric field as it progresses through its cyclotron orbit. On the other hand, when both magnetron and ion axial contributions become significant (illustrated *in extremis* in orbit II), ion packets travel through highly inhomogeneous regions of the ICR cell. Figure 3.6b presents a schematic representation of an ion packet being temporarily positioned in the center of the cell as a result of superimposition of the cyclotron and magnetron motions (see the discussion below).

3.4 Discussion

Kaiser et *al.*, who pioneered EPIC, showed that application of the technique, substantially increases the lifetime of the ICR experiment.(Kaiser and Bruce 2005) These experiments were reproduced on SLCC spectra (fig. 3.2.a) demonstrating that the alteration to the electric field within the cell caused by the electron beam can not only prolong the duration of the signal, but eliminate the nipple effect all together (fig. 3.2.b). In order to analyze its effects on the temporal behavior of the ICR frequency and to minimize all other space-charge related frequency perturbations (except for "self space-charge" of the ions of the same m/z),(Wineland and Dehmelt 1975; Wong and Amster 2007) as was described in the methods and results sections, a single Cesium Iodide cluster (fig. 3.3.a) was isolated for ICR experiments under normal and EPIC conditions. The resulting signals were subjected to the FDM frequency shift calculations (fig. 3.3.b) followed by Fourier Transform in order to find stable harmonic modulations.

The major difference between the two modulation spectra is a much larger peak at the native ICR frequency (fig. 3.4.a) under non-EPIC conditions – a clear indication that the center of the cyclotron orbit is substantially off-center in the XY-plane (a non-zero magnetron component), and the modulations are due to the radial inhomogeneity of the trapping field within its diameter. A virtual elimination of this peak in figure 3.4.b suggests that EPIC shifts the center of the cyclotron orbit back to the center of the cell greatly reducing magnetron motion, which strongly supports earlier findings.(Kaiser and Bruce 2007)

This evidence of the relationship between magnetron motion and the nipple effect will be instrumental in investigation of another tell-tale observation – temporal frequency fluctuations within an isotopic envelope going through the SLCC. An isotopic beat pattern(Hofstadler, Bruce et al. 1994; Easterling, Amster et al. 1999) in the observed ICR signal is not simply a result of superimposition of multiple sinusoids. Had it been, the observed frequencies would not vary in time. It has been shown previously(Aizikov and O'Connor 2006) and can be observed in the pre-nipple stage of the experiments (figure 3.5b) that frequencies "spike" up at the points when the amplitude of the transient is the smallest. This phenomenon can be described as a straight forward manifestation of the fundamentals of the classical principles of ion motion(Brown and Gabrielse 1986) in a Penning trap(Penning 1936) including the space-charge correction:(Jeffries, Barlow et al. 1983)

$$\omega_{\pm} = \frac{\omega_c}{2}\left(1 \pm \sqrt{1 - 4(\frac{2qV_0G_T}{dm} + \frac{q^2\rho G_i}{\varepsilon_0 m}) / \omega_c^2}\right) \tag{2}$$

$$\omega_c = \frac{qB}{m} \tag{3}$$

$$\omega_+ = \omega_c' \tag{4}$$

$$\omega_- = \omega_m \tag{5}$$

where $\omega_c, \omega_m, \omega_c'$ are fundamental cyclotron, magnetron, and reduced cyclotron frequencies, q is the charge, B magnetic field, V_0 trapping potential, m particle's mass, d is the distance between the trapping plates, G_T is the geometry factor of a specific ICR cell, G_i is the geometry factor of an ion cloud, ε_0 permittivity of a vacuum, and, ρ, is the ion density.

Under the high space-charge conditions, when the ion density ρ is maximum, the space-charge correction term in Eq. 2 is maximized and the observed frequency $\omega_c' = \omega_+$ is minimized. These conditions occur when the ion packets of different isotopes are in-phase (the beats of the beat pattern) therefore the minima of the frequency beat pattern in the pre-nipple part of the transient of the experimental SLCC (figure 3.5b) coincide with amplitude maxima. On the other hand, when the packets are in anti-phase, the space-charge effect is minimized and the ω_c' is the largest, which explains the frequency spikes at the amplitude minima.

A steady increase in the magnitude of frequency "spikes" is the manifestation of the positive frequency "drift".(Bruce, Anderson et al. 1993) This behavior can be explained by the isotope beat pattern (ion clouds coming into phase with each other) which scatters and dephases the ion packets reducing ion density. Furthermore, image charge,(Gorshkov, Marshall et al. 1993; Xiang, Grosshans et al. 1993) being oppositely charged, is reflected as attraction of the ions to the ICR cell walls, which slows down the cyclotron motion. Consequently, the detected frequency is reduced by $\Delta\omega$ according to

$$\omega_{eff} = \omega_c - \omega_m - \Delta\omega = \omega_c - \omega_m - \frac{\rho}{4\pi^2 \varepsilon_0 B(r_{trap}^2 - r_{ion}^2)}, \tag{6}$$

where r_{trap} and r_{ion} are cylindrical cell and cyclotron motion radii respectively. Over time, dephasing and expansion of the ion clouds decreases ρ (more rapidly under high space-charge conditions); therefore the detected average frequency shows positive drift.

On the other hand, a simple electrostatics explanation for the nipple and post-nipple behavior fails at the SLCC. For instance, rapid negative frequency shifts ("dips")

(figure 3.2c) corresponding to the "out-of-phase" ion position (abundance minima) violate equation 2 if one neglects consideration of the magnetron/cyclotron orbital geometries. More over, neither loss of ions, nor the spreading of the ion clouds can explain the deviation from the exponential decay in the time domain data and beating in the frequency domain post-SLCC.

As was previously mentioned, a simple columbic explanation of the post-nipple frequency behavior fails. Indeed, initially the ions are tightly bundled into a packet, and the frequency minima corresponds to the isotopic ion packets coming into phase. At such a point, as discussed above, the space-charge is maximum, which causes the observed frequency to minimize (figure 3.5b). The reverse happens later on (figure 3.5c) in the course of the SLCC, when the frequency minimizes ("dips") at the minimum of the amplitude. If frequency minima corresponds to the positions of the highest ion density, and since amplitude corresponds to net ion cloud distance from the cell detection plates, then the *maximum* space-charge condition must be occurring with the *center* of mass of the ion cloud at the center of the cell.

This seeming contradiction disappears in the light of evidence of substantial magnetron expansion obtained in the EPIC experiments. Indeed, since the transient amplitude minima correspond to the center of masses being in the center of the ICR cell (or rather, the furthest away from the detection plates, hence minimum signal intensities), the only feasible explanation to the observed (figure 3.5) post-nipple "dips" is a shift in the ion trajectories. As the magnetron trajectory expands and its radius becomes sufficiently large, ions, when in phase, find themselves periodically positioned (without

loss of momentum) very close the center of the cell as a consequence of the superposition

of the cyclotron and magnetron motions as schematically shown in the figure 3.6.b.
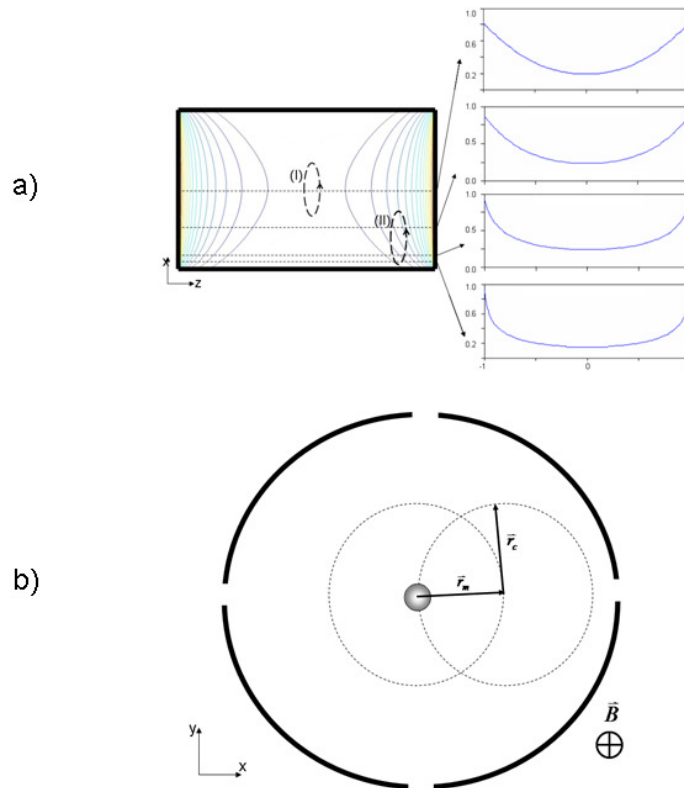
Figure 3.6 a) An illustration of the inhomogeneities in the electric field experienced by a trapped ion packet in a closed, cylindrical ICR cell. When the ions follow the cyclotron orbit close to the middle of the cell (trajectory I), they are subjected to nearly hyperbolic electric potential. As the z and magnetron components start to contribute ions travel through highly inhomogeneous electric field (for example, trajectory II), which perturbs the motion further increasing the magnetron component. The orbits are not drawn to scale. b) A schematic representation of the ions being temporally positioned in the center of the cell as consequence of the superimposition the cyclotron and magnetron orbits. The figure is not drawn to scale.

Thus, the SLCC can be explained by uncorrelated magnetron expansion.

Magnetron motion in a Penning trap always expands(Brown and Gabrielse 1986;

Hendrickson, Hofstadler et al. 1993) under normal conditions. Moreover, the magnetron

expansion rate tends to increase as the magnetron orbit increases due to the increased

gradient in the potential hill.(Honovich 1990) Indeed, in the center of the ICR cell, the trapping potential is nearly hyperbolic, but closer to the edges it squares off (figure 3.6a). So, as ion packets move away from the center of the cell along the magnetron orbit, they are exposed to increasingly inhomogeneous electric fields in both axial and cyclotron motions (figure 3.6a (I)). While some of the ions will experience substantial magnetron expansion, collide with the ICR cell walls, and be neutralized, *all* ions will experience rapid fluctuations in their instantaneous electric fields over their axial and cyclotron oscillations before collision with the cell wall becomes a possibility. These fluctuations in electric field will modulate ω_c' (from equations 2, 3) as well as the axial frequency which will contribute strongly to the dephasing of the ion cloud. In other words, space- and image-charge induced (diocotron) drift shifts ions into the regions of the ICR cell where electric field inhomogeneities cause dephasing, and the rate of expansion governs the SLCC position in time which is itself governed by ion density (equation 6).

It is too early to talk about a computational model for this phenomenon, or an all encompassing formalism capable of quantitative prediction now. Nevertheless, a more thorough investigation focused on analysis of the role excitation radius, ion population, as well as global and local space charge might play in formation of a nipple should give us more understanding of SLCC.

3.5 Summary and Conclusion

This work presented an application of the Filter Diagonalization Method (FDM) in the study of the space-charge in the form of the Spontaneous Loss of Coherence Catastrophe (SLCC). Due to its high resolution on short transients and tolerance to noise,

the FDM made possible detailed frequency chasing experiments, which provide some insight into ion cloud behavior in the ICR cell. The temporal frequency and abundance behavior thus revealed the cause of such a mysterious phenomenon as the SLCC. Specifically, the fact that frequency spikes are observed pre-SLCC that correlate with amplitude minima agrees with the known observation that frequency increases are correlated with low space-charge conditions. The fact that this correlation flips over at the SLCC suggests that the isotope ion packets are temporarily coming back into phase (high space-charge) at the amplitude minima, which is only possible if the magnetron orbit diameter is similar to that of cyclotron motion. This claim is supported by the EPIC experiments, which show that the SLCC is observed only when there is a strong magnetron component. Thus, the SLCC occurs when 1) the image charge drift, the space-charge related scattering, and scattering of ions off neutral molecules result in substantial magnetron expansion, which moves the ion clouds radially into the regions of the cell with large electric field inhomogeneities and 2) when the magnetron orbit expands to approximately the same diameter as the cyclotron orbit diameter.

These findings yet again reinforce the need for reduction of magnetron drift and space-charge induced frequency modulation when pursuing the higher mass accuracy and resolving power capabilities of the FTMS. A number of experimental techniques and cell designs have been proposed in the literature to deal with this issue.(Gabrielse and Mackintosh 1984; Pan, Ridge et al. 1988; Guan and Marshall 1995; Vartanian and Laude 1995; Gillig, Bluhm et al. 1996; Jackson, White et al. 1999; Bruce, Anderson et al. 2000; Heeren, McDonnell et al. 2006; Brustkern, Rempel et al. 2008; Tolmachev, Robinson et

al. 2008; Weisbrod, Kaiser et al. 2008) Clearly EPIC(Kaiser and Bruce 2005; Kaiser and Bruce 2007; Kaiser, Weisbrod et al. 2008) has proven to be a good countermeasure for magnetron expansion and a capable tool to counteract image charge drift and stabilize the transient. Quadrupolar axialization methods should also be revisited.(Savard, Becker et al. 1991; Schweikhard, Guan et al. 1992; Bruce, Anderson et al. 1993; Speir, Gorman et al. 1993; Hasse, Becker et al. 1994; Bruce, Vanorden et al. 1995; Hendrickson, Drader et al. 1995; Hendrickson and Laude Jr. 1995; Pastor, Castoro et al. 1995; O'Connor, Speir et al. 1996) This area of research remains active and such combined methods should help address these issues.

Chapter 4

Vacuum Compatible Sample Positioning Device for MALDI Fourier Transform Ion Cyclotron Resonance Mass Spectrometry Imaging

4.1 Introduction

Major developments in experimental techniques, instrumentation, and software have facilitated the use of mass spectrometers for biological imaging(Caldwell and Caprioli 2005; McDonnell and Heeren 2007) applications. Mass spectrometry imaging (MSI) allows the investigation of the spatial distribution of the molecular compositions within and across selected tissues as well as on the whole organism scale.(Khatib-Shahidi, Andersson et al. 2006) The data produced by application of this technique in the studies of such diseases as Alzheimer's,(Rohner, Staab et al. 2005) caner,(Chaurand, Schwartz et al. 2004) muscular dystrophy,(Touboul, Piednoel et al. 2004) and Parkinson's(Touboul, Piednoel et al. 2004) provides medical community with a qualitatively deeper understanding of the nature of these maladies, while the ability of *in situ* study of the distribution of pharmaceuticals(Hsieh, Chen et al. 2007) promises a significant accelerate in developments of remedies.

Two frequently used desorption and ionization methods for imaging MS are MALDI and Secondary Ion Mass Spectrometry (SIMS), although Desorption Electrospray Ionization (DESI) has recently been employed for imaging experiments as

well.(Wiseman, Ifa et al. 2006) Matrix Assisted Laser Desorption/Ionization (MALDI)(Karas, Bachmann et al. 1987; Tanaka, Waki et al. 1988) mass spectrometry is predominantly extensively utilized in biological applications. Compared to electrospray (ESI)(Fenn, Mann et al. 1989) ionization mass spectrometry, this method has some advantages: specifically lower sensitivity to contaminants, lower detection limits, and the ability to store samples and analyze them minutes (or days) later. Compared to MALDI, SIMS is suitable for studying elements and small molecules usually not exceeding 500 Da, while providing spatial resolution on a sub-micron level.

While MALDI offers an unmatched molecular resolution and range (capable of ionizing whole macromolecules and their non-covalent complexes) its spatial resolution is limited by the laser spot diameter. Even though modification of the laser optics(Caprioli, Farmer et al. 1997; Garden and Sweedler 2000; Spengler and Hubert 2002; Reyzer, Hsieh et al. 2003; Sherrod, Castellana et al. 2007) and such experimental techniques as sample exhaustion(Jurchen, Rubakhin et al. 2005) are capable of producing much smaller "pixels" the typical limit is >50 μm.

All of these methods generate hundreds of sample spots (whether it be a MALDI target spot or a "pixel" in an imaging experiment) which must be analyzed in the mass spectrometer. Such a sample load requires automation. A typical automated source involves a 2D translation stage which positions the MALDI target plates or tissue under ionization beam's focal points. The laser (for MALDI experiments) or a primary ion beam (for SIMS) ionizes the analytes, which are directed into the mass spectrometer's ion optics for analysis. In general, commercial 2D translation stages have a number of

problems associated with operation in vacuum. First, most of the stages (even some sold as "vacuum compatible" at exorbitant prices), are not vacuum compatible in that they are designed with numerous virtual leaks, and use motors and surfaces that must be kept lubricated, albeit quite often with non-vacuum compatible lubricants. Second, the motors and other electrical components are not designed with sufficient heat sinking capability and often overheat and seize or burn out. Third, the feedthroughs these stages required are often inadequate in terms of the RF interference shielding, and the motors and feedback electronics themselves often generate substantial RF noise. Lastly, many instruments are designed horizontally, which requires the sample positioning stage to be mounted vertically and places different stresses on the vertical versus the horizontal positioning motors, loads, and feedback systems.

This article describes and discusses a two-dimensional, vacuum compatible sample positioning stage specifically designed to address these issues. The stage was designed as a vacuum compatible device to operates at pressure around1e-8 mbar. While it's not exactly designed for operation at lower pressures, minor modifications would allow it. Positioning accuracy, RF interference noise, and vacuum compatibility as well as the results from MSI experiments will be discussed.

4.2 Methods

Savinase (synthetic serine protease subtilisin 309) was digested with trypsin and CNBr and 5 μL was separated on a LC Packings nanoLC-system ((Dionex), Amsterdam, NL) with a C_{18} PepMap 100 pre-column (internal diameter 300 um, length 1 mm) and a C_{18} PepMap 100 analytical column (internal diameter 75 um, length 15 cm). The eluents

were 0.1% formic acid and 5% acetonitrile in water (A) and 0.1% formic acid and 5% water in acetonitrile (B). The LC method used a gradient of 20 minutes 0-70% B, followed by a 1 minute gradient of 70-95% B and 10 minutes of 95% B and 12 minutes of 5% B for a total run time of 50 minutes. The capillary was coupled to a SymBiot I sample workstation (Applied Biosystems, Foster City, CA, USA) and the effluent was spotted on a premade MALDI foil (LabConnections, Northborough, MA, USA) in 30 s intervals at a spacing of 1 mm in a 10 x 10 matrix. A 20 minute delay time between the start of the LC method and the start of the spot deposition was used. The foil was coated with a 10 mg/mL solution (60:40 ACN/H_2O (0.2% TFA)) of α-cyano-4-hydroxycinnamic acid with an ImagePrep matrix deposition device (Bruker Daltonics, Billerica, MA, USA) after spotting. Protein identifications were made by a Mascot database search (www.matrixscience.com).

10 μm thick rat brain sections (Harlan Laboratories, Boxmeer, The Netherlands) were prepared at -2O°C in a HM 525 cryomicrotome (Microm International, Walldorf, Germany) and thaw-mounted on indium-tin-oxide coated glass slides (ITO, 4-8 Ω resistance; Delta Technologies, Stillwater, MN). The sections were washed three times with cold 70% ethanol and coated with a 10 mg/mL solution (60:40 ACN/H_2O (0.2% TFA)) of α-cyano-4-hydroxycinnamic acid (Sigma-Aldrich, Zwijndrecht, The Netherlands) with an ImagePrep matrix deposition device (Bruker Daltonics, Billerica, MA, USA).

MALDI FT-ICR MS experiments were performed on a custom built dual source FT-ICR mass spectrometer(Rompp, Taban et al. 2005; Smith, Aizikov et al. 2009)

operating in a 7T unshielded superconducting magnet. The positioning device is

mounted vertically in the MALDI source ~ 2 mm from the entrance to the mass

spectrometer's ion optics. A 355 nm Nd:YAG laser (BrightSolutions, Cura Carpignano,

Italy) is used for desorption/ionization and ions are accumulated in an external octopole

ion trap(Taban, McDonnell et al. 2005) before transfer to a capacitively coupled(Beu and

Laude 1992) cylindrical open ICR cell.(Beu and Laude 1992; Guo, Duursma et al. 2004)

Ions were excited by broadband frequency chirp excitation and detected before a single

zero-fill, Gaussian apodization, and Fourier transform. An AWG3 workflow-based data

station is used for experiment control, data acquisition and analysis.(Taban, van der Burgt

et al. 2008) Images were produced via in-house developed software and visualized as

"datacubes".(Klinkert, McDonnell et al. 2007)

4.3 Design

The design parameters were not limited solely by the requirements of MS imaging

experiments, but were also defined to handle the typical proteomics type samples, for a

versatile vacuum compatible positioning system. The full travel of the stage was required

to be no less then 100 x 100 mm, as to accommodate the microtiter plates (~76 x 89 mm)

commonly used in proteomics work. The speed was set to 2 mm/sec, which would

satisfy both imaging and MALDI FT-ICR MS time requirements, yet it is possible to

further decrease the time of spot to spot travel for the shorter duty cycle analyzers. The

positioning repeatability was set to 1 μm, which is exceeds the requirements for MALDI

MSI experiments, yet with further adjustments can be made to meet the spatial resolution

requirements for SIMS imaging. Additionally, true vacuum compatibility, vertical load,

and low (not detectible by FT-ICR) RF interference noise levels were imperative. Furthermore, to be practical, the devise was to be as small as possible to minimize the volume which needs to be evacuated. Hence, conventional "stacked stage" arrangements having off hanging motors which sweep a significant volume of space as the stage moves was to be avoided in the new design.
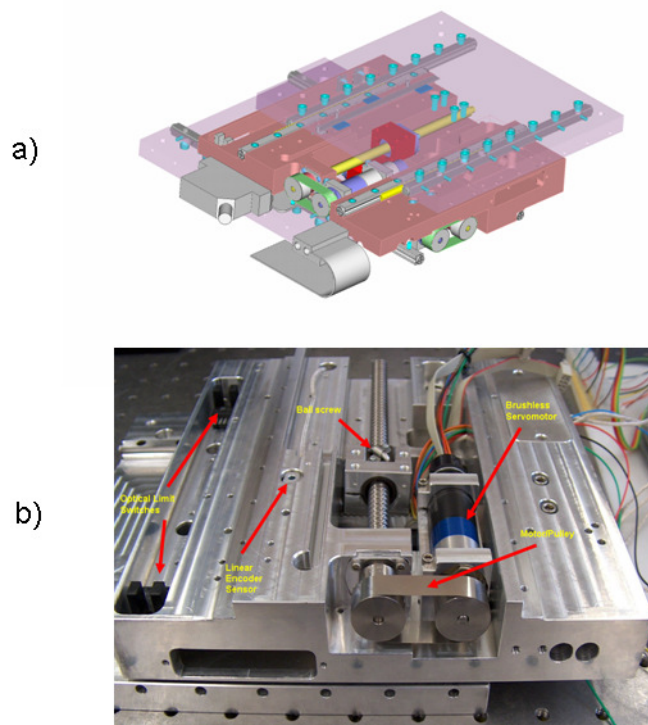
Figure 4.1 The positioning stage is single block three tier design; (a) s blueprint of the fully assembled device with the top tier transparent; (b) a photograph of the middle tier housing all of the mechanical components and sensors.

The final stage design is shown in Figure 4.1. The two-dimensional stage is a three piece single block design: an upper and lower plates and the central block which hosts two axis motors, linear encoders, position limit switches, and two temperature sensors. The system uses ballscrews and crossed roller bearings which require minimal

lubrication; what little lubrication is needed is provided by low vapor pressure PTFE based grease.

Brushless servomotors were used for a number of reasons. Neither linear nor ultrasonic piezomotors, which perform superbly in horizontal setup, are acceptable given the vertical nature of load. Stepper motors are not practical because they tend to generate a lot of heat, dissipation of which is difficult under the vacuum conditions. Brushless servomotors, on the other hand, are easy to tune both in horizontal as well in vertical arrangements. Heat is produced only during motion and heatsinking can be accomplished by trivial thermal grounding, due to placement of the coils on the outside of the case. Additionally, brushless servo motors are durable and do not arc in vacuum.

The motors are mounted to the central block via copper bracket, which allows the block to act as a heat sink. It is only able to dissipate heat through conductive cooling at the bearings and radiative cooling through the environment. The conductive cooling is very inefficient since the bearings are stainless steel (very low heat transfer capacity) and low contact area. A copper band or braid was considered for improving conducting heat transfer, but a quick calculation of the heat transfer of such a band compared to the radiative cooling rate (assuming black body) showed that the heat transfer through the band was negligible. The stage is black anodized to improve the radiative cooling (serendipitously, it also improves surface hardness, but it also increases surface area which could cause problems in UHV operation).

The torque is transferred to the ballscrew via pulleys. The belts for these pulleys are actually small electro welded stainless steel bands, and in order to keep them centered

the pulley wheels are ground to be slightly convex. Tensioning set screws are mounted into the block to allow the pulleys to be tightened properly during testing. The ballscrew is mounted in two places: the pulley bearing assembly (double ball bearing) and the plate, to prevent over-determination of the position, which would result in "jamming". The plates use cross roller bearings, which allows for a much more compact design by both low profile and elimination the need for overhangs otherwise required by recirculating ball bearing.

The system uses 4 optical limit switches (two for each axis). The switch is basically a photodiode/phototransistor pair (see figure 4.1.b) mounted on the central stage body which is interrupted by an aluminum flag mounted on the upper and lower stage plates. This flag blocks the photodiode's signal to the phototransistor when the stage moves to the end of its range of motion, and the electronics signal the stage to stop. Such a system, while similar to a rocker or a magnetic switch involves fewer moving parts and possesses greater positioning accuracy. It is important, however, to verify the cleanliness of the photodiode/phototransistor pair prior to final assembly in vacuum as dust or grease can easily inactivate a limit switch resulting in motor burnout.

The stage control is implemented as a dual loop with the velocity feed-forward (figure 4.2). The feed-forward signal is generated by a trajectory generator, a functionality provided as a part of the Galil® controller. This feature allows for substantial increase in positioning speed especially during the initiation of motion. The outer loop control, which is also handled by the same controller, is a proportional (position) gain controller with the position information fed from the linear encoders. The

inner loop is the Proportional Integral (PI) controller. The proportional (angular position) and integral (velocity) information are received from the servo-motor tachometers and used by the controllers to adjust the current driving the motors.
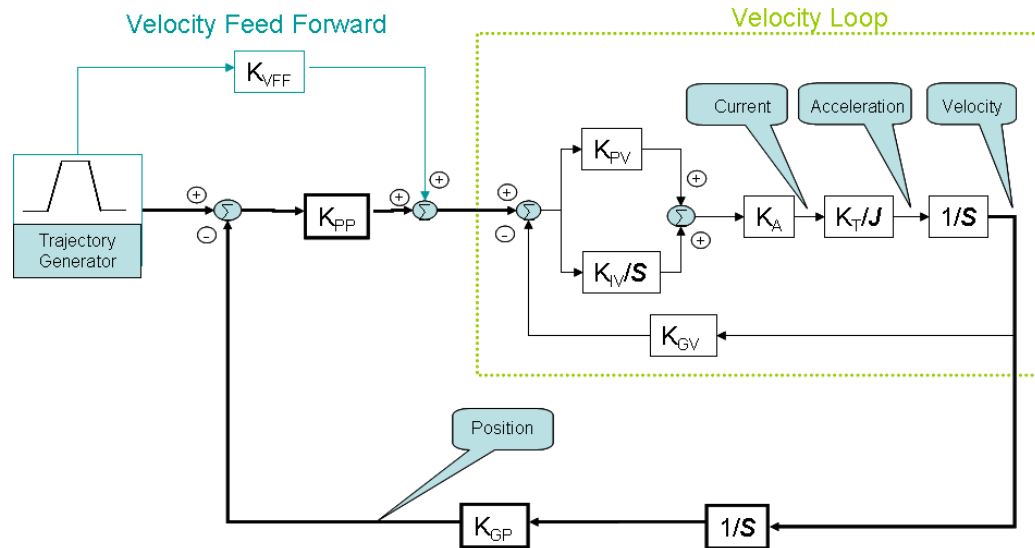
Figure 4.2 The control of the system consisting of the trajectory generator, inner velocity, and outer position loops. The trajectory generator generates both position and velocity commands, with the velocity gain K_{VFF}; the main loop of the control scheme is a proportional only controller with K_{PP} proportional gain and K_{GP} position scaling factor; the inner loop is a proportional integral controller with K_{PV} proportional and K_{IV} integral gains, K_A amp and K_{GV} velocity scaling factors, K_J motor torque and J inertia constants; *1/S* reflects integration in Laplace domain.

The actual position of the load, as was mentioned above, is fed back into the controller via the linear encoder. Although it is possible to bypass linear encoders and use the positioning information directly from the motor rotary encoder (which is easily capable of submicron resolution), this will only provide the controller of the highly accurate angular position of the motor. Since there are multiple mechanical components with different rigidities involved into transferring motor rotation into the linear motion of the stage, the encoder's angular precision cannot be directly mapped to the plate's final positional accuracy. Instead, rotary encoder information is fed back into the motor's amplifier creating a velocity loop. This arrangement significantly simplifies tuning by

reducing the number of interdependent parameters to adjust. In addition, the velocity loop allows not only precise point-to-point movement of the stage but also eases the tuning to follow the desired time trajectory, which makes positioning more accurate (especially given the unequal loads for different axes) while the stage is in motion. Over all, the system performs very similar to a Proportional Integral Derivative (PID) controller with proportional and derivative terms provided explicitly in the from of position in the main and velocity in the inner loops, while the integral component can be though of as a product of integration of the inner proportional term in the main loop.

The sample translational stage requires 48 electrical feedthroughs to control the 2 motors, 4 encoders (2 linear and 2 rotary), 4 limit switches, and a thermocouple. Furthermore, it is critical that the feedthrough and cables are well shielded to reduce RF interference noise, due to the high sensitivity of FT-ICR MS to such noise. The feedthrough used is military standard with strain relief (55 pin) from Detoronics Corporation (South El Monte, CA), but other alternatives are feasible as well, for instance, Caburn MDC (Harwell, UK) manufactures a number of UHV compatible feedthroughs, including two different 50 pin connectors (part numbers 1511007 and 1511008).

4.4 Results

The final assembly of the device is shown in figure 4.3a. Its compact size allows for integration with the majority of existing MALDI sources. Figure 4.3b shows the stage (fully extended in one direction, exposing a motor, a pulley, and one optical limit

switch) mounted on the back source plate of a custom built 7T MALDI FT-ICR MS with high pressure source at Boston University.(Pittman, Thomson et al. 2004) Figure 4.3c is a photograph of the apparatus mounted in the source chamber, taken through a side window of the FT-ICR MS source.
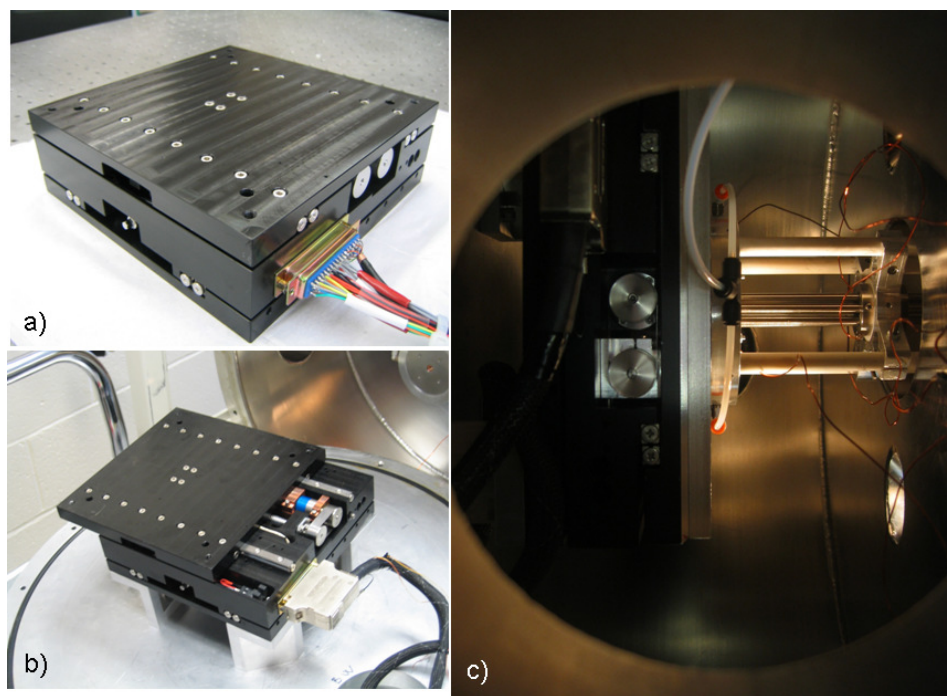
Figure 4.3: Final assembly of the positioning device; (a) lateral view of the stage in its fully compressed form; (b) mounted on the back plate of the MALDI source; (c) inside the MALDI source with a target next to accumulation hexopole (gas inlets for vibrational cooling are seen immediately to the right of the plate).

The software interface is implemented as a lightweight dynamic linked library (dll) wrapper on top of the Galil® DMC software suite. This additional level of abstraction ensures flexibility and ease of access by third party software by hiding the low level routines and significantly lowers the complexity of the interface. A custom built WIN32 application (figure 4.4a) controls the stage for testing, fine tuning, and

manual operation. The application provides access to all functionalities, diagnostic information, and statistics on the device. The stage has also been integrated into other available system control platforms such as the workflow based AWG3 suite.(Mize, Taban et al. 2004; Taban, van der Burgt et al. 2008) A screenshot of the AWG3 GUI stage control for a MS imaging experiment is shown in figure 4.4b.

a)

b)
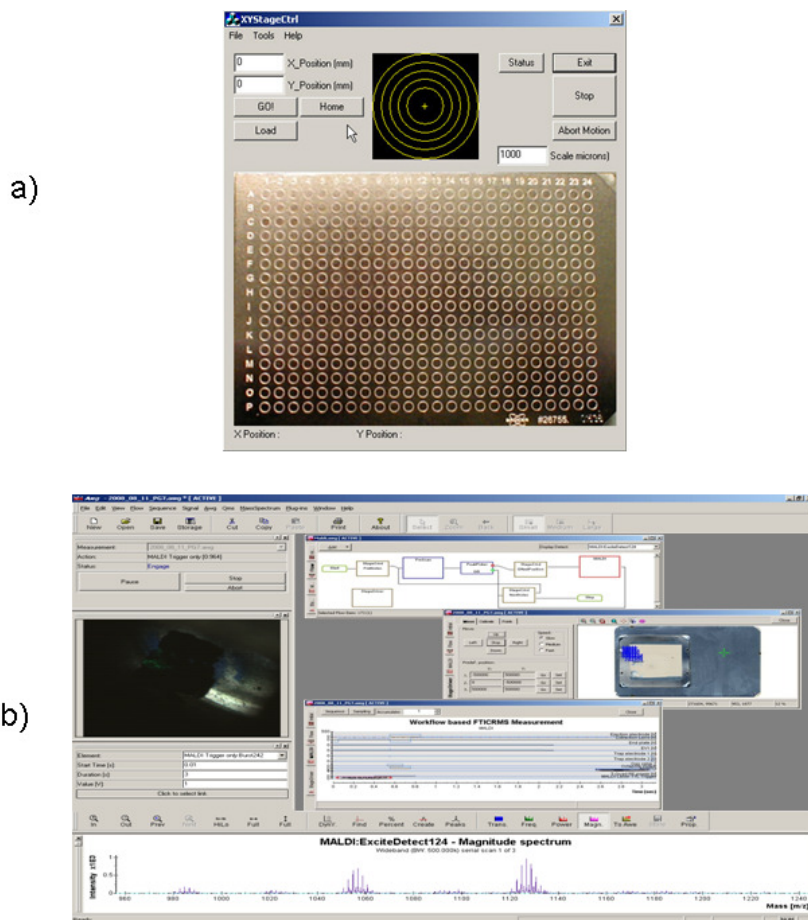
Figure 4.4: Software control interface; (a) a custom-built dedicated application for manual control of the device; (b) stage control GUI integrated into the AWG3 workflow based data acquisition and control system.

The performance capabilities of the positioning stage were tested on the BU 7T FT-ICR MS with the device mounted vertically (fig. 4.3c) in the MALDI source at a

pressure of 1×10^{-8} mbar. The motion speed was set at 2 mm/sec, while acceleration and

deceleration, as well as feed-forward gains were programmatically adjusted for the

optimal positioning accuracy. All tests were conducted using proprietary Gallil®

software tools.

Superimposed plots of the position and the corresponding positional error vs. time

are shown in figure 4.5. The positional plot shows the initial rest at time zero followed

by an acceleration event, steady motion, deceleration, and the final rest position at 1.5

mm roughly corresponding to approximately 0.4 seconds after the initiation. The error

plot indicates that the positional accuracy of the device while moving is under 1 μm and

the jitter that followed fluctuates between 0.1 and 0.2 μm and lasts for the duration of the

movement resulting in a steady state error of 0.1 μm.
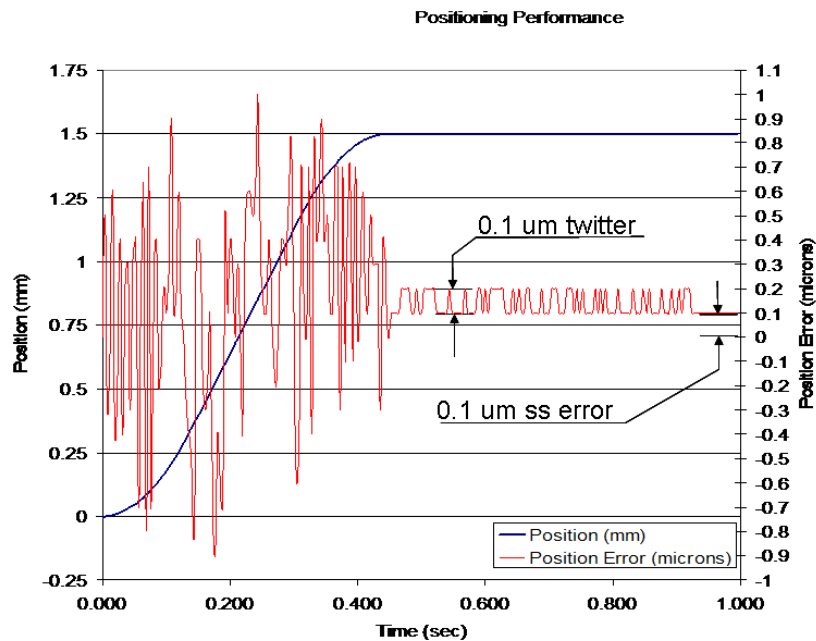
Figure 4.5 Performance evaluation analysis of the system. Blue is the position plot of
the stage superimposed with the corresponding error (red).

The device was also integrated into the AMOLF FT-ICR MS system equipped with a 7T unshielded magnet,(Rompp, Taban et al. 2005) and tested for mass spectrometry imaging applications. For proof of concept as a MALDI MSI positioning system, an HPLC run of the savinase tryptic/CNBr digest was spotted on a MALDI target plate (figure 4.6a). The target was subject to an FT-ICR MS imaging experiment (40 x 40 "pixels") which produced distinct and discrete spatial locations for a number of species species at masses 961.0, 1100.7, 1200.8, 1205.9, 1440.6, 1457.0, 1821.5, 1933.2, 2368.1, and 2593.3Da are shown in figure 4.6b-l. A Mascot PMF database search correctly identified the savinase enzyme with a significant Mascot score of 77 and E-value of .031.
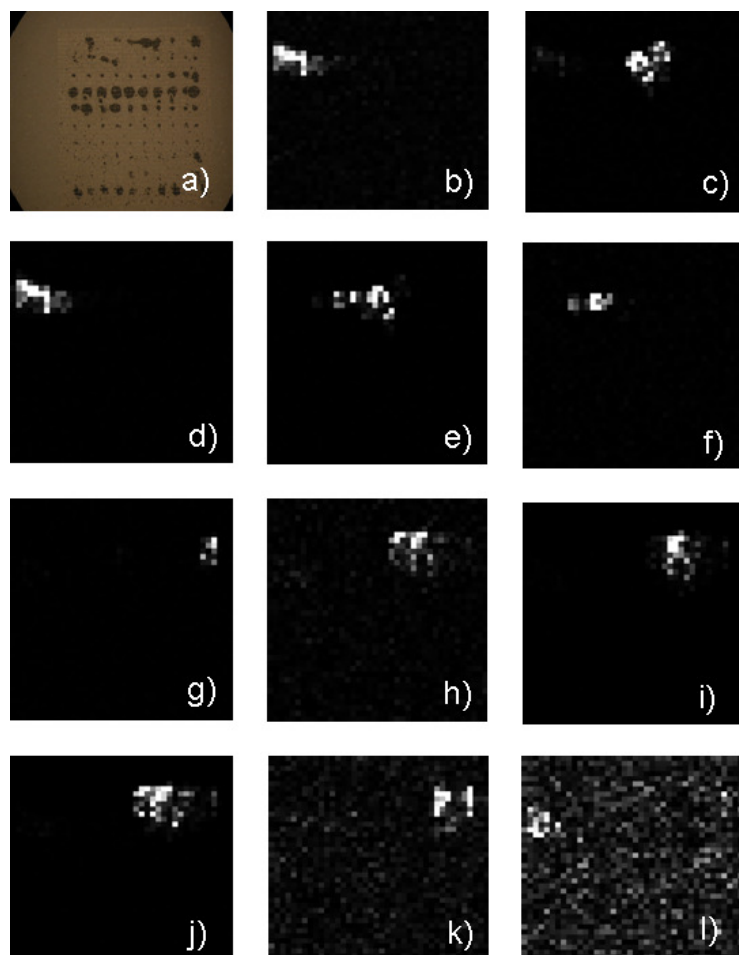
Figure 4.6 An imaging experiment conducted on an LC run of trypsin/CNBr digested savinase enzyme spoted on a MALDI target plate; (a) the plate with the deposited LC run; (b) through (l) special distribution of the compounds with m/z 961, 1101, 1201, 1206, 1440, 1457, 1800, 1821, 1933, 2368, and 2593 Da respectively.

The laser spot size is the limiting factor affecting the resolution of microprobe mode MALDI MS imaging experiments (usually ~50-300 microns). One technique which allows to circumvent this shortcoming is "oversampling".(Jurchen, Rubakhin et al. 2005) A typical oversampling MS imaging experiment consists of complete sample ablation at the initial position followed by moving the sample by a fraction of the laser spot size and collecting spectra (until sample exhaustion as well), hence acquiring sub

laser spot size micron information. To put it to a test, a simple oversampling experiment

with a pixel size of 50 microns (where as the laser spot diameter is 300 microns) was

conducted on a single MALDI spot containing a 50:50 brandykinin, angiotensin mixture

(figure 4.7a) faithfully reproducing their spatial distribution (that of brandykinin on figure

4.7b and angiotensin on 4.7c respectively) even revealing some target surface

imperfection such as the scratch in the lower left part of the dried out droplet appearing

throughout figure 4.7.
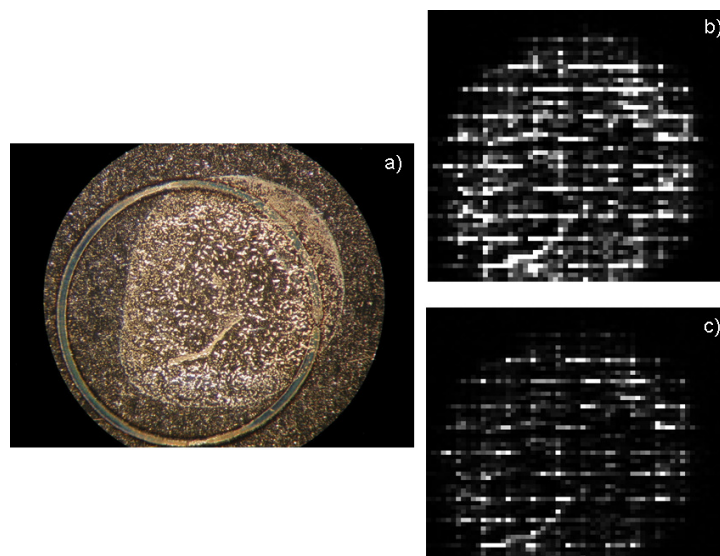
Figure 4.7 Results of the "oversampling" experiment with the roster size of 50 microns
conducted on the 50:50 mixture of brandykinin and angiotensin; (a) the target spot after
the sample deposition; (b) spatial distribution of Bradykinin at 904 Da; (c) special
distribution of angiotensin at 1033 Da.

Figure 4.8a shows a MALDI FT-ICR MS imaging experiment of a rat brain

section at a laser spot diameter of ~300 μm (figure 4.8b,c,d(I)) and an oversampling

experiment a at raster size of 150 μm(figure 4.8b,c,d(II)). The results show distinct

spatial localizations of putative lipids at masses corresponding to 827 Da (b), 768 Da (c),

and 773 Da (d). Oversampling produces a much more detailed and fine images (figure 4.8(II)) compared to the normal mode (figure 4.8(I)), but at the cost of decreased signal-to-noise ratio. This intrinsic trade-off is especially pronounced in figure 4.8d(II) where the compound has a broad distribution across the brain section, yet is not as sharply distinguishable as those in figure 4.8b(II) and 4.8c(II).
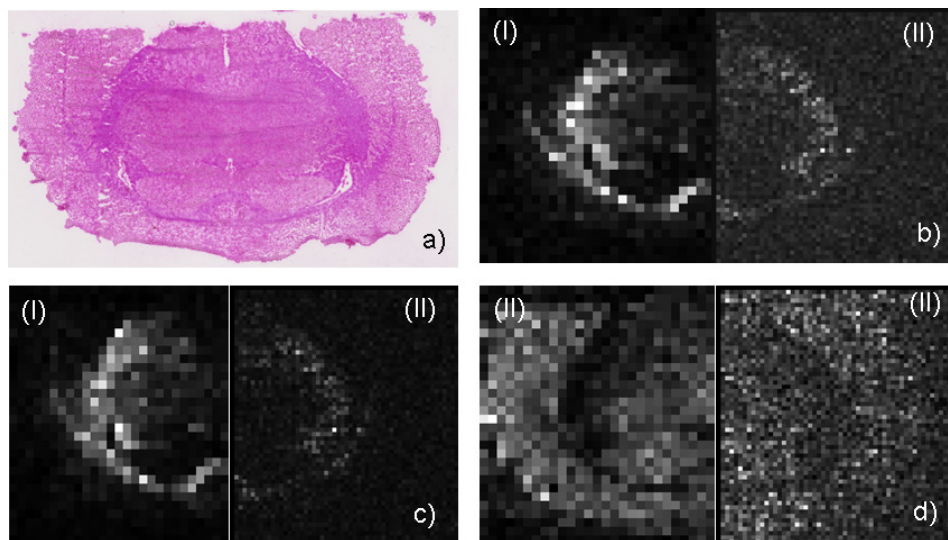
Figure 4.8: FT-ICR mass spectrometry imaging of a coronal rat brain section (a) with roster sizes 300 (I) and 150 (II), monitoring special distribution of putative lipids at 827 Da (b), 768 Da (c), and 773 Da (d).

4.5 Discussion

The primary design goal of this device is to maximize the positioning accuracy, however, minimizing the trajectory error of the device while performing MS imaging experiments is also imperative. "Pixels" must be close for better spatial resolution, but the greater the deviation from the desired trajectory results in a longer settling time for the required positioning accuracy upon motion completion. This leads to an increase in the duty cycle of the experiment, which challenges large area MS imaging experiments.

Here, sub micron trajectory accuracy was achieved with the compartmentalization of the control logic into the velocity and positional loops, as is described in the design section.

Positioning accuracy and speed come with an intrinsic trade-off in the form of settling time. The demonstrated steady state error is 0.1 μm and the amount of twitter does not exceed 0.2 μm, however, the time the stage requires to come to a complete rest upon arriving to its "final destination" is as much as the travel time. Hence, once the minimal amount of under/over-shoots reached (by manipulating feed-forward, acceleration, and deceleration gains), the only way to decrease the settling time is to loosen the accuracy criteria.

The steady state error of 0.1 μm is a very good achievement given the .078 micron resolution of the linear encoders. Reduction of the generally accepted margin of tenfold in respect to the sensor accuracy in PKI controllers is possible mainly due to the design of the control logic. As was described previously, allowed for separate tuning of the proportional and derivative terms (as well as the implicit integral one) in different control loops.

Placing the motors in the central block of the stage (figure 4.1) makes the body of the device act as a heat sink as well as the shield for RF interference. This arrangement modified by use of a copper mounting bracket for the motors (figure 4.3b) proved to be effective against overheating during continuous operation of the motors (over several hours for imaging experiments). Additionally, the sub-detection level of RF interfering noise allows the stage to be moved even during the FT-ICR detection event. Thus, the

only time the stage most definitely must be stationary is during the ionization event only,

leaving the rest of the FT-ICR MS duty cycle for movement to the next raster position;

given the speed of 2mm/sec and .5sec settling time, this does not add a significant

overhead to any MALDI FT-ICR MS imaging experiment time. Moreover, the flexibility

of scheduling the stage movement allows for introduction of internal calibrants.(Mize and

Amster 2000; O'Connor and Costello 2000) Thus utilizing both high resolving power

and mass accuracy of FT-ICR MS for MSI experiments.(Taban, Altelaar et al. 2007;

Cornett, Frappier et al. 2008)

Reported spatial resolution, although substantially improved, was by no means

limited by the device positional accuracy. Reduction of the raster size in oversampling

experiments (figures 4.7 and 4.8) inevitably leads to decreased signal-to-noise levels,

since the decrease of a pixel diameter by a certain factor causes the area to decrease

proportionally to the square of that factor. This decrease in sensitivity, however, can be

diminished to a degree by manipulation of the laser power.(Jurchen, Rubakhin et al.

2005) Another fundamental limit on the resolution of the oversampling experiments is

the "non-square" (Gaussian in most cases) shape of the laser power distribution within a

beam which prevents obtaining sharp borders upon oblation. These and other issues,

such as chemical noise and ion suppression, are especially exacerbated when imaging

biological tissues, which are inherently complex and lead to the possibility of only

fractionally improving spatial resolution, as shown in figure 4.8(II).

4.6 Conclusions

The design goals of building a general purpose vacuum compatible positioning device for MALDI FT-ICR MS imaging have been met and its capabilities were demonstrated. The size, range of motion, ability to operate in vacuum for hours uninterrupted, undetectable levels of RF interference noise, speed, and positional accuracy makes this stage suitable for a wide range of applications ranging from automated offline MALDI MS analysis to the most detailed MALDI MS imaging experiments. Although 0.1 μm positioning accuracy might seem somewhat excessive for the purposes, recent developments in laser optics within mass spectrometry community(Caprioli, Farmer et al. 1997; Garden and Sweedler 2000; Spengler and Hubert 2002; Reyzer, Hsieh et al. 2003; Sherrod, Castellana et al. 2007) allows acquiring MALDI with submicron laser spot diameters. Clearly for such small areas laser power must be significantly increased causing excessive fragmentation, yet vibrational cooling(Krutchinsky, Chernushevich et al. 1998; Laiko, Baldwin et al. 2000; O'Connor and Costello 2001; Ivleva, Elkin et al. 2003; Moyer, Budnik et al. 2003; O'Connor, Budnik et al. 2003; Ivleva, Sapp et al. 2005) should prove itself useful to reduce such fragmentation.

In regards to SIMS imaging, the positional accuracy provided by the stage is sufficient for C_{60} primary ion sources, but should be increased by the factor of ten at least for gold or cesium primary ion beams. The current design can be easily modified to these specifications through the use of different optical linear encoders, or by switching to shorter wavelength detecting photo elements.

Chapter 5

MALDI Fourier Transform Ion Cyclotron Resonance Mass Spectrometry Imaging: Instrumentation and Methods

5.1 Introduction

Mass spectrometry imaging combines molecular (mass) information with spatial information from complex surfaces (e.g. biological tissues).(Heeren, McDonnell et al. 2006; Reyzer and Caprioli 2007) Current instrumental and method developments aim to improve one or both of these facets. Time-of-flight secondary-ion mass spectrometry (ToF-SIMS), stigmatic MALDI-ToF ion-microscope and highly focused microprobe experiments (via MALDI or SIMS) allow high spatial resolution to sub-micrometer scale.(Chandra, Smith et al. 2000; Chandra 2003; Altelaar, van Minnen et al. 2005; McDonnell, Piersma et al. 2005; Altelaar, Klinkert et al. 2006; Arlinghaus, Kriegeskotte et al. 2006; Altelaar, Luxembourg et al. 2007; Chaurand, Schriver et al. 2007; Fletcher, Rabbani et al. 2008; Nie, Francis et al. 2008) On the other hand, high performance mass spectrometers (e.g. FT-ICR MS(Marshall, Hendrickson et al. 1998), LTQ-Orbitap(Makarov 2000) are now being used for complimentary high mass resolving power and high mass accuracy MS for identification of observed species.(Taban, Altelaar et al. 2007; Cornett, Frappier et al. 2008; Landgraf, Conaway et al. 2009) Here, we describe instrumentation and methodology for a custom-built MALDI source for FT-ICR mass spectrometry imaging.

The utility of MALDI FT-ICR for the direct analysis of biological tissues has been demonstrated for peptides from crab neurons(Kutz, Schmidt et al. 2004), crab sinus glands(Stemmler, Bruns et al. 2007), and a wide array of decapod neural tissues.(Stemmler, Bruns et al. 2007; Dickinson, Wiwatpanit et al. 2009) Further, MALDI FT mass spectrometry imaging has been used to image peptides and lipids in rat brain(Taban, Altelaar et al. 2007; Verhaert, Pinkse et al. 2009) and drugs and metabolites from rat kidney and liver, as well as mouse brain.(Cornett, Frappier et al. 2008) These studies demonstrate the need for high mass resolving power to resolve isobaric species and the advantage of high mass accuracy for the identification of analytes and MS/MS fragments.

Here we describe an external MALDI source, with associated software upgrades, that enables FT-ICR mass spectrometry imaging over large areas. Instrumental considerations for improving the speed and sensitivity of FT-ICR MS imaging will be discussed. A LC-MALDI run was "imaged" to test the new configuration in a data- and position-dependent MS/MS mode. A coronal rat brain section was imaged to assess the applicability of the system to tissue analysis, where over 200 unique peaks are observed. Mass selected images of selected lipids display different spatial distributions

5.2 Methods

Acetonitrile (BioSolve, Valkenswaard, NL) and acetic acid (JT Baker, Phillipsburg, NJ, USA) were used without prior purification. Savinase (synthetic serine protease subtilisin 309) was digested with trypsin and CNBr and 5 µl was separated on a LC Packings nanoLC-system ((Dionex), Amsterdam, NL) with a C18 PepMap 100 pre-

column (internal diameter 300 um, length 1 mm) and a C18 PepMap 100 analytical

column (internal diameter 75 um, length 15 cm). The eluents were 0.1% formic acid and

5% acetonitrile in water (A) and 0.1% formic acid and 5% water in acetonitrile (B). The

LC method was 50 minutes with a gradient of 20 minutes 0-70% B, followed by a 1

minute gradient 70-95% B and 10 minutes of 95% B and 12 minutes of 5% B. The

capillary was coupled to a SymBiot I sample workstation (Applied Biosystems, Foster

City, CA, USA) and effluent was spotted at intervals of 30 s and a spacing of 1 mm (10 x

10 matrix) on a premade 2,5-dihydroxybenzoic acid (DHB) MALDI foil

(LabConnections, Northborough, MA, USA). The delay time between the start of the LC

run and spot deposition was 20 minutes.

A 10 μM thick coronal section of rat brain (Harlan Laboratories, Boxmeer, The

Netherlands) was prepared in a Microm HM 525 cryomicrotome (Microm International,

Walldorf, Germany) at -2OºC and placed on indium-tin-oxide coated glass slides (ITO, 4-

8 Ω resistance; Delta Technologies, Stillwater, MN). The section was washed with cold

(-20 ºC) ethanol (70% in H_2O) and coated with ~20 layers of a 100 mg/mL soultion (2:1

ACN/H_2O (0.2% TFA)) of α-cyano-4-hydroxycinnamic diethylamine salt with a Bruker

ImagePrep matrix deposition device.
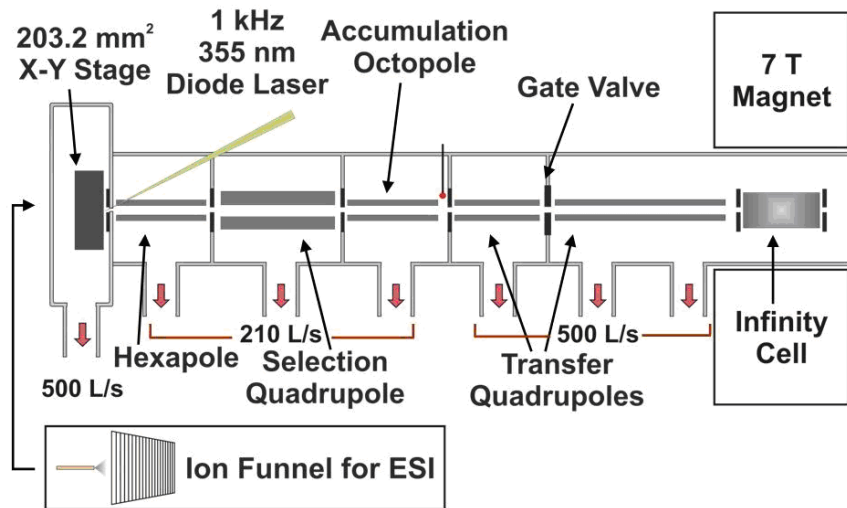
Figure 5.1 Schematic of the AMOLF 7 Tesla MALDI/ESI FT-ICR mass spectrometer. The source features a 203.2 mm2 X-Y stage for MALDI that can be replaced with an electro-dynamic ion-funnel for ESI.

All experiments were performed on a heavily modified Bruker Apex 70E FT-ICR MS.(Rompp, Taban et al. 2005) Figure 5.1 shows a schematic of the new instrument configuration. A 355 nm Nd:YAG laser (1,000 Hz repetition rate; BrightSolutions, Cura Carpignano, Italy) is coupled to the source through a 3 m tapered fiber optic cable (800-200 uM, Fiberguide Industries, Stirling, NJ, USA). The beam is collimated after the fiber optic cable and aligned through the hexapole rods and conductance limit (4 mm) onto the sample surface, which is ~2 mm from the hexapole entrance. The laser power, start time and output frequency are controlled from the data station. In addition, a 337 nm N_2 laser (Laser Science, Inc., Franklin, MA, USA) can also be coupled to the system. A 203.2 mm^2 translational X-Y stage with 10 cm^2 range of motion (Fraunhofer USA, Brookline, MA, USA) allows for the analysis of large sample areas. (Aizikov, et al. 2009) For ESI, the MALDI stage is removed and replaced with an electrodynamic ion funnel(Shaffer,

Tang et al. 1997; Shaffer, Tolmachev et al. 1999; Ibrahim, Tang et al. 2006) and operated

in nano-ESI mode.

Ions from the surface are injected into a short (75 mm) transfer hexapole, pass

through a mass selective quadropole (ABB Extrel, Pittsburg, PA, USA) before storage

(0.1-1 s) in a 170 mm accumulation octopole (with helium cooling gas). External ion

accumulation allows for the accumulation of a large number of laser shots at high

repetition rate. In addition, calibrants from an adjacent sample(Mize and Amster 2000;

O'Connor and Costello 2000) can be stored in the octopole while analyte ions are

collected, and the entire packet sent to the ICR cell simultaneously. Ejection electrodes

are used for efficient extraction of ions into two transfer quadropoles (253 and 889 mm)

(ABB Extrel, Pittsburg, PA).(Wilcox, Hendrickson et al. 2002; Taban, McDonnell et al.

2005) The instrument can be equipped with either a capacitively coupled cylindrical

open ICR cell(Guo, Duursma et al. 2004) or a Bruker Infinity cell,(Caravatti and

Allemann 1991) where ions are cooled with an argon pulse gas(Savard, Becker et al.

1991) before broadband frequency (chirp) excitation and direct-mode detection. An

AWG3 workflow-based data station is used for experiment control, data acquisition and

analysis.(Mize, Taban et al. 2004; Taban, van der Burgt et al. 2008)

5.3 Results and Discussion

The new source was designed around an X-Y translational stage with high

position accuracy (< 0.4 μm under vertical load), with a 10x10 cm range of motion for

analysis of large samples. Stage control is managed through a new "StageDriver" node

in the AWG3 flow-based control software, as shown in Figure 5.2. Variable speed

movement is controlled by "joystick" control and predefined positions can be stored. The sample stage is calibrated by a simple 3-point (or more) calibration routine of the live feed of the sample stage with respect to a scan of the sample plate. Regions of interest with user defined raster size can be defined by a polygon or a simple grid. "Stage command" nodes in the workflow define stage movements such as an offset of the current position, a "go to position" command and a decision to wait for the stage to stop movement. The stage position is stored as a variable and can be used for position-dependent experiments.
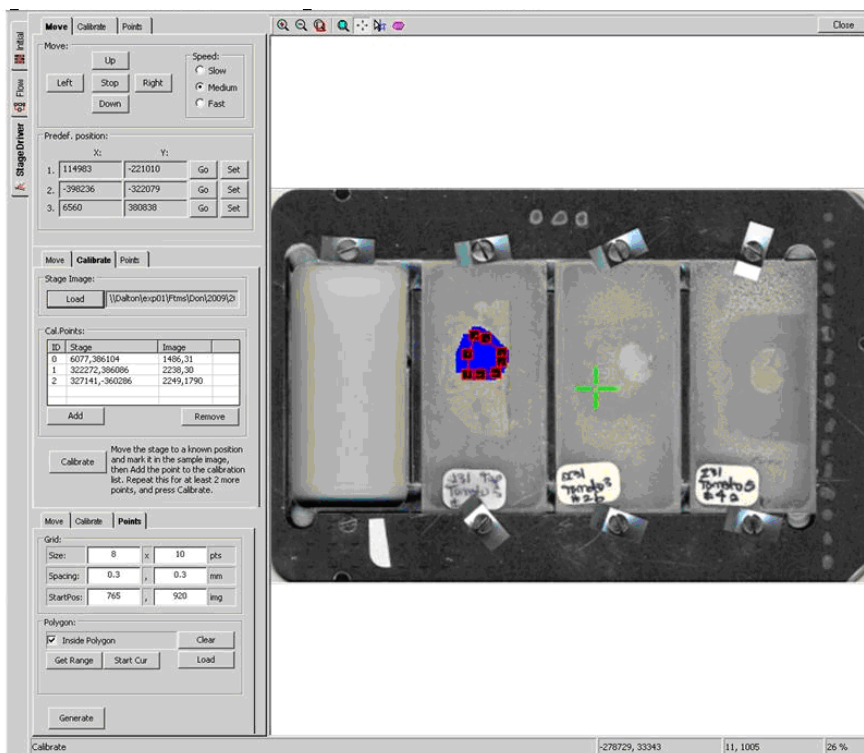
Figure 5.2 The new "StageDriver" node within the AWE instrument control software for stage movement, calibration and selection of analysis areas.

Figure 5.3 shows a MALDI FT-ICR MS "images" for selected peptides from a LC-MS/MS data-dependent run of a trypsin/CNBr digest of Synthetic Subtilisin 309 Gene (Savinase), and an overlay of m/z 1200.8048 (red; NPSWSNVQIR) and it's y8 product ion (m/z 989.6202, blue; SWSNVQIR) (Fig. 5.3, top). The workflow is shown in Figure 5.2, bottom. Here, a prescan was collected and evaluated by the *PeakPicker* node to determine if peaks were present, followed by declustering of detected peaks in the *ClusterList* node. If at least one cluster was found, the stage was offset and the most abundant peak from the prescan was SWIFT isolated(Guan and Marshall 1996) and fragmented by SORI-CID(Gauthier, Trautman et al. 1991; Heck, Koning et al. 1991). This workflow can be modified to fragment specific target ions (i.e. a MRM like experiment) or to store the mass of fragmented ions to insure the same ion is not fragmented multiple times.
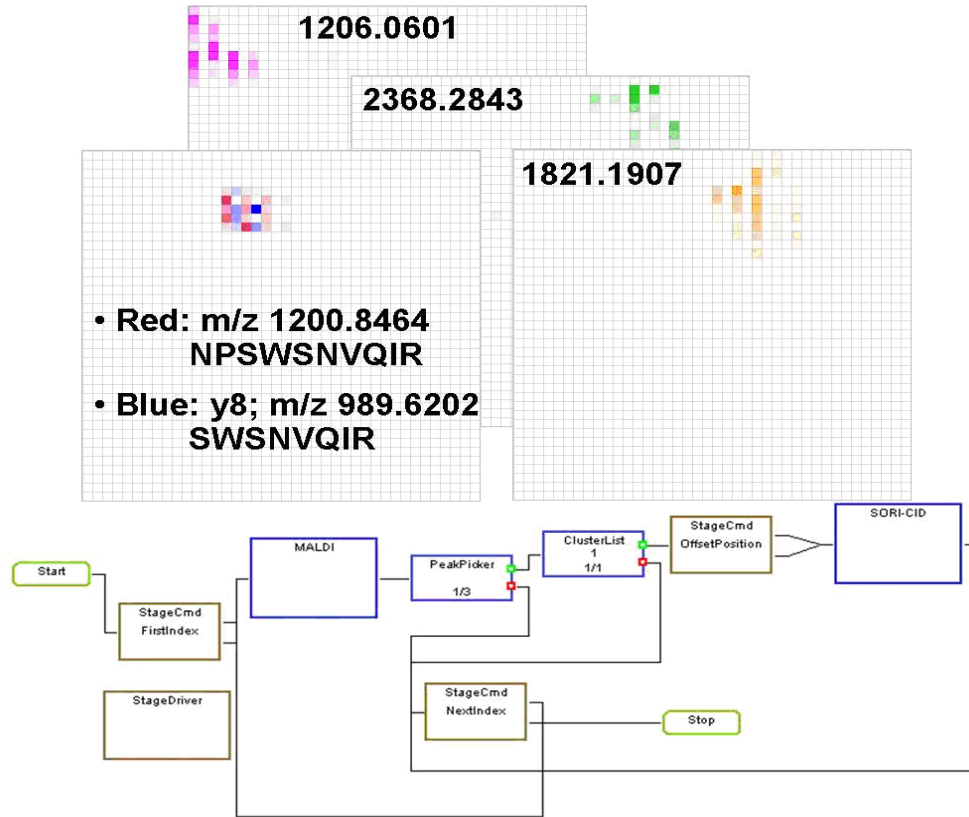
Figure 5.3 Top: FT-ICR MS "images" for selected peptides from a LC MALDI MS/MS run of trypsin/CNBr digested synthetic subtilisin 309 gene (savinase). Red and blue indicate the parent and y8 fragment of the tryptic peptide at m/z 1200.8464. The grid indicates the raster positions of 300 μm. Bottom: The data-dependent workflow used for the LC MALDI run.
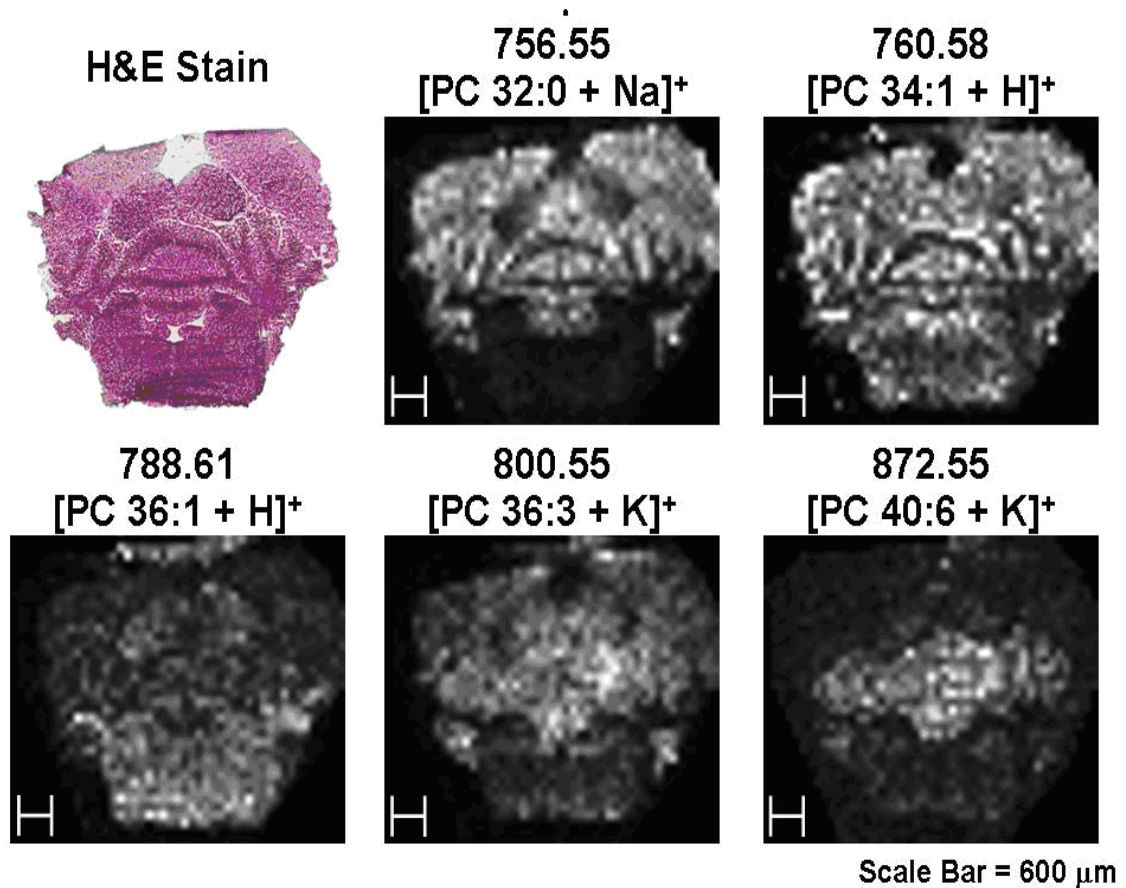
Figure 5.4 Mass selected images of five lipids from a positive-ion MALDI FT-ICR MS imaging experiment of a coronal rat brain section collected at 150 μm raster size. The mass spectrum was binned into 0. 1 Da segments for easy handling and navigation of the dataset. Scale bar = 600 μm. The optical image shows post-analysis hematoxylin/eosin chemical staining.

A rat brain coronal section was used to test the tissue imaging capabilities of the new source. Mass selected images of 5 lipids, acquired at a raster size of 150 μm, are found in Figure 5.4, as well as an optical image of the section stained post-analysis with hematoxylin/eosin. In addition, ~200 unique peaks (> S/N 5:1) were observed from m/z 400-1200. In-house developed software was used to create a "datacube" of the X-Y

correlated mass spectra, in which data can be easily navigated and mass selected images exported.(Klinkert, McDonnell et al. 2007) The time-domain data was zero-filled once and Gaussian apodized before fast Fourier transform and insertion into the datacube. The large number of spectra from an FT-ICR MS imaging experiment, here 1476, requires spectral binning in order to reduce the datacube size, here a bin size of 0.1 Da was used. Lipid assignments were made using LIPID MAPS (LIPID Metabolites and Pathways Strategy; http://www.lipidmaps.org) with a mass tolerance of 0.1 Da with regards to the average measured mass.

5.4 Conclusions

We have constructed a dedicated MALDI source for FT-ICR mass spectrometry imaging. Software updates allow data- and position-dependent workflow based MS imaging experiments as demonstrated with a LC-MALDI MS/MS experiment. Mass resolved images of lipids from a rat brain section demonstrate the utility of the new source for biological tissue measurements. Future work will focus on increased mass resolving power, accurate mass across the *entire* dataset and on-tissue tandem MS strategies.

Chapter 6

Conclusions and Further Work

6.1 Conclusions

MSI is an emerging MS methodology to characterize spatial variation of biomolecules across samples with unmatched accuracy and sensitivity, which has great promise to facilitate biomarker discovery and molecular diagnosis, among other applications. The two major challenges of this technique remain the unambiguous identification of biologically relevant compounds and their precise spatial localization. By developing computational methodologies to explore deleterious space-charge and magnetron motion phenomena in FT-ICR MS, which limit mass accuracy and resolution, and by developing instrumentation to improve spatial resolution in FT-ICR MS imaging experiments, this work addresses both of these challenges.

While FT-ICR mass spectrometers provide, by far, the most accurate mass measurement and highest resolving power of all available mass analyzers, an aspect that is critical to the unambiguous assignment of chemical composition to the analytes, the nature and geometry of the ICR trap allow for the occurrence of potentially coupled space-charge and magnetron motion ion effects. Space charge effects arise due to Coulombic interactions of the ion clouds within the ICR cell. Magnetron motion is a consequence of the hyperbolic shape of the trapping potential, is always expanding, and exposes the ion packets to increasing inhomogeneities in the trapping field. Both of these effects lead, among other undesirable effects, to instabilities that increase both the peak

width and the uncertainty in peak position, while decreasing the duration of the ICR

signal, hence they reduce FT-ICR MS resolving power and mass accuracy.

Here, in the first part of this work, the application of a recently developed high resolution

spectral analysis technique capable of extracting resonance frequencies and amplitudes

from very short transient signals, called the filter diagonalization method (FDM), has

been detailed for the investigation of space-charge related phenomena inside the

detection cell of a FT-ICR mass spectrometer. The FDM analysis of signals produced by

ions in an FT-ICR revealed a novel space-charge induced rapid isotope-beat ICR

frequency modulation. This previously unappreciated isotope beat was shown to reach up

to +/- 400 ppm even on high quality spectra. Furthermore, the FDM analysis

methodology was applied to the investigation of the previously observed Spontaneous

Loss of Coherence Catastrophe FT-ICR phenomenon which had never before been

conclusively explained. This analysis revealed conclusively for the first time that the

Spontaneous Loss of Coherence Catastrophe is directly related to space charge and

magnetron expansion effects, consisting of a complex combination of factors occurring

concurrently, governed by electrostatics and ion packet trajectories. The detailed insight

into these effects that this FDM analysis had provided furthers the ability to understand

and overcome these perturbing phenomena in order to obtain the highest possible

resolution and mass accuracy.

Along with high mass accuracy, high spatial positional accuracy is critical for high

quality and meaningful MSI. Unfortunately, currently available sample positioning

robotics have limited accuracy and range of motion, which imposes limits on the size and spatial resolution of the MS images that are possible with this technology.

In an effort to overcome these limitations, a high precision sample positioning robotic stage for biological MSI applications, that is vacuum compatible and built for accommodation with an FT-ICR MS source, has been designed, constructed, performance tested, and demonstrated functionally in the context of a biological application, as described in the second part of this work. The XY-positioning stage was installed into the ionization sources of three MALDI FT-ICR MS instruments and shown to perform under 10-8 mbar vacuum. It functioned along its entire 100x100 mm X and Y ranges of motion with an error in positioning accuracy less than 0.4 microns and no detectible RF noise. This functionality was exploited in two application demonstrations: two chemo-spatial maps of rat brain tissue selections were constructed with 150 micron spatial resolution, which revealed multiple lipid species with distinct spatial localizations. These performance characteristics greatly exceed current state-of-the-art robotics that are commercially available for MALDI MSI and enable MS images with a spatial resolution that was hither-to impossible. Moreover, they overcome problem of X-Y stage positional accuracy as a factor limiting the spatial resolution of MSI, thereby shifting the focus of potential further technical developments to improve spatial resolution away from stage design

6.2 Future Work

Further improvements in spatial accuracy of the positioning device, possible through the utilization of more precise optical encoders, should lead to even greater

utility provided by this piece of robotics. However, the current stage implementation will allow for dramatically improved resolution and diversity of utility when incorporated into other types of sources that provide higher resolution ionization techniques, such as SIMS or MALDI with higher laser focusing optics. Future work designed to demonstrate the full functionality of the current stage design might include high resolution SIMS imaging of tissue samples, interrogation of bound partners in high resolution protein or nucleic acid array experiments, or blind TLC MALDI experiments, among many others.

The utility of FDM in FT-ICR spectral analysis, as demonstrated in this work, holds great promise in a variety of possible applications. The most immediate one is the analysis of simulated ion behavior and verification of experimental data in the development of more sensitive and accurate ICR detection cells.

Apart from instrumentation development, the fundamental understanding of underlying causes of ICR frequency instabilities that is provided by the FDM analysis are very important. In addition to the phenomena of SLCC and isotope induced ICR frequency modulations, other yet to be discovered underlying factors might be responsible for frequency perturbations. Through FDM analysis a greater understanding of these factors should lead to new mathematical methodologies designed to account and correct for these undesirable effects.

The use of the FDM should not be limited to the FT-ICR technique. Spectral analysis of data from other resonant traps, such as Orbitrap is feasible. It might provide numerous advantages over currently employed signal processing methods. The application of the FDM in Orbitrap data analysis might lead to substantial reduction in

the duty cycle, which will inevitably lead to the increase in experimental throughput and utility of this types of instruments.

References

Adamson, J. T. and K. Hakansson (2007). "Electron capture dissociation of oligosaccharides ionized with alkali, alkaline earth, and transition metals." Analytical Chemistry **79**(7): 2901-2910.

Aizikov, K., R. Mathur, et al. (2009). "The Spontaneous Loss of Coherence Catastrophe in Fourier Transform Ion Cyclotron Resonance Mass Spectrometry." Journal of the American Society for Mass Spectrometry **20**(2): 247-256.

Aizikov, K. and P. B. O'Connor (2006). "Use of the filter diagonalization method in the study of space charge related frequency modulation in Fourier transform ion cyclotron resonance mass spectrometry." Journal of the American Society for Mass Spectrometry **17**(6): 836-843.

Altelaar, A. F. M., I. Klinkert, et al. (2006). "Gold-enhanced biomolecular surface imaging of cells and tissue by SIMS and MALDI mass spectrometry." Analytical Chemistry **78**(3): 734-742.

Altelaar, A. F. M., S. L. Luxembourg, et al. (2007). "Imaging mass spectrometry at cellular length scales." Nature Protocols **2**(5): 1185-1196.

Altelaar, A. F. M., J. van Minnen, et al. (2005). "Direct molecular Imaging of Lymnaea stagnalis nervous tissue at subcellular spatial resolution by mass spectrometry." Analytical Chemistry **77**(3): 735-741.

Amster, I. J. (1996). "Fourier Transform Mass Spectrometry." Journal of Mass Spectrometry **31**(12): 1325-1337.

Anderson, E., Z. Bai, et al. (1999). LAPACK Users' Guide. Philadelphia, PA, Society for Industrial and Applied Mathematics.

Arlinghaus, H. F., C. Kriegeskotte, et al. (2006). "Mass spectrometric characterization of elements and molecules in cell cultures and tissues." Applied Surface Science **252**(19): 6941-6948.

Aston, F. W. (1919). "A positive ray spectrograph." Philosophical Magazine Series 6 **38**: 707-716.

Belov, M. E., R. Zhang, et al. (2003). "Automated gain control and internal calibration with external ion accumulation capillary liquid chromatography-electrospray ionization-fourier transform ion cyclotron resonance." Analytical Chemistry **75**(16): 4195-4205.

Beu, S. C. and D. A. Laude, Jr. (1992). "Elimination of Axial Ejection during Excitation with a Capacitively Coupled Open Trapped-Ion Cell for FTICRMS." Analytical Chemistry **64**: 177-180.

Beu, S. C. and D. A. Laude, Jr. (1992). "Open trapped ion cell geometries for FT/ICR/MS." International Journal of Mass Spectrometry and Ion Physiscs **112**: 215-230.

Brown, B., G. Gabrielse, et al. (1997). "Comparing the Antiproton and Proton and Progress toward Cold Antihydrogen." Nuclear Physics B(Suppl 56A): 326-335.

Brown, L. S. and G. Gabrielse (1986). "Geonium Theory: Physics of a Single Electron or Ion in a Penning Trap." Reviews of Modern Physics **58**: 233-311.

Bruce, J. E., G. A. Anderson, et al. (2000). "Obtaining more accurate Fourier transform ion cyclotron resonance mass measurements without internal standards using multiply charged ions." Journal of the American Society for Mass Spectrometry **11**(5): 416-421.

Bruce, J. E., G. A. Anderson, et al. (1993). "Selected-ion accumulation from an external electrospray ionization source with a Fourier-transform ion cyclotron resonance mass spectrometer." Rapid Communications in Mass Spectrometry **7**(10): 914-919.

Bruce, J. E., G. A. Anderson, et al. (1993). "Time-Base Modulation For the Correction of Cyclotron Frequency Shifts Observed in Long-Lived Transients From Fourier-Transform Ion-Cyclotron-Resonance Mass Spectrometry of Electrosprayed Biopolymers." Rapid Communications in Mass Spectrometry **7**(8): 700-703.

Bruce, J. E., G. A. Anderson, et al. (2000). "A novel high-performance Fourier transform ion cyclotron resonance cell for improved biopolymer characterization." Journal of Mass Spectrometry **35**(1): 85-94.

Bruce, J. E., S. L. Vanorden, et al. (1995). "Selected ion accumulation of noncovalent complexes in a Fourier-transform ion cyclotron resonance mass spectrometer." Journal of Mass Spectrometry **30**(1): 124-133.

Brustkern, A. M., D. L. Rempel, et al. (2008). "An electrically compensated trap designed to eighth order for FT-ICR mass Spectrometry." Journal of the American Society for Mass Spectrometry **19**(9): 1281-1285.

Caldwell, R. L. and R. M. Caprioli (2005). "Tissue profiling by mass spectrometry - A review of methodology and applications." Molecular & Cellular Proteomics **4**(4): 394-401.

Caprioli, R. M., T. B. Farmer, et al. (1997). "Molecular Imaging of Biological Samples - Localization of Peptides and Proteins Using Maldi-Tof Ms." Analytical Chemistry **69**(23): 4751-4760.

Caravatti, P. and M. Allemann (1991). "The Infinity Cell - a New Trapped-Ion Cell with Radiofrequency Covered Trapping Electrodes for Fourier-Transform Ion-Cyclotron Resonance Mass-Spectrometry." Organic Mass Spectrometry **26**(5): 514-518.

Chabala, J. M., K. K. Soni, et al. (1995). "High-Resolution Chemical Imaging with Scanning Ion Probe Sims." International Journal of Mass Spectrometry and Ion Processes **143**: 191-212.

Chandra, S. (2003). "SIMS ion microscopy as a novel, practical tool for subcellular chemical imaging in cancer research." Applied Surface Science **203**: 679-683.
Chandra, S., D. R. Smith, et al. (2000). "Subcellular imaging by dynamic SIMS ion microscopy." Analytical Chemistry **72**(3): 104a-114a.

Chaurand, P., K. E. Schriver, et al. (2007). "Instrument design and characterization for high resolution MALDI-MS imaging of tissue sections." Journal of Mass Spectrometry **42**(4): 476-489.

Chaurand, P., S. A. Schwartz, et al. (2004). "Integrating histology and imaging mass spectrometry." Analytical Chemistry **76**(4): 1145-1155.

Chaurand, P., S. A. Schwartz, et al. (2004). "Profiling and imaging proteins in tissue sections by MS." Analytical Chemistry **76**(5): 86a-93a.

Chen, J. H. and V. A. Mandelshtam (2000). "Multiscale filter diagonalization method for spectral analysis of noisy data with nonlocalized features." Journal of Chemical Physics **112**(10): 4429-4437.

Clauser, K. R., P. Baker, et al. (1999). "Role of accurate mass measurement (+/- 10 ppm) in protein identification strategies employing MS or MS MS and database searching." Analytical Chemistry **71**(14): 2871-2882.

Comisarow, M. B. (1985). "Fundamentals of Fourier-Transform Ion-Cyclotron Resonance Mass-Spectroscopy." Abstracts of Papers of the American Chemical Society **189**(APR-): 194-Anyl.

Comisarow, M. B. and A. G. Marshall (1974). "Fourier Transform Ion Cyclotron Resonance Spectroscopy." Chemical Physics Letters **25**: 282-283.

Comisarow, M. B. and A. G. Marshall (1976). "Theory of Fourier Transform Ion Cyclotron Resonance Mass Spectroscopy. I. Fundamental Equations and Low-Pressure Line Shape." Journal of Chemical Physics **64**: 110-119.

Cooley, J. W. and J. W. Tukey (1965). "Fast Fourier Transform algorithm." Mathematics of Computation **19**: 297-301.

Cornett, D. S., S. L. Frappier, et al. (2008). "MALDI-FTICR imaging mass spectrometry of drugs and metabolites in tissue." Analytical Chemistry **80**(14): 5648-5653.

Cutler, R. G., J. Kelly, et al. (2004). "Involvement of oxidative stress-induced abnormalities in ceramide and cholesterol metabolism in brain aging and Alzheimer's disease." Proceedings of the National Academy of Sciences of the United States of America **101**(7): 2070-2075.

Dempster, A. J. (1918). "A new Method of Positive Ray Analysis." Physical Review **11**(4): 316 LP - 325.

Dickinson, P. S., T. Wiwatpanit, et al. (2009). "Identification of SYWKQCAFNAVSCFamide: a broadly conserved crustacean C-type allatostatin-like peptide with both neuromodulatory and cardioactive properties." Journal of Experimental Biology **212**(8): 1140-1152.

Easterling, M. L., I. J. Amster, et al. (1999). "Isotope beating effects in the analysis of polymer distributions by Fourier transform mass spectrometry." Journal of the American Society for Mass Spectrometry **10**(11): 1074-1082.

Easterling, M. L., T. H. Mize, et al. (1997). "Maldi Ftms Analysis of Polymers - Improved Performance Using an Open Ended Cylindrical Analyzer Cell." International Journal of Mass Spectrometry & Ion Processes **169**: 387-400.

Easterling, M. L., T. H. Mize, et al. (1999). "Routine part-per-million mass accuracy for high-mass ions: Space-charge effects in MALDI FT-ICR." Analytical Chemistry **71**(3): 624-632.

Engen, J. R., T. E. Smithgall, et al. (1999). "Comparison of SH3 and SH2 domain dynamics when expressed alone or in an SH(3+2) construct: The role of protein dynamics in functional regulation." Journal of Molecular Biology **287**(3): 645-656.

Farrar, T. C., J. W. Elling, et al. (1992). "Application of Linear Prediction to Fourier-Transform Ion-Cyclotron Resonance Signals for Accurate Relative Ion Abundance Measurements." Analytical Chemistry **64**(22): 2770-2774.

Fenn, J. B., M. Mann, et al. (1989). "Electrospray ionization for mass spectrometry of large biomolecules." Science **246**(4926): 64-71.

Fletcher, J. S., S. Rabbani, et al. (2008). "A New Dynamic in Mass Spectral Imaging of Single Biological Cells." Analytical Chemistry **80**(23): 9058-9064.

Flora, J. W., J. C. Hannis, et al. (2001). "High-mass accuracy of product ions produced by SORI-CID using a dual electrospray ionization source coupled with FTICR mass spectrometry." Analytical Chemistry **73**(6): 1247-1251.

Gabrielse, G. and F. C. Mackintosh (1984). "Cylindrical Penning Traps with Orthogonalized Anharmonicity Compensation." International Journal of Mass Spectrometry and Ion Processes **57**(1): 1-17.

Garden, R. W. and J. V. Sweedler (2000). "Heterogeneity within MALDI samples as revealed by mass spectrometric imaging." Analytical Chemistry **72**(1): 30-36.

Gauthier, J. W., T. R. Trautman, et al. (1991). "Sustained off-resonance irradiation for CAD involving FTMS. CAD technique that emulates infrared multiphoton dissociation." Analytica Chimica Acta **246**: 211-225.

Gillig, K. J., B. K. Bluhm, et al. (1996). "Ion motion in a Fourier transform ion cyclotron resonance wire ion guide cell." International Journal of Mass Spectrometry **158**: 129-147.

Gorshkov, M. V., A. G. Marshall, et al. (1993). "Analysis and Elimination of Systematic Errors Originating from Coulomb Mutual Interactions and Image Charge in FT/ICR Precise Mass Difference Measurements." Journal of the American Society for Mass Spectrometry **4**: 855-868.

Guan, S. and A. G. Marshall (1995). "Ion traps for fticrms: principles and design of geometric electric configurations." International Journal of Mass Spectrometry and Ion Processes **146/147**: 261-296.

Guan, S., M. C. Wahl, et al. (1993). "Elimination of frequency drift from fourier transform ion cyclotron resonance mass spectra by digital quadrature heterodyning: Ultrahigh mass resolving power for laser-desorbed molecules." Analytical Chemistry **65**(24): 3647-3653.

Guan, S., M. C. Wahl, et al. (1993). "Elimination of frequency drift from FTICR mass spectra by digital quadrature heterodyning: ultrahigh mass resolving power for laser-desorbed molecules." Analytical Chemistry. **65**: 3647-3653.

Guan, S. H. and A. G. Marshall (1995). "Ion Traps For Fourier Transform Ion Cyclotron Resonance Mass Spectrometry - Principles and Design of Geometric and Electric Configurations." International Journal of Mass Spectrometry & Ion Processes **146**: 261-296.

Guan, S. H. and A. G. Marshall (1996). "Stored Waveform Inverse Fourier Transform (Swift) Ion Excitation in Trapped-Ion Mass Spectometry - Theory and Applications." International Journal of Mass Spectrometry & Ion Processes **158**: 5-37.

Guan, S. H. and A. G. Marshall (1997). "Linear Prediction Cholesky Decomposition Vs Fourier Transform Spectral Analysis For Ion Cyclotron Resonance Mass Spectrometry." Analytical Chemistry **69**(6): 1156-1162.

Guo, X. H., M. Duursma, et al. (2004). "Design and performance of a new FT-ICR cell operating at a temperature range of 77-438 K." International Journal of Mass Spectrometry **231**(1): 37-45.

Hannis, J. C. and D. C. Muddiman (2000). "A dual electrospray ionization source combined with hexapole accumulation to achieve high mass accuracy of biopolymers in fourier transform ion cyclotron resonance mass spectrometry." Journal of the American Society for Mass Spectrometry **11**(10): 876-883.

Hasse, H. U., S. Becker, et al. (1994). "External Ion Accumulation in a Penning Trap with Quadrupole Excitation Assisted Buffer Gas Cooling." International Journal of Mass Spectrometry and Ion Processes **132**: 181-191.

Heck, A. J. R., L. J. d. Koning, et al. (1991). "Mass-specific selection of ions in FTICRMS." Rapid Communications in Mass Spectrometry **5**: 406-414.

Heeren, R. M. A., L. A. McDonnell, et al. (2006). "Why don't biologists use SIMS? A critical evaluation of imaging MS." Applied Surface Science **252**(19): 6827-6835.

Hendrickson, C. L., J. J. Drader, et al. (1995). "Simplified application of quadrupolar excitation in Fourier-transform ion cyclotron resonance mass spectrometry." Journal of the American Society for Mass Spectrometry **6**(5): 448-452.

Hendrickson, C. L., S. A. Hofstadler, et al. (1993). "Initiation of Coherent Magnetron Motion Following Ion Injection into a Fourier-Transform Ion-Cyclotron

Resonance Trapped Ion Cell." International Journal of Mass Spectrometry and Ion Processes **123**(1): 49-58.

Hendrickson, C. L. and D. A. Laude Jr. (1995). "Quadrupolar axialization for improved control of electrosprayed proteins in FTICR mass spectrometry." Analytical Chemistry **67**(10): 1717-1721.

Herzog, R. F. K. and F. P. Viehböck (1949). "Ion Source for Mass Spectrography." Physical Review **76**(6): 855 LP - 856.

Hofstadler, S. A., J. E. Bruce, et al. (1994). "Isotopic Beat Patterns in Fourier Transform Ion Cyclotron Resonance Mass Spectrometry - Implications For High Resolution Mass Measurements of Large Biopolymers." International Journal of Mass Spectrometry & Ion Processes **132**(1-2): 109-127.

Honovich, J. P. (1990). "Non-quadrupolar potential in dual trap: effect on ion transfer." International Journal of Mass Spectrometry and Ion Processes **101**: 21.

Hoog, C. L. d. and M. Mann (2004). "Proteomics." Annual Review of Genomics and Human Genetics **5**: 267-293.

Hsieh, Y., J. Chen, et al. (2007). "Mapping pharmaceuticals in tissues using MALDI imaging mass spectrometry." Journal of Pharmacological and Toxicological Methods **55**(2): 193-200.

Hu, H. T., A. A. De Angelis, et al. (2000). "The multidimensional filter diagonalization method - II. Application to 2D projections of 2D, 3D, and 4D NMR experiments." Journal of Magnetic Resonance **144**(2): 357-366.

Hu, H. T., Q. N. Van, et al. (1998). "Reference deconvolution, phase correction, and line listing of NMR spectra by the 1D filter diagonalization method." Journal of Magnetic Resonance **134**(1): 76-87.

Ibrahim, Y., K. Q. Tang, et al. (2006). "Improving mass spectrometer sensitivity using a high-pressure electrodynamic ion funnel interface." Journal of the American Society for Mass Spectrometry **17**(9): 1299-1305.

Ivleva, V. B., Y. N. Elkin, et al. (2003). "Coupling Thin Layer Chromatography with High Pressure Matrix Assisted Laser Desorption/Ionization Fourier Transform Mass Spectrometry for the Analysis of Ganglioside Mixtures." Analytical Chemistry: **76**(21): 6484-6491.

Ivleva, V. B., L. M. Sapp, et al. (2005). "Ganglioside analysis by thin-layer chromatography matrix-assisted laser desorption/ionization orthogonal time-of-

flight mass spectrometry." Journal of the American Society for Mass Spectrometry **16**(9): 1552-1560.

Jackson, G. S., F. M. White, et al. (1999). "Matrix-shimmed ion cyclotron resonance ion trap simultaneously optimized for excitation, detection, quadrupolar axialization, and trapping." Journal of the American Society for Mass Spectrometry **10**(8): 759-769.

Jebanathirajah, J. A., J. L. Pittman, et al. (2005). "Characterization of a new qQq-FTICR mass spectrometer for post-translational modification analysis and top-down tandem mass Spectrometry of whole proteins." Journal of the American Society for Mass Spectrometry **16**(12): 1985-1999.

Jeffries, J. B., S. E. Barlow, et al. (1983). "Theory of Space Charge Shift of ICR Frequences." International Journal of Mass Spectrometry & Ion Processes **54**: 169-187.

Jurchen, J. C., S. S. Rubakhin, et al. (2005). "MALDI-MS imaging of features smaller than the size of the laser beam." Journal of the American Society for Mass Spectrometry **16**(10): 1654-1659.

Kaiser, N. K. and J. E. Bruce (2005). "Observation of increased ion cyclotron resonance signal duration through electric field perturbations." Analytical Chemistry **77**(18): 5973-5981.

Kaiser, N. K. and J. E. Bruce (2007). "Reduction of ion magnetron motion and space charge using radial electric field modulation." International Journal of Mass Spectrometry **265**(2-3): 271-280.

Kaiser, N. K., C. R. Weisbrod, et al. (2008). "Reduction of axial kinetic energy induced perturbations on observed cyclotron frequency." Journal of the American Society for Mass Spectrometry **19**(4): 467-478.

Karas, M. and F. Hillenkamp (1988). "Laser desorption ionization of proteins with molecular masses exceeding 10,000 daltons." Analytical Chemistry **60**(20): 2299-301.

Karas, M. I., D. Bachmann, et al. (1987). "Matrix-Assisted Ultraviolet Laser Desorption of Non-Volatile Compounds." International Journal of Mass Spectrometry & Ion Processes. **78**: 53-68.

Khatib-Shahidi, S., M. Andersson, et al. (2006). "Direct molecular analysis of whole-body animal tissue sections by imaging MALDI mass spectrometry." Analytical Chemistry **78**(18): 6448-6456.

King, R., R. Bonfiglio, et al. (2000). "Mechanistic investigation of ionization suppression in electrospray ionization." Journal of the American Society for Mass Spectrometry **11**(11): 942-950.

Kleinfeld, A. M., J. P. Kampf, et al. (2004). "Transport of C-13-oleate in adipocytes measured using multi imaging mass Spectrometry." Journal of the American Society for Mass Spectrometry **15**(11): 1572-1580.

Klinkert, I., L. A. McDonnell, et al. (2007). "Tools and strategies for visualization of large image data sets in high-resolution imaging mass spectrometry." Review of Scientific Instruments **78**(5): 053756

Knochenmuss, R., A. Stortelder, et al. (2000). "Secondary ion-molecule reactions in matrix-assisted laser desorption/ionization." Journal of Mass Spectrometry **35**(11): 1237-1245.

Kruse, R. and J. V. Sweedler (2003). "Spatial profiling invertebrate ganglia using MALDI MS." Journal of the American Society for Mass Spectrometry **14**(7): 752-759.

Krutchinsky, A. N., I. V. Chernushevich, et al. (1998). "Collisional Damping Interface for an Electrospray Ionization Time-of-Flight Mass Spectrometer." Journal of the American Society for Mass Spectrometry **9**(6): 569-579.

Kussmann, M., E. Nordhoff, et al. (1997). "Matrix-Assisted Laser Desorption/Ionization Mass Spectrometry Sample Preparation Techniques Designed For Various Peptide and Protein Analytes." Journal of Mass Spectrometry **32**(6): 593-601.

Kutz, K. K., J. J. Schmidt, et al. (2004). "In situ tissue analysis of neuropeptides by MALDI FTMS in-cell accumulation." Analytical Chemistry **76**(19): 5630-5640.

Laiko, V. V., M. A. Baldwin, et al. (2000). "Atmospheric pressure matrix-assisted laser desorption/ionization mass spectrometry." Analytical Chemistry. **72**(4): 652-7.

Landgraf, R. R., M. C. P. Conaway, et al. (2009). "Imaging of Lipids in Spinal Cord Using Intermediate Pressure Matrix-Assisted Laser Desorption-Linear Ion Trap/Orbitrap MS." Analytical Chemistry **81**(20): 8488-8495.

Lawrence, E. O. and M. S. Livingston (1932). "The Cyclotron." Physical Review. **40**: 19.

Ledford, E. B., Jr., D. L. Rempel, et al. (1984). "Mass calibration law for quadrupolar potential." Analytical Chemistry **56**: 2744-2748.

Leymarie, N., C. E. Costello, et al. (2003). "Electron capture dissociation initiates a free radical reaction cascade." <u>Journal of the American Chemical Society</u> **125**(29): 8949-8958.

Loo, J. F., M. D. Krahling, et al. (1990). "Accurate Ion Abundance Measurements in ICR/MS by Linear Prediction." <u>Rapid Communications in Mass Spectrometry</u> **4**: 297-299.

Lorenz, S. A., E. P. Maziarz, et al. (1999). "Electrospray ionization Fourier transform mass spectrometry of macromolecules: The first decade." <u>Applied Spectroscopy</u> **53**(1): 18A-36A.

Makarov, A. (2000). "Electrostatic axially harmonic orbital trapping: A high-performance technique of mass analysis." <u>Analytical Chemistry</u> **72**(6): 1156-1162.

Makarov, A. and E. Denisov (2009). "Dynamics of Ions of Intact Proteins in the Orbitrap Mass Analyzer." <u>Journal of the American Society for Mass Spectrometry</u> **20**(8): 1486-1495.

Mandelshtam, V. (2003). "On harmonic inversion of cross-correlation functions by the filter diagonalization method." <u>Abstracts of Papers of the American Chemical Society</u> **225**: U435-U435.

Mandelshtam, V. A. (2001). "FDM: the filter diagonalization method for data processing in NMR experiments." <u>Progress in Nuclear Magnetic Resonance Spectroscopy</u> **38**(2): 159-196.

Mandelshtam, V. A. (2003). "On harmonic inversion of cross-correlation functions by the filter diagonalization method." <u>Journal of Theoretical & Computational Chemistry</u> **2**(4): 497-505.

Mandelshtam, V. A. and H. S. Taylor (1997). "A low-storage filter diagonalization method for quantum eigenenergy calculation or for spectral analysis of time signals." <u>Journal of Chemical Physics</u> **106**(12): 5085-5090.

Mandelshtam, V. A. and H. S. Taylor (1998). "Harmonic inversion of time signals and its applications (vol 107, pg 6756, 1997)." <u>Journal of Chemical Physics</u> **109**(10): 4128-4128.

Mandelshtam, V. A., H. S. Taylor, et al. (1998). "Application of the filter diagonalization method to one- and two-dimensional NMR spectra." <u>Journal of Magnetic Resonance</u> **133**(2): 304-312.

Mann, S. and S. Haykin (1992). "Adaptive Chirplet Transform - an Adaptive Generalization of the Wavelet Transform." Optical Engineering **31**(6): 1243-1256.

Marple, S. L. (1987). Digital spectral analysis: with applications. Upper Saddle River, NJ, Prentice-Hall, Inc.

Marshall, A. G. (1979). "Theoretical Signal-to-Noise Ratio and Mass Resolution in Fourier Transform Ion Cyclotron Resonance Mass Spectrometry." Analytical Chemistry **51**: 1710-1714.

Marshall, A. G. (2000). "Milestones in Fourier transform ion cyclotron resonance mass spectrometry technique development [Review]." International Journal of Mass Spectrometry **200**(1-3): 331-356.

Marshall, A. G. and C. L. Hendrickson (2001). "Charge reduction lowers mass resolving power for isotopically resolved electrospray ionization Fourier transform ion cyclotron resonance mass spectra." Rapid Communications in Mass Spectrometry **15**(3): 232-235.

Marshall, A. G., C. L. Hendrickson, et al. (1998). "Fourier Transform Ion Cyclotron Resonance Mass Spectrometry - A Primer." Mass Spectrometry Reviews **17**(1): 1-35.

Masselon, C., A. V. Tolmachev, et al. (2002). "Mass measurement errors caused by "local" frequency perturbations in FTICR mass spectrometry." Journal of the American Society for Mass Spectrometry **13**(1): 99-106.

Mathur, R., R. W. Knepper, et al. (2007). "A low-noise, wideband preamplifier for a Fourier-transform ion cyclotron resonance mass spectrometer." Journal of the American Society for Mass Spectrometry **18**(12): 2233-2241.

Mathur, R. and P. B. O'Connor (2006). "Design and implementation of a high power rf oscillator on a printed circuit board for multipole ion guides." Review of Scientific Instruments **77**(11)

Matteo Frigo and S. G. Johnson (2005). The design and implementation of FFTW3. Proceedings of the IEEE. **55** (1), 111–119 (2007)

McDonnell, L. A. and R. M. A. Heeren (2007). "Imaging mass spectrometry." Mass Spectrometry Reviews **26**(4): 606-643.

McDonnell, L. A., S. R. Piersma, et al. (2005). "Subcellular imaging mass spectrometry of brain tissue." Journal of Mass Spectrometry **40**(2): 160-168.

Mikhail E. Belov, G. A. A., Mark A. Wingerd,, K. T. Harold R. Udseth, David C. Prior, Kenneth R. Swanson,, et al. (2004). "An Automated High Performance Capillary Liquid Chromatography-Fourier Transform Ion Cyclotron Resonance Mass Spectrometer for High-Throughput Proteomics." <u>Journal of the American Society for Mass Spectrometry</u> **15**(2): 212-232.

Mize, T. H. and I. J. Amster (2000). "Broad-band ion accumulation with an internal source MALDI-FTICR-MS." <u>Analytical Chemistry</u> **72**(24): 5886-5891.

Mize, T. H., I. Taban, et al. (2004). "A modular data and control system to improve sensitivity, selectivity, speed of analysis, ease of use, and transient duration in an external source FTICR-MS." <u>International Journal of Mass Spectrometry</u> **235**(3): 243-253.

Moyer, S. C., B. A. Budnik, et al. (2003). "Attomole Peptide Analysis by High Pressure Matrix-Assisted Laser Desorption/Ionization Fourier Transform Mass Spectrometry." <u>Analytical Chemistry</u> **75**(23): 6449-6454.

Neuhauser, D. (1990). "Bound-State Eigenfunctions from Wave-Packets - Time-]Energy Resolution." <u>Journal of Chemical Physics</u> **93**(4): 2611-2616.

Neuhauser, D. (1994). "Circumventing the Heisenberg Principle - a Rigorous Demonstration of Filter-Diagonalization on a Licn Model." <u>Journal of Chemical Physics</u> **100**(7): 5076-5079.

Nie, H. Y., J. T. Francis, et al. (2008). "Imaging subcellular features of a sectioned rat brain using time-of-flight secondary ion mass spectrometry and scanning probe microscopy." <u>Applied Surface Science</u> **255**(4): 1079-1083.

Nikolaev, E. N., R. M. A. Heeren, et al. (2007). "Realistic modeling of ion cloud motion in a Fourier transform ion cyclotron resonance cell by use of a particle-in-cell approach." <u>Rapid Communications in Mass Spectrometry</u> **21**(22): 3527-3546.

Nikolaev, E. V., N. V. Miluchihin, et al. (1995). "Evolution of an ion cloud in a FTICRMS druing signal deteciton: its influence onf spectral line shape and position." <u>International Journal of Mass Spectrometry and Ion Processes</u> **148**: 145-157.

Norbeck, A. D., M. E. Monroe, et al. (2005). "The utility of accurate mass and LC elution time information in the analysis of complex proteomes." <u>Journal of the American Society for Mass Spectrometry</u> **16**(8): 1239-1249.

O'Connor P, B. (2002). Boston University Data Analysis. www.bumc.bu.edu/ftms

O'Connor, P. B., B. A. Budnik, et al. (2003). "A High Pressure Matrix-Assisted Laser Desorption Fourier Transform Mass Spectrometry Ion Source Designed to Accommodate Large Targets with Diverse Surfaces." Journal of the American Society for Mass Spectrometry **15**(1): 128-132.

O'Connor, P. B., C. A. Costello, et al. (2002). "A High Voltage RF Oscillator for Driving Multipole Ion Guides." Journal of the American Society for Mass Spectrometry **13**(12): 1370-1375.

O'Connor, P. B. and C. E. Costello (2000). "Internal calibration on adjacent samples (InCAS) with Fourier transform mass spectrometry." Analytical Chemistry **72**(24): 5881-5885.

O'Connor, P. B. and C. E. Costello (2001). "A High Pressure Matrix-Assisted Laser Desorption/Ionization Fourier Transform Mass Spectrometry Ion Source for Thermal Stabilization of Labile Biomolecules." Rapid Communications in Mass Spectrometry **15**: 1862-1868.

O'Connor, P. B., J. L. Pittman, et al. (2006). "A new hybrid electrospray Fourier transform mass spectrometer: design and performance characteristics." Rapid Communications in Mass Spectrometry **20**(2): 259-266.

O'Connor, P. B., J. P. Speir, et al. (1996). "Quadrupolar axialization of large multiply charged ions." Journal of Mass Spectrometry **31**(5): 555-559.

Ong, S. E. and M. Mann (2006). "A practical recipe for stable isotope labeling by amino acids in cell culture (SILAC)." Nature Protocols **1**(6): 2650-2660.

Pan, Y., D. P. Ridge, et al. (1988). "Harmonic Signal Enhancement in Ion-Cyclotron Resonance Mass-Spectrometry Using Multiple Electrode Detection." International Journal of Mass Spectrometry and Ion Processes **84**(3): 293-304.

Pastor, S. J., J. A. Castoro, et al. (1995). "High-mass analysis using quadrupolar excitation ion cooling in a Fourier-transform mass spectrometry." Analytical Chemistry **67**(2): 379-384.

Paul, W. (1990). "Electromagnetic Traps for Charged and Neutral Particles." Angewandte Chemie-International Edition in English **29**(7): 739-748.

Penning, F. M. (1936). "Die Glimmentladung Bei Niedrigem Druck..." Physica **3**(9): 873-894.

Pierson, J., J. L. Norris, et al. (2004). "Molecular profiling of experimental Parkinson's disease: Direct analysis of peptides and proteins on brain tissue sections by MALDI mass spectrometry." Journal of Proteome Research **3**(2): 289-295.

Pittman, J. L. and P. B. O'Connor (2005). "A minimum thickness gate valve with integrated ion optics for mass spectrometry." Journal of the American Society for Mass Spectrometry **16**(4): 441-445.

Pittman, J. L., B. A. Thomson, et al. (2004). A novel hybrid instrument using a commercial electrospray ionization source with a high-performance FTMS for proteomics applications. Proceedings of the 52nd ASMS Conference, Nashville, TN.

Press, W. H., B. P. Flannery, et al. (1986). Numerical Recipes. New York, NY, Cambridge University Press.

Puglielli, L., R. E. Tanzi, et al. (2003). "Alzheimer's disease: the cholesterol connection." Nature Neuroscience **6**(4): 345-351.

Reyzer, M. L. and R. M. Caprioli (2007). "MALDI-MS-based imaging of small molecules and proteins in tissues." Current Opinion in Chemical Biology **11**(1): 29-35.

Reyzer, M. L., Y. S. Hsieh, et al. (2003). "Direct analysis of drug candidates in tissue by matrix-assisted laser desorption/ionization mass spectrometry." Journal of Mass Spectrometry **38**(10): 1081-1092.

Rohner, T. C., D. Staab, et al. (2005). "MALDI mass spectrometric imaging of biological tissue sections." Mechanisms of Ageing and Development **126**(1): 177-185.

Rompp, A., I. M. Taban, et al. (2005). "Examples of Fourier transform ion cyclotron resonance mass spectrometry developments: from ion physics to remote access biochemical mass spectrometry." European Journal of Mass Spectrometry **11**(5): 443-456.

Roy, R., B. G. Sumpter, et al. (1991). "Novel Methods for Spectral-Analysis." Physics Reports-Review Section of Physics Letters **205**(3): 109-152.

Savard, G., S. Becker, et al. (1991). "A new cooling technique for heavy ions in a Penning trap." Physics Letters A **158**: 247-252.

Savitski, M. M., I. A. Ivonin, et al. (2004). "Shifted-basis technique improves accuracy of peak position determination in Fourier transform mass spectrometry." Journal of the American Society for Mass Spectrometry **15**(4): 457-461.

Schwartz, S. A., M. L. Reyzer, et al. (2003). "Direct tissue analysis using matrix-assisted laser desorption/ionization mass spectrometry: practical aspects of sample preparation." Journal of Mass Spectrometry **38**(7): 699-708.

Schweikhard, L., S. H. Guan, et al. (1992). "Quadrupolar Excitation and Collisional Cooling for Axialization and High-Pressure Trapping of Ions in Fourier-Transform Ion-Cyclotron Resonance Mass-Spectrometry." International Journal of Mass Spectrometry and Ion Processes **120**(1-2): 71-83.

Scigelova, M. and A. Makarov (2006). "Orbitrap mass analyzer - Overview and applications in proteomics." Proteomics: 16-21.

Senko, M. W. IsoPro. http://members.aol.com/msmssoft/

Senko, M. W., C. L. Hendrickson, et al. (1997). "External Accumulation of Ions For Enhanced Electrospray Ionization Fourier Transform Ion Cyclotron Resonance Mass Spectrometry." Journal of the American Society for Mass Spectrometry **8**(9): 970-976.

Shaffer, S. A., K. Q. Tang, et al. (1997). "A Novel Ion Funnel For Focusing Ions At Elevated Pressure Using Electrospray Ionization Mass Spectrometry." Rapid Communications in Mass Spectrometry **11**(16): 1813-1817.

Shaffer, S. A., A. Tolmachev, et al. (1999). "Characterization of an improved electrodynamic ion funnel interface for electrospray ionization mass spectrometry." Analytical Chemistry **71**(15): 2957-2964.

Shen, Y. F., N. Tolic, et al. (2001). "High-throughput proteomics using high efficiency multiple-capillary liquid chromatography with on-line high-performance ESI FTICR mass spectrometry." Analytical Chemistry **73**(13): 3011-3021.

Sherrod, S. D., E. T. Castellana, et al. (2007). "Spatially dynamic laser patterning using advanced optics for imaging matrix assisted laser desorption/ionization (MALDI) mass spectrometry." International Journal of Mass Spectrometry **262**(3): 256-262.

Smith, D. F., K. Aizikov, et al. (2009). "MALDI FT-ICR Mass Spectrometry Imaging Instrumentation and Methods." in preparation.

Smith, J. O. (2003). Mathematics of the Discrete Fourier Transform (DFT).

Speir, J. P., G. S. Gorman, et al. (1993). "Remeasurement of ions using quadrupolar excitation Fourier-transform ion cyclotron resonance spectrometry." Analytical Chemistry **65**(13): 1746-1752.

Spengler, B. (2004). "De novo sequencing, peptide composition analysis, and composition-based sequencing: A new strategy employing accurate mass determination by Fourier transform ion cyclotron resonance mass spectrometry." Journal of the American Society for Mass Spectrometry **15**(5): 703-714.

Spengler, B. and M. Hubert (2002). "Scanning microprobe matrix-assisted laser desorption ionization (SMALDI) mass spectrometry: Instrumentation for sub-micrometer resolved LDI and MALDI surface analysis." Journal of the American Society for Mass Spectrometry **13**(6): 735-748.

Stemmler, E. A., E. A. Bruns, et al. (2007). "Mass spectrometric identification of pEGFYSQRYamide: A crustacean peptide hormone possessing a vertebrate neuropeptide Y (NPY)-like carboxy-terminus." General and Comparative Endocrinology **152**(1): 1-7.

Stolzenberg, H., G. Audi, et al. (1990). "Accurate Mass Determination of Short-lived Isotopes by a Tandem Penning Trap Mass Spectrometer." Physiscs Review Letters **65**: 3104-3107.

Taban, I. M., A. F. M. Altelaar, et al. (2007). "Imaging of peptides in the rat brain using MALDI-FTICR mass spectrometry." Journal of the American Society for Mass Spectrometry **18**(1): 145-151.

Taban, I. M., L. A. McDonnell, et al. (2005). "SIMION analysis of a high performance linear accumulation octopole with enhanced ejection capabilities." International Journal of Mass Spectrometry **244**(2-3): 135-143.

Taban, L. M., Y. E. M. van der Burgt, et al. (2008). "A novel workflow control system for Fourier transform ion cyclotron resonance mass spectrometry allows for unique on-the-fly data-dependent decisions." Rapid Communications in Mass Spectrometry **22**(8): 1245-1256.

Tanaka, K., H. Waki, et al. (1988). "Protein and Polymer Analyses up to m/z 100000 by Laser Ionization Time-of-Flight Mass Spectrometry." Rapid Communications Mass Spectrometry **2**: 151-153.

Thomson, J. J. (1910). "Rays of positive electricity." Philosophical Magazine A: Physics of Condensed Matter: Defects and Mechanical Properties **20**: 752-767.

Thomson, J. J. (1913). Rays of positive electricity. Proceedings of the Royal Society.

Tolmachev, A. V., E. W. Robinson, et al. (2008). "Trapped-ion cell with improved DC potential harmonicity for FT-ICR MS." Journal of the American Society for Mass Spectrometry **19**(4): 586-597.

Touboul, D., H. Piednoel, et al. (2004). "Changes in phospholipid composition within the dystrophic muscle by matrix-assisted laser desorption/ionization mass spectrometry and mass spectrometry imaging." European Journal of Mass Spectrometry **10**(5): 657-664.

Vartanian, V. H. and D. A. Laude (1995). "Optimization of a Fixed-Volume Open Geometry Trapped Ion Cell for Fourier-Transform Ion-Cyclotron Mass-Spectrometry." International Journal of Mass Spectrometry and Ion Processes **141**(3): 189-200.

Verhaert, P. D. E. M., M. Pinkse, et al. (2009). Tissue Imaging of neuropeptides by MALDI Orbitrap MS. Proceedings of 57th American Society for Mass

Spectrometry Conference on Mass Spectrometry and Allied Topics., Philadelphia, PA.
Wall, M. R. and D. Neuhauser (1995). "Extraction, through Filter-Diagonalization, of General Quantum Eigenvalues or Classical Normal-Mode Frequencies from a Small Number of Residues or a Short-Time Segment of a Signal .1. Theory and Application to a Quantum-Dynamics Model." Journal of Chemical Physics **102**(20): 8011-8022.

Wall, M. R. and D. Neuhauser (1995). "Filter-Diagonalization - a New Method for the Computation of Eigenstates." Abstracts of Papers of the American Chemical Society **209**: 249-PHYS.

Wang, M. and A. G. Marshall (1988). "High-Resolution Multiple-Ion Simultaneous Monitoring by Means of Multiple-Foldover Fourier Transform Ion Cyclotron Resonance Mass Spectrometry." Analytical Chemistry **60**: 341-344.

Weisbrod, C. R., N. K. Kaiser, et al. (2008). Series, Trapping Ring Electrode Cell (TREC): A novel ICR cell for ultra-high sensitivity, resolution, and mass measurement accuracy. the 56th ASMS Conference on Mass Spectrometry and Allied Topics, Denver, CO.

Wilcox, B. E., C. L. Hendrickson, et al. (2002). "Improved ion extraction from a linear octopole ion trap: SIMION analysis and experimental demonstration." Journal of the American Society for Mass Spectrometry **13**(11): 1304-1312.

Wineland, D. J. and H. G. Dehmelt (1975). "Line shifts and widths of axial, cyclotron, and G-2 resonances in tailored, stored electron (ion) cloud." International Journal of Mass Spectrometry and Ion Processes **16**: 338.

Wiseman, J. M., D. R. Ifa, et al. (2006). "Tissue imaging at atmospheric pressure using desorption electrospray ionization (DESI) mass spectrometry." Angewandte Chemie-International Edition **45**(43): 7188-7192.

Wong, R. L. and I. J. Amster (2007). "Experimental evidence for space-charge effects between ions of the same mass-to-charge in Fourier-transform ion cyclotron resonance mass spectrometry." International Journal of Mass Spectrometry **265**(2-3): 99-105.

Xiang, X., P. B. Grosshans, et al. (1993). "Image Charge-Induced Ion Cyclotron Orbital Frequency Shift for Orthorhombic and Cylindrical FT/ICR Ion Traps." International Journal of Mass Spectrometry and Ion Processes **125**: 33-43.

Yergey, J. A. (1983). "A general approach to calculating isotopic distributions for mass spectrometry." International Journal of Mass Spectrometry and Ion Processes **52**: 337-349.

Zenobi, R. and R. Knochenmuss (1998). "Ion formation in MALDI mass spectrometry [Review]." Mass Spectrometry Reviews **17**(5): 337-366.

Zubarev, R. and M. Mann (2007). "On the proper use of mass accuracy in proteomics." Molecular & Cellular Proteomics **6**(3): 377-381.

Zubarev, R. A., N. L. Kelleher, et al. (1998). "Electron Capture Dissociation of Multiply Charged Protein Cations - a Nonergodic Process." Journal of the American Chemical Society **120**(13): 3265-3266.

Zubarev, R. A., N. A. Kruger, et al. (1999). "Electron capture dissociation of gaseous multiply-charged proteins is favored at disulfide bonds and other sites of high hydrogen atom affinity." Journal of the American Chemical Society **121**(12): 2857-2862.

Curriculum Vitae

Konstantin Aizikov

Education

2009	Ph.D. Electrical Engineering, Boston University, Boston
	Thesis: Novel Computation and Instrumentation Methodologies in Fourier
	Transform Ion Cyclotron Resonance Mass Spectrometric Imaging.
2009	M.S. Bioinformatics, Boston University, Boston
2009	M.S. Software Engineering, Boston University, Boston
1997	B.S. Chemistry, Brandeis University, Waltham MA

Experience:

2004-2009	Research assistant at Boston University School of Medicine, Mass Spectrometry Resource, Boston MA
2007	Bioinformatics consultant at The Institute for Molecular Medicine, CA
2002-2004	Software design engineer at MacroHard, Inc., Boston, MA
2000-2002	Software engineer at Shym Technologies, Inc., Newtown MA
1999-2000	Software engineer at Teradyne, Inc., Boston, MA

Journal Publications:

1. Aizikov K.; Smith D.F..; Chargin D.A.; Ivanov S.; Lin T.Y.; Heeren, R.M.A.; O'Connor P.B. Vacuum Compatible SamplePositioning Device for MALDI FT-ICR MS Imaging *in submission* **2009**

2. Smith, D. F.; Aizikov, K.; Duursma, M.; Spaanderman, D. J.; McDonnell, L. A.; O'Connor, P. B.; Heeren, R. M. A. MALDI FT-ICR Mass Spectrometry Imaging Instrumentation and Methods *in submission* **2009**

3. Aizikov, K.; Mathur, R.; O'Connor, P. B. The Spontaneous Loss of Coherence Catastrophe in Fourier Transform Ion Cyclotron Resonance Mass Spectrometry *J. Am. Soc. Mass Spectrom.* **2009**, *20*, 247-256.

4. Lin, C.; Mathur, R.; Aizikov, K.; O'Connor, P.B. First Signal on the Cryogenic Fourier-Transform Ion Cyclotron Resonance Mass Spectrometer. *J. Am. Soc. Mass Spectrom.* **2007**, 18 2090-2093.

5. Aizikov, K; O'Connor, P.B. Use of the Filter Diagonalization Method in the Study of Space Charge Related Frequency Modulation in Fourier Transform Ion Cyclotron

Posters and Invited Talks:

1. Aizikov K, Lin TY, Lin C, O'Connor PB. Automated MALDI Stage for Imaging MS. *Annual Cardiovascular Proteomic Center and Boston University School of Medicine Mass Spectrometry Resource Advisory Meeting.* Boston, MA May, 2009

2. Li X, Cui W, Yao C, <u>Aizikov K</u>, Lin TY, Sargaeva NP, Lin C, O'connor PB. Glutamine Deamidation: Differentiation of Glutamic Acid and γ-Glutamic Acid in Peptides by Electron Capture Dissociation. *Proceedings of the 56nd ASMS Conference*; Philadelphia, PA, 2009.

3. Sargaeva NP, Yao C, Lin TY, Cui W, <u>Aizikov K</u>, Li X, Lin C, O'Connor PB. ECD and EID of Amyloid Beta 17-28, 1-40, and Synthetic Beta-Substance P. *Proceedings of the 56nd ASMS Conference*; Philadelphia, PA, 2009.

4. <u>Aizikov K</u>, Smith FD, Chargin DA, Ivanov S, Perlman DH, Lin TY, Sargaeva NP, Heeren RMA, O'connor PB. Automated Vacuum Compatible Sample Positioning Device for Imaging Mass Spectrometry. *Proceedings of the 56nd ASMS Conference*; Philadelphia, PA, 2009.

5. Lin TY, Mathur R, Lin C, <u>Aizikov K</u>, Knepper RW, O'Connor PB. An Amplitude and Frequency Stabilized High Power Oscillator for Mass Filtering and Driving Multipole Ion Guides. *Proceedings of the 56nd ASMS Conference*; Philadelphia, PA, 2009.

6. Yao C, Sargaeva NP, Cui W, Li X, Lin TY, <u>Aizikov K</u>, Lin C, O'Connor PB. Top-down ECD Mass Spectrometry of Calmodulin Deamidation. *Proceedings of the 56nd ASMS Conference*; Philadelphia, PA, 2009.

7. Lin TY, Mathur R, Lin C, <u>Aizikov K</u>, Knepper RW, O'Connor PB. An Amplitude and Frequency Stabilized High Power Oscillator for Mass Filtering and Multipole Ion Guides. *The 11th Annual MASSEP.org GBMSDG Symposium*, Boston, MA, 2009

8. <u>Aizikov K</u>, Smith DF, Chargin DA, Ivanov S, Perlman DH, Lin TY, Sargaeva NP, Heeren RMA, O'Connor PB. Automated Vacuum Compatible Sample Positioning Device for Imaging Mass Spectrometry. *7th North American FTMS Conference*, Key West, FL, 2009

9. Smith DF, Duursma MC, Czornak K, <u>Aizikov K</u>, O'Connor PB, Heeren RMA. Development of Instrumentation and Methods for FT-ICR Imaging Mass spectrometry. *7th North American FTMS Conference*, Key West, FL, 2009

10. Mathur R, Lin C, <u>Aizikov K</u>, Knepper RW, and O'Connor PB. A Novel, High Sensitivity Cryogenic Fourier Transform Ion Cyclotron Resonance Mass Spectrometer. *56th ASMS Conference on Mass Spectrometry and Allied Topics*, Denver, CO, June 2008.

11. <u>Aizikov K</u>, Sargaeva NP, Cournoyer JJ, Lin C, and O'Connor PB. Experimental Evidence of Ion Cyclotron Resonance Frequency Modulations Induced by Inhomogeneities of the Trapping Electric Field. *Proceedings of the 56nd ASMS Conference*; Denver, Co, 2008.

12. <u>Aizikov K</u>, Mathur R, O'Connor PB. The Spontaneous Loss of Coherence Catastrophe in FTMS. *Proceedings of the 55nd ASMS Conference*; Indianapolis, IN, 2007.

13. Mathur R, Lin C, <u>Aizikov K</u>, Knepper RW, O'Connor PB. Low Noise Preamplifier for Cryogenic Fourier Transform Ion Cyclotron Resonance Mass Spectrometry. *Proceedings of the 55nd ASMS Conference*; Indianapolis, IN, 2007.

14. O'Connor PB, Lin C, Mathur R, <u>Aizikov K</u>, Cournoyer JJ, Kaur P, Ivleva VB and Zhao C. A Fourier Transform Ion Cyclotron Resonance Mass Spectrometer Designed to Operate at Cryogenic Temperatures. *Proceedings of the 54nd ASMS Conference*; Seattle, WA, 2005.

15. <u>Aizikov, K</u>.; O'Connor, P.B. Use of the Filter Diagonalization Method in the Study of Space Charge Related Frequency Modulation in FTMS. *Proceedings of the 53nd ASMS Conference*; San Antonio, TX, 2005.

16. Kaur, P.; <u>Aizikov, K</u>.; Budnik, B.A.; O'Connor, P.B. MASSPIKE (Mass SPectrum Interpretation and Kernal Extraction) for Biological Samples. *Proceedings of the 53nd ASMS Conference*; San Antonio, TX, 2005. Kaur, P.; <u>Aizikov, K</u>.; O'Connor, P.B. Improved Algorithms for Interpretation of High Resolution Mass Spectra. *Proceedings of the 52nd ASMS Conference*; Nashville, TN,

17. Lin C, Mathur R, <u>Aizikov K</u>, and O'Connor PB. Development of the CryoFTMS. *9th NHLBI Proteomics Initiative Investigators Meeting*, Boston, MA, April 2007. Aizikov K, O'Connor PB, Use of the Filter Diagonalization Method in the Study of Space Charge Related Frequency Modulation in FTMS. *Annual Cardiovascular Proteomic Center Meeting.* Boston, MA Sept, 2005

Curriculum Vitae

Konstantin Aizikov

Education

2010	Ph.D. Electrical Engineering, Boston University, Boston
	Thesis: Novel Computation and Instrumentation Methodologies in Fourier Transform Ion Cyclotron Resonance Mass Spectrometric Imaging.
2009	M.S. Bioinformatics, Boston University, Boston
2002	M.S. Software Engineering, Boston University, Boston
1997	B.S. Chemistry, Brandeis University, Waltham MA

Experience:

2004-2009	Research assistant at Boston University School of Medicine, Mass Spectrometry Resource, Boston MA
2007	Bioinformatics consultant at The Institute for Molecular Medicine, CA
2002-2004	Software design engineer at MacroHard, Inc., Boston, MA
2000-2002	Software engineer at Shym Technologies, Inc., Newtown MA
1999-2000	Software engineer at Teradyne, Inc., Boston, MA

Journal Publications:

1. Aizikov K.; Smith D.F..; Chargin D.A.; Ivanov S.; Lin T.Y.; Heeren, R.M.A.; O'Connor P.B. Vacuum Compatible SamplePositioning Device for MALDI FT-ICR MS Imaging *in submission* **2009**

2. Smith, D. F.; Aizikov, K.; Duursma, M.; Spaanderman, D. J.; McDonnell, L. A.; O'Connor, P. B.; Heeren, R. M. A. MALDI FT-ICR Mass Spectrometry Imaging Instrumentation and Methods *in submission* **2009**

3. Aizikov, K.; Mathur, R.; O'Connor, P. B. The Spontaneous Loss of Coherence Catastrophe in Fourier Transform Ion Cyclotron Resonance Mass Spectrometry *J. Am. Soc. Mass Spectrom.* **2009**, *20*, 247-256.

4. Lin, C.; Mathur, R.; Aizikov, K.; O'Connor, P.B. First Signal on the Cryogenic Fourier-Transform Ion Cyclotron Resonance Mass Spectrometer. *J. Am. Soc. Mass Spectrom.* **2007**, 18 2090-2093.

5. Aizikov, K; O'Connor, P.B. Use of the Filter Diagonalization Method in the Study of Space Charge Related Frequency Modulation in Fourier Transform Ion Cyclotron

Posters and Invited Talks:

1. Aizikov K, Lin TY, Lin C, O'Connor PB. Automated MALDI Stage for Imaging MS. *Annual Cardiovascular Proteomic Center and Boston University School of Medicine Mass Spectrometry Resource Advisory Meeting.* Boston, MA May, 2009

2. Li X, Cui W, Yao C, <u>Aizikov K</u>, Lin TY, Sargaeva NP, Lin C, O'connor PB. Glutamine Deamidation: Differentiation of Glutamic Acid and γ-Glutamic Acid in Peptides by Electron Capture Dissociation. *Proceedings of the 56nd ASMS Conference*; Philadelphia, PA, 2009.

3. Sargaeva NP, Yao C, Lin TY, Cui W, <u>Aizikov K</u>, Li X, Lin C, O'Connor PB. ECD and EID of Amyloid Beta 17-28, 1-40, and Synthetic Beta-Substance P. *Proceedings of the 56nd ASMS Conference*; Philadelphia, PA, 2009.

4. <u>Aizikov K</u>, Smith FD, Chargin DA, Ivanov S, Perlman DH, Lin TY, Sargaeva NP, Heeren RMA, O'connor PB. Automated Vacuum Compatible Sample Positioning Device for Imaging Mass Spectrometry. *Proceedings of the 56nd ASMS Conference*; Philadelphia, PA, 2009.

5. Lin TY, Mathur R, Lin C, <u>Aizikov K</u>, Knepper RW, O'Connor PB. An Amplitude and Frequency Stabilized High Power Oscillator for Mass Filtering and Driving Multipole Ion Guides. *Proceedings of the 56nd ASMS Conference*; Philadelphia, PA, 2009.

6. Yao C, Sargaeva NP, Cui W, Li X, Lin TY, <u>Aizikov K</u>, Lin C, O'Connor PB. Top-down ECD Mass Spectrometry of Calmodulin Deamidation. *Proceedings of the 56nd ASMS Conference*; Philadelphia, PA, 2009.

7. Lin TY, Mathur R, Lin C, <u>Aizikov K</u>, Knepper RW, O'Connor PB. An Amplitude and Frequency Stabilized High Power Oscillator for Mass Filtering and Multipole Ion Guides. *The 11th Annual MASSEP.org GBMSDG Symposium*, Boston, MA, 2009

8. <u>Aizikov K</u>, Smith DF, Chargin DA, Ivanov S, Perlman DH, Lin TY, Sargaeva NP, Heeren RMA, O'Connor PB. Automated Vacuum Compatible Sample Positioning Device for Imaging Mass Spectrometry. *7th North American FTMS Conference*, Key West, FL, 2009

9. Smith DF, Duursma MC, Czornak K, <u>Aizikov K</u>, O'Connor PB, Heeren RMA. Development of Instrumentation and Methods for FT-ICR Imaging Mass spectrometry. *7th North American FTMS Conference*, Key West, FL, 2009

10. Mathur R, Lin C, <u>Aizikov K</u>, Knepper RW, and O'Connor PB. A Novel, High Sensitivity Cryogenic Fourier Transform Ion Cyclotron Resonance Mass Spectrometer. *56th ASMS Conference on Mass Spectrometry and Allied Topics*, Denver, CO, June 2008.

11. <u>Aizikov K</u>, Sargaeva NP, Cournoyer JJ, Lin C, and O'Connor PB. Experimental Evidence of Ion Cyclotron Resonance Frequency Modulations Induced by Inhomogeneities of the Trapping Electric Field. *Proceedings of the 56nd ASMS Conference*; Denver, Co, 2008.

12. <u>Aizikov K</u>, Mathur R, O'Connor PB. The Spontaneous Loss of Coherence Catastrophe in FTMS. *Proceedings of the 55nd ASMS Conference*; Indianapolis, IN, 2007.

13. Mathur R, Lin C, <u>Aizikov K</u>, Knepper RW, O'Connor PB. Low Noise Preamplifier for Cryogenic Fourier Transform Ion Cyclotron Resonance Mass Spectrometry. *Proceedings of the 55nd ASMS Conference*; Indianapolis, IN, 2007.

14. O'Connor PB, Lin C, Mathur R, Aizikov K, Cournoyer JJ, Kaur P, Ivleva VB and Zhao C. A Fourier Transform Ion Cyclotron Resonance Mass Spectrometer Designed to Operate at Cryogenic Temperatures. *Proceedings of the 54nd ASMS Conference*; Seattle, WA, 2005.

15. Aizikov, K.; O'Connor, P.B. Use of the Filter Diagonalization Method in the Study of Space Charge Related Frequency Modulation in FTMS. *Proceedings of the 53nd ASMS Conference*; San Antonio, TX, 2005.

16. Kaur, P.; Aizikov, K.; Budnik, B.A.; O'Connor, P.B. MASSPIKE (Mass SPectrum Interpretation and Kernal Extraction) for Biological Samples. *Proceedings of the 53nd ASMS Conference*; San Antonio, TX, 2005. Kaur, P.; Aizikov, K.; O'Connor, P.B. Improved Algorithms for Interpretation of High Resolution Mass Spectra. *Proceedings of the 52nd ASMS Conference*; Nashville, TN,

17. Lin C, Mathur R, Aizikov K, and O'Connor PB. Development of the CryoFTMS. *9th NHLBI Proteomics Initiative Investigators Meeting*, Boston, MA, April 2007. Aizikov K, O'Connor PB, Use of the Filter Diagonalization Method in the Study of Space Charge Related Frequency Modulation in FTMS. *Annual Cardiovascular Proteomic Center Meeting*. Boston, MA Sept, 2005